UTS UNIVERSITY OF TECHNOLOGY SYDNEY

Removing the Battery Recharge/Replacement Burden of Internet-of-Things Wireless Sensor Nodes Using Thermoelectric Energy Harvesting

by Amer Hawchar

Thesis submitted in fulfilment of the requirements for the degree of

Doctor of Philosophy

under the supervision of A/Prof. Nick Bennett & Dr. Mickey Clemon

University of Technology Sydney
Faculty of Engineering and IT

August 2024

CERTIFICATE OF ORIGINAL AUTHORSHIP

I, Amer Hawchar declare that this thesis, is submitted in fulfilment of the requirements for the award of Doctor of Philosophy, in the Faculty of Engineering and IT at the University of Technology Sydney.

This thesis is wholly my own work unless otherwise referenced or acknowledged. In addition, I certify that all information sources and literature used are indicated in the thesis.

This document has not been submitted for qualifications at any other academic institution.

This research is supported by the Australian Government Research Training Program.

Signature: Production Note: Signature removed prior to publication.

Date: 09/08/2024

Acknowledgments

The author would like to firstly acknowledge his family for providing financial and emotional support throughout the duration of this thesis. He would also like to acknowledge his supervisor A/Prof Nick Bennett for providing support with regards to the research, theoretical information and experimental methodologies of this research project. Finally, he would like to thank both breweries, Young Henrys and Hawke's brewery for allowing experimentation within the breweries to obtain experimental results.

Publications

First Author Publications

Amer Hawchar, Solomon Ould, and Nick S. Bennett. “Carbon Dioxide Monitoring inside an Australian Brewery Using an Internet-of-Things Sensor Network.” *Sensors* 22, no. 24 (December 2022): 9752. https://doi.org/10.3390/s22249752.

Second Author Publications

Nick S. Bennett, Amer Hawchar, and Aidan Cowley. “Thermal Control of CubeSat Electronics Using Thermoelectrics.” *Applied Sciences* 13, no. 11 (May 2023): 6480. https://doi.org/10.3390/app13116480.

Abstract

The release of fermentation carbon dioxide (CO_2) was investigated in this research thesis, with regards to its effects on raising CO_2 levels inside an Australian brewery. Using 3 wireless Internet-of-Things (IoT) sensor nodes, it was determined that, at times, the CO_2 levels inside the brewery far exceeded safe limits, indicated by the maximum CO_2 level recorded being in excess of 18,000 ppm. The identification of differences in measured CO_2 at different times and locations throughout the brewery also revealed that a single hard-wired CO_2 sensor, which is typically used as the detection standard in breweries, may be inadequate to support indoor air quality monitoring. This strengthened the need to have a network of wireless IoT CO_2 sensor modes inside breweries. One identified constraint was the short battery life of current Wi-Fi IoT sensor nodes. In order to increase this battery life, LoRa was analysed alongside Wi-Fi by developing three wireless IoT sensor nodes that measured the CO_2 concentration. The LoRa sensor node achieved a battery runtime that was more than 17 times greater than the Wi-Fi sensor node, equivalent to a decreased power consumption of over 94%. This significant decrease in power consumption in conjunction with no decrease in signal range and penetrability was a significant step towards creating a feasible network of wireless CO_2 sensor nodes, however the battery life was still a burden, therefore further improvements were required. A thermoelectric generator (TEG) system was then developed to recover brewery waste heat from the hot pipe outlet of two steam boilers within an Australian brewery, converting it into electricity to recharge the battery of a CO_2 sensor node. The TEG was successful at removing the battery recharge/replacement burden of the developed sensor node, evidenced by its ability to keep the battery charged with no input from any user/source over the (32 days) test period, while the sensor node was active and monitoring CO_2 levels. The TEG was capable of producing a maximum and average power output of approximately 2.5 W and 1.02 W (period of 10 hours) respectively, while generating an average of approximately 7.29 Wh of useable energy daily, allowing for the estimate that it can support a network of LoRa IoT sensor nodes, thus creating a wireless IoT sensor network that can uniformly monitor CO_2 throughout the brewery supporting a safer working environment.

Table of Contents

List of Figures

List of Tables

1. Introduction

The Environmental Protection Agency (EPA), which are the regulatory body for regulating air quality in the United States, have stated that indoor pollutant concentrations can exceed outdoor levels by 100 times, while they also rank poor air quality in the top five environmental risks to public health [1]. Importance must therefore be placed on ensuring that indoor air quality (IAQ) within domestic residences and workplaces is free of elevated levels of pollutants that may cause long/short term injury. Poor IAQ can create risks that are equally relevant worldwide, yet, as stated by Morawska et al. (2024) [2], most countries do not have legislated IAQ performance standards for public spaces that address concentrations of indoor air pollutants. Their research concludes that long-term benefits to public health, well-being and productivity are likely to outweigh short-terms costs associated with the implementation of systems to monitor and maintain adequate air quality standards, therefore, deriving new methods to monitor IAQ is relevant, due to the need to enforce standards which may require non-intrusive, fit-and-forget sensing methods that can be implemented within residences or workplace environments.

1.1 CO_2 Monitoring

Carbon dioxide (CO_2) is both a colourless and odourless gas that exists at concentrations of approximately 400 parts-per-million (ppm) in the atmosphere, however indoor levels can be several times higher. CO_2 is often produced indoors by the human respiratory system and the combustion of fossil fuels. In recent years, CO_2 levels indoors have been used as a proxy to assess IAQ [3–5]. Cognitive performance can be impacted by CO_2 levels exceeding 1,000 ppm, effecting decision making and problem solving ability [6–9], while CO_2 levels exceeding 10,000 ppm can result in physiological impairment, resulting in increased respiratory rate, respiratory acidosis, metabolic stress (decreased blood calcium or urine phosphorus), increased brain blood flow, and increased minute ventilation [10–13].

In 2005, the Australian Standard 5034 [14] came into effect to reduce the risks associated with the hazards of compressed and refrigerated gases in the workplace, which included CO_2. A key element of AS5034-2005 was the requirement for gas monitors in non-ventilated areas. The standard states that CO_2 monitors must be installed in non-ventilated areas with the intention

of keeping concentrations below 5,000 ppm, however monitors are only required to sound when levels are above 15,000 ppm and again at 30,000 ppm.

Workplaces that produce CO_2 intentionally or unintentionally within their manufacturing processes are at risk of creating poor IAQ. An example is breweries, who generate CO_2 as a result of fermentation, where yeast turns glucose into alcohol and CO_2, a process that is crucial in beer production. Technology exists to capture and re-use the CO_2 resulting from fermentation for beer carbonation; however, this technology is not accessible to smaller breweries due to its high costs. In that case, CO_2 is normally vented from the fermentation tanks directly to the indoor environment, while CO_2 for carbonation is purchased separately and delivered via trucks which directly pump the CO_2 into large indoor/outdoor storage tanks. The CO_2 released via venting from fermentation and the unintentional elevation of concentrations from refilling CO_2 storage tanks may result in CO_2 levels above safe limits, creating cognitive/physiological side effects. Since working in a brewery requires manual tasks, e.g. using forklifts, lifting heavy products, and hosing down equipment which may leave the floor wet, this may ultimately increase the risk of work-related injuries occurring, therefore adequate monitoring is required.

Breweries in Australia are only legally required to use one single hard-wired CO_2 monitoring system [Figure 1] to track IAQ/CO_2 and prevent possible health issues [14]. Using one fixed sensor within a brewery leads to some areas being unmonitored, which may unknowingly expose workers to elevated CO_2 levels that in turn may create unsafe working environments.

This research project will firstly determine if using a single hard-wired CO_2 monitoring system in an Australian craft brewery is adequate for monitoring CO_2. If deemed inadequate, an effective way of combatting the existence of unmonitored CO_2 areas and potential CO_2 exposure would be to add more monitoring sensors, such as the one shown in [Figure 1]. Potential issues with this approach include that, firstly, several hard-wired connections would need to be implemented to accommodate multiple fixed sensors, while some sensors may need to be implemented in areas where this is impossible, therefore, the most effective approach would be to utilize wireless Internet-of-Things (IoT) sensor networks that can monitor CO_2 throughout the workplace in multiple locations.

Figure 1. An example of a hard-wired CO_2 monitoring system used in an Australian brewery.

1.2 Low-Power Sensing

Industry 4.0 has led to the rapid growth of large wireless IoT sensor networks that can monitor multiple and various environmental conditions, for example, a wireless IoT sensor network can be created to monitor the CO_2 concentration inside a brewery using an array of sensors to ensure workers are not subjected to unsafe workplace environments, however the biggest drawback of wireless IoT sensor technology is battery power, with most IoT technologies utilizing power intensive wireless protocols such as Wi-Fi, this limits battery life increasing the reluctance of widespread adoption due to a consistent battery recharge/replacement burden.

Low-Power Wide Area Networks (LPWAN) have been developed with the intention of reducing the power requirements of wireless IoT technologies for various applications and end uses. Several LPWAN technologies are present in the market today such as SigFox, NB-IoT and LoRaWAN. Unlike SigFox and NB-IoT, LoRaWAN offers good range, penetration, private network deployments, and easy integration with a number of world-wide network platforms such as The Things Network (TTN). It is for these reasons, along with its open access specifications, that LoRaWAN has received attention from research communities since its first appearance on the market [15].

Secondly, this research project will investigate the effectiveness of LoRa to improve and potentially remove the battery recharge/replacement burden of IoT sensor technology, however if LoRa cannot adequately remove the aforementioned, this thesis will lastly experimentally analyse if LoRa can be utilized in conjunction with energy harvesting techniques to remove this burden, allowing wireless IoT sensor nodes to be powered indefinitely and increasing the feasibility of portable sensor nodes, this would therefore allow for IAQ monitoring throughout the brewery, or other workplaces, thus reducing the possibility of dangerous unmonitored areas.

1.3 Energy Harvesting

Wireless IoT sensor nodes typically contain a battery as a main source of power. The battery is used to power the communications board and sensor portions of the sensor node. The main issue with batteries is with regards to the fact that they need to be replaced and/or recharged every so often creating a burden and reluctance for IoT adoption.

Several energy harvesting techniques exist; however, it is important to consider which is the most practical to implement within a brewery. Solar energy harvesting via indoor photovoltaics (PV) is a potential option, however many breweries contain areas of low-lighting with low availability of harvestable energy [16]. Mechanical energy harvesting, such as piezoelectric harvesting is another option, yet it is likely to be impractical due to there being no obvious consistent source of harvestable energy available within a brewery, with the same applying to RF energy harvesting. Thermal energy harvesting is probably the most viable method to harvest energy within a brewery due to the abundance of waste heat available, such as that which is radiated from boilers and connecting pipework.

Thermoelectric modules harvest waste heat by converting it into electricity when a temperature difference is present between the module's top and bottom surfaces. Thermoelectric generator (TEG) systems contain thermoelectric modules sandwiched between a heat sink and a heat source. The heatsink rejects heat at the cold-side allowing for consistent waste heat to pass through the module, while the heat source provides the heat input to the module. Previous systems in the literature demonstrate that power in the 0.1 - 4 W range is achievable with a size and scale of system that could be implemented in a brewery.

This research project will lastly investigate the feasibility of using a TEG to harvest waste heat within a brewery manufacturing setting and generate electricity to remove the battery recharge/replacement burden of wireless IoT sensor nodes.

This thesis will achieve the aforementioned by firstly providing a literature review (Chapter 2) that outlines current literature pertaining to IAQ, IoT sensors, and energy harvesting techniques with emphasis on thermoelectrics, manufacturing waste heat, and finally, previously developed TEG systems. The literature review will help form three research questions that will be stated in the final subsection of Chapter 2. The methodology of the work and experiments undertaken will then be described in Chapter 3, followed by the results and discussion in Chapter 4. Finally, the conclusions and future work will be discussed to complete this thesis.

1.4 The Novelty

The novelty of this research project can be categorised as follows:

- IAQ monitoring
    - This research project aims to address the need for comprehensive and continuous monitoring of CO_2 levels throughout the manufacturing workplace, to ensure safe working environments by investigating if current CO_2 measurement protocols in breweries are adequate.
- Reducing power requirements
    - This work will also aim to minimise the power consumption of wireless CO_2 sensor nodes by reducing the consumption of all hardware to as low as possible, something that has not been done before for this category of sensor.
- Thermoelectric energy harvesting
    - This research project will then aim to remove the battery recharge/replacement burden of wireless IoT sensor technologies by utilizing thermoelectric energy harvesting and manufacturing waste heat within a brewery setting for the creation of a TEG system coupled with a wireless IoT CO_2 sensor node, for the first time.

In summary, the novelty of this research project lies in the innovative combination of thermoelectric technology, waste heat recovery, IoT connectivity, and a specific industrial

application to address a practical challenge – with the potential future impact to provide detailed and continuous IAQ monitoring throughout the manufacturing workplace to support safe working environments and remove potential unforeseen side effects of unsafe IAQ.

2. Literature Review

The section herein contains a literature review that outlines current literature pertaining to indoor air quality (IAQ), IoT sensors, and energy harvesting techniques, with emphasis on thermoelectrics, manufacturing waste heat, and finally, past developed TEG systems. This literature review will help form three research questions that will be addressed in this thesis.

2.1 Indoor Air Quality (IAQ)

The main pollutants with regard to IAQ are particle matter (PM), volatile organic compounds (VOCs), nitrous oxides (NO_X), ozone (O_3), sulfur dioxide (SO_2), and carbon oxides (CO and CO_2). Other pollutants include heavy metals, aerosols, radon (Rn), pesticides, biological allergens and microorganisms [17].

PM is defined as fine carbonaceous particles that are associated with absorbed organic chemicals and reactive metals [17]. PM is caused by particles that migrate from outdoor environments, or particles generated indoors via cooking, combustion of fossil fuels, smoking, or machine operation [17]. PM of diameter <0.1 μm are of extreme concern as they can be inhaled deep into the lung's alveoli, which can affect the lungs and heart, potentially leading to serious health injuries [17–19].

VOCs are gaseous organic compounds that contain chemicals emitted from liquids or solids [20], and formaldehyde is the most common [17]. VOCs are released from cooking, smoking, use of cleaning or personal care products, indoor chemical reactions, penetration of outdoor air, and building materials [21–25]. VOCs can affect humans via inhalation, ingestion, or dermal contact [17]. Long-term exposure can potentially cause cancer [26].

NO_X consists of nitric oxide (NO) and nitrogen dioxide (NO_2) gases, commonly caused by combustion sources [27]. Elevated levels of NO_X can cause increased asthmatic reactions and respiratory damage [27].

Ozone is produced by the photochemical reactions of atmospheric O_2, NO_x, and VOCs [17]. Ozone reacts with indoor pollutants, which can create products that irritate humans, via inhalation or skin exposure, and damage materials [17, 28]. Ozone indoors emerges mainly from electrical devices and penetration of the outdoor air [29].

Sulfur dioxide is a gas that is most commonly produced by the combustion of fossil fuels and can combine with aerosols or PMs [30]. SO_2 is emitted indoors by vented gas appliances, oil furnaces, tobacco smoke, kerosene heaters, and coal or wood stoves [31]; however, it can also enter indoor spaces via penetration from outdoor air [32]. The hourly concentration of SO_2 indoors is often below 20 ppb [33]. Exposure to SO_2 can impair respiratory function via inhalation [17].

CO_X consists of carbon monoxide (CO) gas and carbon dioxide (CO_2) gas. CO gas is produced indoors by combustion processes; however, it can also enter indoor spaces via the penetration of outdoor air [34]. The average concentration of CO indoors without a combustion source is equal to 0.5–5 ppm; however, when a gas stove is added, CO levels can rise higher than 30 ppm [17]. Exposure to low concentrations of CO can impact cardiovascular and neurobehavioral processes, while high concentrations can cause unconsciousness or death [35].

2.1.1 Carbon Dioxide (CO_2)

CO_2 is both colourless and odorless, therefore it cannot be seen or smelt creating an extreme safety risk for environments with high CO_2 levels due to the unforeseen dangers. Safety standards such as the Australian Standard 5034 [14] are in place to prevent extremely high levels of CO_2 exceeding 15,000 ppm that potentially can lead to irreparable health effects, however no Australian standards are currently in place for monitoring low-level CO_2 in the workplace. This is concerning as low-level CO_2 has been documented to impact cognitive performance exceeding 1,000 ppm, which includes decision making and problem resolution [6–9], while levels exceeding 10,000 ppm results in impaired physiological effects such as increased respiratory rate, respiratory acidosis, metabolic stress (decreased blood calcium or urine phosphorus), increased brain blood flow, and increased minute ventilation [10–13].

Low-level CO_2 needs to be monitored in workplaces where employees are consistently performing manual tasks such as, lifting, forklift operation, etc. Exposure to low-level CO_2 for such employees can result in impaired cognitive performance, which in turn, may lead to unforeseen workplace accidents.

Breweries generate CO_2 as a by-product of fermentation, something which is vital to beer manufacturing which is consistently occurring within their workplace. Alonso-Moreno and

Garcia-Yuste (2016) stated that approximately 12.7 million tonnes of CO_2 was released from fermentation processes used to produce wine and spirits [36]. A considerable amount of CO_2 is released during fermentation; from 100 g of glucose, approximately 51.1 g of ethanol and 48.9 g of CO_2 are produced [37]. Craft breweries typically lack the technology to recapture this generated CO_2 leading to the gas directly being vented into the unventilated indoor atmosphere. Craft breweries also purchase CO_2 and have it directly pumped into large indoor/outdoor storage tanks via delivery trucks, if indoor, this process can also lead to CO_2 being unintentionally vented indoors. CO_2 release due to fermentation and carbonation present a combined risk that may lead CO_2 levels indoors to consistently be higher than desirable, which increases the probability of employees being exposed to CO_2 side-effects that may impair employee health and performance, while also potentially increasing workplace accidents.

2.2 CO_2 Sensors

Traditional CO_2 sensors use Non-Dispersive InfraRed (NDIR) technology that measures CO_2 by shining infrared (IR) light through a sample of gas. CO_2 molecules absorb 4.2 to 4.4 μm wavelengths of infrared, therefore the degree to which the aforementioned wavelengths are absorbed provides a signature indicating the CO_2 concentration of the sample gas.

New innovative methods of measuring CO_2 have emerged which also use NDIR, however instead of using a filament as the source of generating IR, the new methods use LEDs, this reduces the power consumption of the sensor drastically due to the efficiency of LEDs and their ability to be tuned to only produce the required infrared wavelengths. This power decrease increases the feasibility of using CO_2 sensors within a wireless IoT sensor framework.

Industry 4.0 has led to the adoption of large IoT sensor networks that improve manufacturing conditions by monitoring machine operation and IAQ to ensure both machine and staff are performing within optimal conditions. Wireless IoT sensor nodes typically require a power source, a motherboard/computing unit, a sensor, and a wireless gateway. The power source needs to be sufficient to provide enough power to both the sensor and motherboard/computing unit, a factor which is important when considering different sensors with different power requirements coupled with different wireless protocols. A motherboard/computing unit is required to provide a means for the sensor to send and receive data while also allowing the

sensor to be programmed to the particular use case. Finally, a wireless gateway is required as a medium between the wireless sensor node and the internet.

IoT sensors are subjected to multiple applications within the manufacturing industry, therefore multiple types of IoT sensors exist, each with a specific purpose. Some common IoT sensors are as follows [38]:

- Position/Presence/Proximity
- Motion/Velocity/Displacement
- Temperature/Humidity/Moisture
- Acoustic/Sound/Vibration
- Chemical/Gas
- Force/Load/Torque/Strain/Pressure
- Machine/Vision/Optical/Ambient Light
- Electric/Magnetic

2.2.1 Wireless Protocols for CO_2 Sensing

Several studies using Wi-Fi as the wireless protocol for IoT IAQ monitoring systems have been conducted, such as the work done by the authors in references [39–42].

In reference [39], Jiang et al. (2011) developed MAQS, a personalized mobile sensing system for IAQ monitoring. MAQS differed from other systems by allowing users to carry portable indoor location tracking sensors that provided personalized IAQ information. To improve accuracy and energy efficiency, MAQS included an accurate temporal n-gram augmented Bayesian room localization method that requires few Wi-Fi fingerprints; an air exchange rate based IAQ sensing method, which measured general IAQ using CO_2 sensors; and finally, a zone-based proximity detection method for collaborative sensing which enabled data sharing among users. MAQS supported accurate personalized IAQ monitoring and quantitative analysis with high energy efficiency.

In reference [40], Marques et al. (2019) developed the iAirCO_2 system, a method that real-time monitored indoor CO_2 levels using IoT. The iAirCO_2 was composed of a hardware prototype for ambient data collection, web/smartphone software for data collection via Wi-Fi, and an

SQL Server. The primary reason was to enhance living environments by providing IAQ data that can be accessed by doctors in order to support medical diagnostics.

Kodali et al. (2020) [41] developed a wireless air pollution monitoring system that sent alerts to the user via Wi-Fi when concentrations of pollutants were beyond safe limits. The system monitored pollutants such as, nitrogen dioxide (NO_2), ammonia, sulphur dioxide (SO_2), radon, carbon monoxide (CO), carbon dioxide (CO_2), and benzene. The system differed from others in the sense that it allowed the alerts to be received by the user on their mobile phone from any distance irrespective of whether it is connected to the internet. The system used the NodeMCU Dev board v1.0 and the MQ135 air quality sensor.

In reference [42], Fernández-Ramos et al. (2020) developed a portable device based on a colorimetric sensor to determine the atmospheric level of CO_2 gas. The system consisted of a low-cost low-power System on a Chip (SoC) microcontroller with integrated Wi-Fi, a sensing membrane to determine CO_2 ppm, and finally, a user-friendly application to monitor and log the CO_2 measurements when the system is connected to a Wi-Fi network. The system was used to determine the CO_2 level inside classrooms in several secondary schools. It was concluded that the concentration of CO_2 in some school classrooms was higher than the desired limits with regards to influencing student health, safety, productivity, and comfort, therefore demonstrating the need to control this parameter to ensure appropriate IAQ.

2.2.1.1 Low-Power Sensors

Table 1 contains a comparison of popular wireless protocols that are often utilized for IoT sensor technologies [43].

Worldwide Interoperability for Microwave Access (Wi-Max) is a wireless broadband communications technology based on the IEE 802.16 standard that was developed in 2001, it can provide high speed data over a large range. Wi-Max can reach speeds of 70 mbps with a max range of 50 km, although the speed is less than Wi-Fi, the range is 50 times more, therefore Wi-Max is a great option for rural areas that do not have access to hardwired internet connection lines.

Table 1. Comparison of wireless protocols, adapted from [43].

Protocol	Range	TTN Compatibility	Power Consumption	Network Type	Data Rate
LoRa	**100 km**	**Yes**	**Very Low**	LPWAN	250 kbps
Wi-Max	50 km	No	Medium	MAN	70 mbps
LTE	28 km	No	Medium	GERAN	1 gbps
Wi-Fi	1 km	No	High	WLAN	7000 mbps
ZigBee	100 m	No	Low	Mesh	0.25 mbps
Bluetooth	35 m	No	Very Low	P2P	1 mbps
Z-Wave	30 m	No	Very Low	Mesh	0.1 mbps

The Zigbee protocol was developed in 2003 as an open global market connectivity standard with the intention of addressing the low cost/power needs of wireless IoT networks. Zigbee is a packet-based protocol that operates on the IEEE 802.15.4 specification. Zigbee devices create a mesh network that enables data transfer via a central node connected to a gateway that connects to the internet. The biggest drawback of ZigBee is its minimal range of 100 m.

Z-Wave was developed in 1999 by Zensys, a Danish company located in Copenhagen. Z-Wave uses low energy radio waves to communicate between devices within a mesh network. Z-Wave can allow for wireless control of smart home devices. The biggest drawback of Z-wave is also its minimal range of 30 m.

When compared with other LPWAN protocols, the LoRa protocol has very low power consumption while also having the largest range of up to 100 km, LoRa also has TTN integration which is one of the easiest methods of pushing data to the cloud with relatively little

setup from the end-user, however, the biggest drawback of LoRa is its minimal data rate capabilities of 250 kbps. This limited data rate capability will most likely be adequate for IoT sensor nodes due to their limited need for bandwidth, therefore LoRa would be the best wireless protocol for this research projects use case.

The LoRa protocol is a physical layer that has been patented by Semtech in 2014 [44], its Chirp Spread Spectrum (CSS) radio modulation is based on [45] and works by producing a chirp signal. A chirp is a time profile of the instantaneous frequency that changes over the time interval T from a frequency f_0 to f_1 [15]. The LoRa physical layer operates within the 433, 868 and 915 MHz frequency bands, with Australia using the 915 MHz frequency band.

The LoRaWAN medium access control (MAC) protocol is an open-source protocol standardized by the LoRa Alliance [46] that runs on top of the LoRa [44] physical layer [15]. The LoRaWAN MAC layer provides the mechanism that enables communication between multiple devices and network gateway(s) [15]. In order for LoRaWAN networks to cover large distances, the LoRaWAN network architecture has a star topology, therefore the end devices can only communicate with LoRaWAN gateways and not directly with each other [47]. Multiple gateways are connected to a central network server, with the LoRaWAN gateways being only responsible for forwarding raw data packets from end nodes towards the network server in UDP/IP packets and the network server being mainly responsible for sending downlink packets and MAC commands towards end devices [15]. The communication terminates at the application servers that can be owned by third parties such as The Things Network, while multiple application layers can be connected to a single network server [15].

The LoRaWAN connection allows for customizability when it comes to data rate (DR) and transmission power (TX) of the connection. The data rate can vary from 0-15 with 0-5 having the least amount of bandwidth (125 kHz) for the AU915-928 band and is therefore best suited for low powered connections. Table 2 contains the DR properties for the AU915-928 band, highlighting that a change in data rate also leads to a change in bit rate and spreading factor (chirp rate).

The TX is the Equivalent Isotropically Radiated Power (EIRP), which is the radiated output power referenced to an isotropic antenna radiating power equally in all directions with its gain

expressed in dBi [48]. The default max EIRP is +30dBm with a decrease leading to a shorter range of signal [48].

Table 2. Data rate properties for LoRaWAN AU915-928 band adapted from [48].

Data Rate	Configuration (Spreading Factor/Bandwidth)	Bitrate (bit/sec)
0	LoRa: SF12 / 125 kHz	250
1	LoRa: SF11 / 125 kHz	440
2	LoRa: SF10 / 125 kHz	980
3	LoRa: SF9 / 125 kHz	1760
4	LoRa: SF8 / 125 kHz	3125
5	LoRa: SF7 / 125 kHz	5470

LoRa and LoRaWAN have been researched extensively in the past with multiple papers exploring their use cases as IoT wireless protocols such as the work done in [43, 49, 50]

Wu et al. (2018) [49] developed a wearable IoT sensor node to monitor harmful environmental conditions for safety applications via LoRa wireless technology. The proposed sensor node was low-power and supported multiple environmental sensors and a LoRa based gateway was used to connect the sensors to the internet. The system focused on monitoring carbon monoxide, carbon dioxide, ultraviolet, and some general environmental parameters. Surrounding environmental data was gathered by the wearable node in real-time and then transmitted to a remote cloud server, allowing the data to be displayed to authorized users through a web-based application located in the cloud server. The user could also be alerted via a mobile application when an emergency occurred.

In reference [50], Lee and Ke (2018) developed a LoRa mesh networking system for large-area monitoring of IoT applications by deploying 19 LoRa end devices over an 800 m × 600 m area at a university campus with a gateway that collected data at 1 min intervals. The proposed LoRa mesh networking system achieved an average of 88.49% PDR, compared to the star-network topology used by LoRa achieving only 58.7% under the same conditions. This was one of the

first papers discussing LoRa mesh networking in detail and evaluating its performance via real experiments.

In reference [43] Ould and Bennett (2022) tested the power consumption of several LoRaWAN boards to determine which had the least amount of power consumption for the IoT use case. It was determined that the boards all had varying power consumption with the Grasshopper LoRaWAN board having the least amount of power consumption using, on average, approximately 1.18 Ws of energy, while the E5 Full used approximately 2.15 Ws, the E5 Mini 2.28 Ws, and finally, the Pycom 15.6 Ws.

2.2.1.2 IAQ Use Cases

Several papers have been written with emphasis on IAQ such as in references [51–57].

In reference [51], Abraham and Li (2014) developed a simplified ZigBee system for IAQ monitoring applications using the Arduino platform, the system consisted of a low-cost CO_2, VOC, and temperature and humidity sensors, however the system did not provide any mobile computing solution for IAQ evaluation or analytics. The outcome was to reduce indoor air pollution to improve public health.

Kim et al. (2014) [52] developed a system that monitored particulate matter, ozone, carbon monoxide, carbon dioxide, nitrogen oxides, sulfur dioxide, VOCs, temperature, and humidity. The system contained a protype sensor module which used a Raspberry Pi, while incorporating a smoothing algorithm to prevent temporary sensor errors and an aggregation algorithm to reduce the network traffic and power consumption, however as the system used a raspberry pi it was not cost effective. The main focus was to monitor IAQ on a real-time basis in urban ecosystems.

In reference [53] Pitarma at al. (2017) developed a wireless sensor network for monitoring and collection of IAQ using Arduino, XBee modules/microsensors and ZigBee protocol. Temperature, humidity, carbon monoxide, CO_2 and luminosity data were monitored and later accessed via an android application and a web portal. The purpose of this research was to provide an effective IAQ assessment to prevent sick building syndrome.

Moon et al. (2017) [54] developed an IoT-based sensor that was used to monitor the air quality inside a factory to help managers maintain optimum working conditions for their employees by measuring temperature, humidity, CO_2 level, dust, and odour sensor data. The proposed system was robust and able to accurately measure the environmental condition inside the factory in real-time.

Husein et al. (2019) [55] developed a real-time and long range air pollution monitoring system for indoor and outdoor environments. The system consisted of a wireless sensor network that used LoRa technology for data communication between all nodes and sensors. 3 nodes were distributed within 900 m of the gateway for measuring the concentration of carbon monoxide (CO), carbon dioxide (CO_2) and nitrogen oxide (NO). The paper demonstrates thar LoRa technology is very suitable for the air pollution system especially in long range transmission compared to other wireless transmission technologies. The sensor nodes used the Arduino UNO R3 microcontroller board due to its low cost and ease of use, while the sensors used were the MQ7, MQ2, and MQ135.

CO_2 IAQ monitoring inside craft breweries using IoT technology is relatively new and therefore prior research is limited; however, in reference [56], Huizen (2020) developed a wearable system that used IoT to monitor brewery IAQ. The main drawback of the system was its bulkiness, making it difficult to implement within a brewery, due to the inclusion of a Raspberry Pi, camera, power supply and CO_2 sensor that had to be worn like a backpack at all times, making it difficult to access tight spaces, and creating extra layers that brewery workers may be reluctant to wear due to the high temperatures in a brewery. There is a need to therefore create a more practical solution.

Twahirwa et al. (2021) [57] developed an air pollution monitoring system which used the LoRa enabled IoT framework. Two sensors capable of monitoring CO_2 and $PM_{2.5}$ were deployed in the cafeteria kitchen and laboratory room of the University of Rwanda, College of Science and Technology. The measured data was then sent to the cloud via a LoRaWAN gateway, allowing the end users the ability to query the system and access the data together with the analytic information via the developed web-based user interface dashboard. Analysis of the data over a period of 11 months demonstrated CO_2 levels in excess of 800 ppm and $PM_{2.5}$ concentration

levels exceeding 100 ppm in the kitchen environment, while maximum values of 500 and 0 ppm for CO_2 and $PM_{2.5}$ were observed in the laboratory room respectively.

2.2.1.3 Other Use Cases

IAQ is not the only use case for IoT in the workplace, multiple studies have been conducted in the manufacturing industry demonstrating significant advantages of utilizing IoT based sensors to improve working conditions, preventing erroneous designs, providing fault diagnosis/quality prediction, and helping managers with better decision making [58]. References [59–62] are examples of studies conducted with regards to other use cases in the manufacturing industry.

Salamone et al. (2017) [59] proposed an environmental monitoring system based on low-cost IoT sensors for preventing errors during the design phase in additive manufacturing by measuring temperature and humidity data. It was revealed that the proposed system could help prevent errors during the design phase in additive manufacturing by monitoring for optimal manufacturing conditions.

In reference [60], Lee et al. (2018) proposed a system that utilized IoT sensors and machine learning to predict the quality of a product and optimize operation control. The effectiveness of the system was investigated alongside metal casting. The system effectively predicted the quality of the metal that was casted and efficiently improved operational control.

Calderón Godoy and González Pérez (2018) [61] investigated the integration of IoT sensors within the SCADA system for effective migration of legacy systems to the fourth industrial revolution framework. The proposed system was feasible and is expected to help managers during the migration of legacy systems to the industry 4.0 framework.

In reference [62], Li et al. (2018) proposed IoT sensors for fault diagnosis of mine hoisting equipment. It was concluded that the proposed IoT sensors can help by collecting complete diagnosis data, thus improving diagnosis results.

2.2.1.4 Signal Propagation

Multiple studies have been conducted investigating the signal propagation capabilities and drawbacks of both Wi-Fi and LoRa such as in references [63, 64].

Suherman (2018) [63] investigated the effect that various indoor building materials had on Wi-Fi signal propagation. The first set of experiments consisted of an obstacle that was made of either wood, metal or concrete that was placed between an ESP8266 and a smartphone hotspot at varying distances. The second set of experiments consisted of introducing a metal reflector to aid with bypassing a concrete wall. It was concluded that average Wi-Fi signal level decreased with an increase in distance, while the concrete obstacle absorbed the most signal followed by metal and lastly wood. Average signal strength fluctuated from -66.27 to -58.9 dBm for concrete and wood respectively indicating the vast impact building materials can have on signal strength indoors. While the introduction of a reflector was able to increase signal strength from -68.69 to -62.13 indicating that reflective material indoors can allow Wi-Fi signals to reflect around obstacles.

In reference [64], Liang et al. (2020) investigated the effect that building materials had on LoRa signal propagation indoors by placing a LoRa transmit module on the 7^{th} floor of a building with 3 receiving modules on the same floor to investigate penetration through cement walls, receiving modules were then placed on other floors to investigate penetration through reinforced concrete floors. It was determined that LoRa's penetration capability through walls was excellent as a packet delivery ratio (PDR) of $\geq$ 99.2% was achieved when using TX(10). LoRa's penetration capability through reinforced concrete however, was also determined to be excellent as floors 3, 6, 8, 12 achieved a PDR of approximately $\geq$ 90% with TX(10) and approximately $\geq$ 98% with TX(20), therefore LoRa was able to penetrate through at least 4 reinforced slabs of concrete before signal strength was significantly degraded.

2.2.2 Wireless IoT Sensor Power Requirements

The current and power requirements of a wireless IoT sensor node are extremely important as they determine the severity of the battery recharge/replacement burden that is typically linked to wireless IoT sensor node adoption.

The first component to consider when determining current requirements of a wireless IoT sensor node is the motherboard/computing unit which is responsible for receiving and transmitting data from components connected to it such as a CO_2 sensor. The wireless protocol of the motherboard/computing unit is strongly linked to how much current it requires during operation, for example, a unit that transmits over Wi-Fi, such as the Sparkfun ESP32 Thing

board, will typically require, according to the manufacturer's website [65], approximately 150 mA (540 mW) for Wi-fi transmissions. A LoRa board on the other hand, such as the Grasshopper LoRaWAN board only consumes approximately 35 mA (126 mW) during LoRa transmissions [43]. Just by considering the motherboard/computing unit, it is evident how severe the battery recharge/replacement burden may be if the wrong components are chosen.

The next component to consider is the sensor portion of the wireless IoT sensor node. Different sensor types that measure different parameters may have different current requirements, for example, a sensor that measures CO_2 may have different current consumption when compared to a sensor that measures temperature, however, it is even possible for sensors that measure the same parameter to have different current consumptions due to new innovative methods of measuring the parameter, for example an Adafruit SCD30 CO_2 sensor which uses an old filament method of measuring CO_2 consumes approximately 19 mA (68.4 mW), according to the manufacturers website [66], while a new innovated LED sensor such as the Cozir LP3 consumes approximately 1 mA (3.5 mW), according to its datasheet.

2.2.2.1 Types of Batteries

The ever-increasing demand for non-renewable energy has led to the rise of renewable energy and energy harvesting technologies, however such technologies often rely on energy storage devices to operate such as batteries, therefore the type of battery used along with its power characteristics are of high importance [67].

Batteries are devices that have the capability of storing energy by converting chemical reactions to electrical energy, thus transporting electrons from the negative to the positive electrode during charging or discharging [67]. There are 2 main types of batteries, the first being primary batteries which are non-rechargeable and the second being secondary batteries which are rechargeable by applying a reverse current to the battery [67].

A battery usually contains an electrochemical cell which has materials for the anode and cathode, with oxidization or reduction occurring at the anode or cathode [67]. The electrochemical cell also contains an electrolyte which is a chemical solution where the anode and cathode are immersed, the solution allows for the exchange of electrons between the anode

and cathode, therefore allowing for the chemical reaction to occur, thus creating electricity [67].

The main power characteristics of a battery along with their respective definitions are as follows [67]:

- Quantity of energy: Is the energy storage capacity produced by the electrochemical reaction which is measured in Wh and is the product of the output voltage and the maximum deliverable current of the battery.
- Maximum deliverable current: Is the amount of A that a battery can supply to the load.
- Internal resistance: Is the internal resistance of the battery that is generated by the composition and physical conditions of the battery electrolyte, the electrodes and contact with the current collector or electrolyte interface.
- Discharge depth: Is the percentage of the total battery capacity used in a discharge process.
- Lifespan: Is the number of charge-discharge cycles without noticeably negative effects on the operation of the battery.
- Self-discharge parameter: Is the energy stored in the battery that is self-discharged.

Different battery types contain different materials or elements that produce the electrochemical processes within the battery [67]. Different battery types along with their specific power characteristics are listed in Table 3.

A lead acid (Pb-Ac) battery is composed of a lead dioxide anode and a matrix or sponge lead at the cathode, while the electrolyte can either be a liquid such as sulfuric acid or a paste with a pressure regulated valve [67]. The advantages, disadvantages, and applications of a lead acid battery are as follows [67]:

- Advantages: A lead acid battery is low cost, can tolerate intensive use, contains highly studied technology, while also being high voltage per cell (2 V), has high efficiency (50 - 92 %), and is recyclable.
- Disadvantages: High weight due to the lead resulting in low power density (30 to 40 Wh/kg), has considerably large self-discharge rate (> 20 %/month), small number of lifecycles (500 to 800 cycles), and does not allow fast charging.

- Applications: Uninterruptible Power Supply Systems (UPS), power management, grid stabilization, and starting systems (automobiles).

Table 3. Comparison of power characteristics of different battery types [67].

Parameter / Technology	Pb-Ac	Ni-Cd	Ni-MH	Li-ion	Li-Po
Cell voltage (V * cell)	2 V	1.2 V	1.2 V	3.3 V	3.7 V
Self-discharge (% / month)	> 20%	10%	30%	8%	5%
Lifecycles	500-800	1500-2000	300-500	2000 V	> 1000
Life time (years)	5 – 15	10–20	10–15	2 – 5	2 – 7
Specific energy (Wh / Kg)	30-40	40-60	30-80	100-250	130-200
Efficiency	50%-92%	70%-90%	66%	80%-95%	90%-95%
Overload tolerance	-	V. Good	Good	V. Bad	V. Bad
Impact robustness	Good	V. Good	Good	V. Bad	V. Bad
High temperature work	Mean	V. Good	Mean	V. Bad	V. Bad

A Nickel-Cadmium (Ni-Cd) battery is composed of a cadmium anode and a nickel hydroxide cathode, while the electrolyte is composed of potassium hydroxide. The advantages, disadvantages, and applications of a Ni-Cd battery are as follows [67]:

- Advantages: Contains well studied technology, has good behaviour at different environmental temperatures, has a large number of lifecycles (1500 - 2000), has small internal resistance, while also being higher in power density (40 - 60 Wh/kg).
- Disadvantages: Is an expensive technology, deprecated by the use of other types of batteries, has considerably large self-discharge rate (10 % monthly), and is low voltage per cell (1.2 V).
- Applications: Backup and energy storage, portable devices, and energy management.

A Nickel-Metal Hydride (Ni-MH) battery is composed of a nickel hydroxide anode and a metal hydride cathode, it is a modification or improvement of the nickel-cadmium battery [67]. The advantages, disadvantages, and applications of a Ni-MH battery are as follows [67]:

- Advantages: Contain all the advantages of Ni-Cd batteries plus, they have a higher energy density (30 - 80 Wh/kg).
- Disadvantages: Has high self-discharge rate (30 % / month), is low voltage per cell (1.2 V), has lifecycles of 300 - 500 charges, and has a longer charge time than Ni-Cd batteries.
- Applications: Backup, energy storage and energy management.

Lithium ion (Li-Ion) batteries contain lithium in both electrodes with graphite in the cathode and lithium in the anode [67]. The most common type of Li-Ion batteries are lithium-cobalt oxide, lithium-cobalt phosphate and lithium manganese oxide [67]. The chemical process is based on the insertion-disinsertion of lithium ions [67]. The advantages, disadvantages, and applications of a Li-Ion battery are as follows [67]:

- Advantages: Has high energy density (100 - 250 Wh/kg), has low self-discharge rate (8 %/month), contains high voltage per cell (3.3V - 4.0V), and has a long lifespan (2 - 5 years).
- Disadvantages: Requires a charging circuit, has a lifespan of 2 - 5 years regardless of being used, has rapid degradation of the electrodes if it is completely discharged, can be susceptible to high temperatures, and it expensive in comparison with other technologies such as Pb-Ac.
- Applications: Portable devices (e.g. IoT sensors), electric vehicles, and renewable energy systems.

Lithium polymer (Li-Po) batteries are a modification of traditional Li-Ion batteries by containing a solid polymer electrolyte, allowing for the creation of smaller batteries [67]. The advantages, disadvantages, and applications of a Li-Po battery are as follows [67]:

- Advantages: Contains high power density (130 - 200 Wh/kg). has reduced volume and weight compared to Li-Ion batteries, and low self-discharge rate (5 %/month).
- Disadvantages: It is expensive, it can have a higher internal resistance when compare with Li-Ion, can be punctured easy, and it requires charge control.
- Applications: Portable devices (e.g. IoT sensors).

When creating wireless IoT sensors that are portable, large consideration must be put towards battery capacity and size. It is evident from Table 3 that the battery chemistries with the best Wh/kg are Li-Ion and Li-Po batteries, it is for this reason that they are the best options when paired with portable IoT sensors, however when comparing both technologies even closer it appears that the traditional Li-Ion battery is overall preferred due to it being more cost efficient and less prone to puncture.

2.2.2.2 Battery Recharge/Replacement Burden

Table 4 contains the estimated current consumption of 4 differing wireless IoT sensor node configurations using the components outlined above. It can be seen from Table 4 that the best-case scenario includes a sensor node which consumes approximately 36 mA, while the worst-case scenario includes a sensor node which consumes 169 mA.

Now considering the last component of a wireless IoT sensor node, which is the battery, it can be determined approximately after how many hours each sensor node would need to be charged. For a wireless IoT sensor node it can be concluded that lithium-ion batteries are the most suitable option due to reasons aforementioned.

Table 4. Estimated current requirements and battery life of different wireless IoT sensor node configuration.

Configuration	**Estimated Current Consumption (mA)**	**Estimated Battery Life (hours) (1,000 mAh)**
Grasshopper + LP3	36 mA	27.8
Grasshopper + SCD30	54 mA	18.5
ESP32 + LP3	151 mA	6.6
ESP32 + SCD30	169 mA	5.9

Choosing a 1,000 mAh battery for the sake of comparison, the estimated battery life of each sensor node is now contained in Table 4. It can be seen from Table 4 that estimated battery life various from 27.8 - 5.9 hours, thus highlighting that a battery recharge/replacement burden

does indeed exist and how the severity of the aforementioned burden can be reduced with optimised technologies.

It should be noted that while the battery recharge/replacement burden may be able to be reduced via changing components contained within the wireless IoT sensor node, further improvements would need to be investigated in order to optimise component current consumption further and remove the aforementioned burden completely.

2.3 Energy Harvesting

With the ever-increasing demand for wireless sensor nodes on the rise, several issues have arisen with regards to IoT technology, one of such issues is with regards to the maintenance that is required to replace and recharge sensor node batteries producing a cumbersome and more costly to implement solution. There has been, in recent years, considerable interest in the development of systems capable of extracting useful electrical energy from existing environmental sources for WSNs, due to the relatively slow improvements in battery technology and power requirements of such sensor nodes [68]. Such environmental sources may include, electromagnetic radiation, thermal gradients, vibration and other forms of motion [68].

Electromagnetic radiation contains regions on the spectrum where ambient energy is very high and regions where it is much lower [68]. Photovoltaic (PV) systems convert visible light (typically sunlight) into electrical power, such systems are well established and provide relatively high efficiency (approx. 15 %) over a range of wavelengths [68], these systems also are cost effective and provide voltage and current levels that are close to those required for sensor nodes [68]. The harvestable electrical power available from PV systems over a 24 h period is approximately 2 W/m^2 outdoors, in temperate locations with high dependency on clear weather and direct sunlight, while harvesting indoors can typically provide 0.15 W/m^2 of electrical energy [68].

Radio signals can be used to power passive electronic devices such as radio frequency identification (RFID) tags, however the radio signals require careful tuning, require large antennas to harvest useable power, and are only typically capable of transmitting power over a distance of a few metres [68].

Sources of mechanical energy can be grouped in 3 categories, those dependent on motion which is always constant, such as fluid-flow used in turbines, those dependent on intermittent motion such as piezoelectric sensors in a football, and those dependent on vibrations [68]. Steady state mechanical sources such as wind and water flow can be harvested via using natural channels, pipes, or a rotating shaft [68]. Wind turbines and hydroelectricity plants are just a few examples of systems which utilize steady state mechanical sources for electrical power generation. Intermittent mechanical sources are sources in which motion can be cyclic, however the energy is only available for part of the cycle [68]. Some examples of intermittent mechanical sources include, vehicles driving over an energy harvesting plate and intermittent human activity (e.g. walking/typing) [68]. Starner (1996) [69] investigated the potential energy available from harvesting using intermittent mechanical sources. Starner concluded that the potential harvestable energy ranged from 7 mW to 67 W with finger typing and lower limb movement respectively. Vibration energy is available in most built environments with the energy extracted from a vibration source being dependent on the amplitude of the vibration and its frequency [68]. An example of a vibrational mechanical source would be a domestic freezer which has shown to have a fundamental frequency of 50 Hz with an acceleration amplitude of 0.1 m/s^2 in [68]. Piezo electric material exhibit the characteristic that if they are mechanically strained they generate an electricity field proportional to the strain [68], this therefore allows them to harvest energy from intermittent and vibrational mechanical sources.

Harvesting thermal energy from a thermal source requires a thermal gradient, typically leading to greater temperature differences resulting in greater energy conversion efficiency [68]. Thermoelectrics is a potential method of harvesting thermal energy and converting it into electricity when a temperature gradient is present [70]. An example of a potential heat source is a room heater, with a typically domestic hot water radiator typically delivering approximately 1.4 kW/m^2 when heated to 50 °C, therefore only a small section of the radiator would be required to harvest useable energy [68]. Another example of a heat source is the human body, however small differences between the temperature of the human body and the ambient environment results in only 6.4 W of harvestable power from the entire human body, this fact along with the facts that harvesting energy from a human's body will typically only take place on part of the body as well as the temperature of the harvested area will reduce as a result, also reducing harvestable power further, leads to the conclusion that minimal power can be harvested from the human body [68], with Starner (1996) [69] concluding that potential

harvestable energy from a device covering the human neck could only potentially deliver 0.2 - 0.32 W.

2.3.1 Thermoelectrics

2.3.1.1 Seebeck Effect – Thermoelectric Energy Harvesting

Thermoelectrics is the process of harvesting energy through the use of the Seebeck effect, The Seebeck effect was discovered by Thomas J. Seebeck in 1821, he discovered that electricity could be generated by a circuit made from two dissimilar wires when one of the junctions was heated, creating a temperature difference [Figure 2] [70]. The voltage generated is proportional to the temperature difference at both junctions, as shown in Equation 1 [70], where α is known as the Seebeck coefficient and ΔT is the temperature delta from both junctions.

$$V = \alpha \Delta T \tag{1}$$

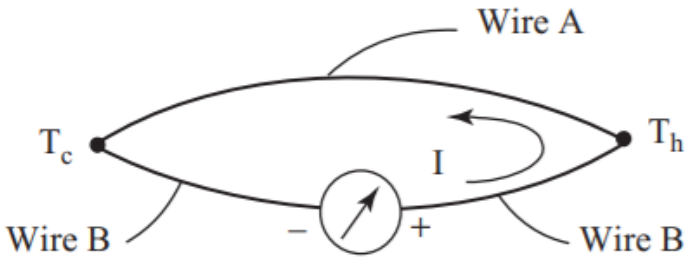

Figure 2. Seebeck effect - current generation from temperature difference [70].

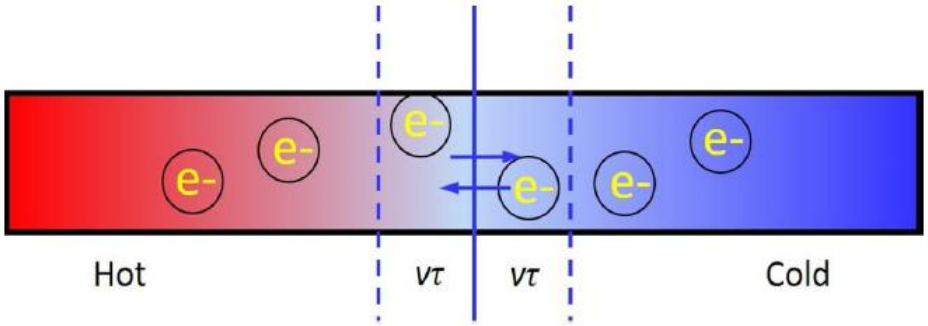

Figure 3. Seebeck effect - electron transfer from hot- to cold-side [71].

Figure 3 shows in more detail the electron transfer when a TEG is implemented, and a temperature difference is present. Electrons and holes are free to move and carry charge,

however when a temperature gradient is present along the hot and cold-side faces, they move from the hot-side to the cold-side. It is this build-up of charged carriers that results in power generation and output [71].

2.3.1.2 Peltier and Thomson Effect

The Peltier effect of thermoelectrics is coupled with thermoelectric refrigeration and states that when current flows across a junction between two different wires, it is found that heat must be continuously added or subtracted at the junction in order to keep its temperature constant as depicted in Figure 4 [70]. This heat is proportional to the current flow and changes sign when the current is reversed [70].

The Thomson effect is similar to the Peltier effect and states that when current flows in a wire with a temperature gradient, heat is absorbed or liberated across the wire depending on the material and the direction of the current [70]. The Thomson heat is proportional to both the electric current and the temperature gradient [70].

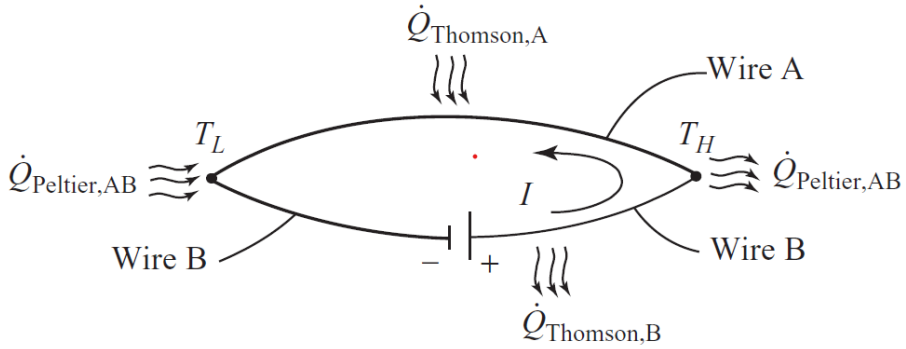

Figure 4. Peltier and Thomson effect - current supplied producing temperature difference [70].

2.3.1.3 Thermoelectric Characteristics

Thermoelectrics has been widely researched in the literature for its ability to harvest energy from thermal based sources and convert it into electricity. Thermoelectrics relies on the principles of the Seebeck effect to generate electricity while the Peltier effect is relied upon for thermoelectric refrigeration [70]. TEGs have a long lifecycle due to their stationary parts and solid-state structure making them highly reliable, they typically have low efficiency of 5 - 6%,

therefore researchers are mostly focused on increasing efficiencies and not enough research is contributed to engineering and improving applications that can be best utilized by thermoelectrics in its current state.

TEGs harvest thermal energy by utilizing thermoelectric modules that consist of p and n-type semiconductor elements connected electrically in series and thermally in parallel sandwiched between two high thermally conductive but low electrically conductive ceramic plates, these plates are often referred to as the cold-side for the lower temperature plate and hot-side for the higher temperature plate [Figure 5] [70]. When the temperature of one side is hotter than the other, heat is transferred through the module and an electrical current is generated [70]. Once a resistive load is attached electricity can flow and power devices such as IoT sensor technology.

The figure of merit, Z, shown in Equation 2, assesses a material's thermoelectric capabilities for both energy harvesting and refrigeration by taking into account the materials Seebeck coefficient, thermal conductivity and electrical resistivity, where α is the Seebeck coefficient, ρ is the electrical resistivity, and k is the thermal conductivity [70].

$$Z = \frac{\alpha^2}{\rho k} \tag{2}$$

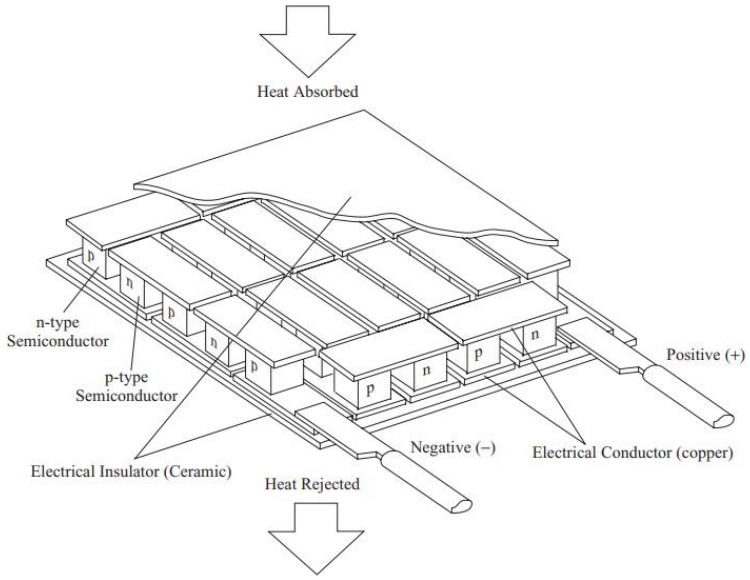

Figure 5. Thermoelectric module schematic [70].

The maximum conversion efficiency of a TEG can be represented by Equation 3 [70], where T_c and T_h are the cold and hot-side temperatures respectively, $\bar{T}$ is the average of the aforementioned temperatures, and η_c is the Carnot cycle thermal efficiency that can be calculated using Equation 4.

$$\eta_{mc} = \eta_c \frac{(1+Z\bar{T})^{\frac{1}{2}}-1}{(1+Z\bar{T})^{\frac{1}{2}}+\frac{T_c}{T_h}} \tag{3}$$

$$\eta_c = 1 - \frac{T_c}{T_h} \tag{4}$$

2.3.1.4 Power Characteristics

When it comes to thermoelectric modules and how they work when harvesting manufacturing waste heat, 4 power characteristics are important to outline. The first being open-circuit voltage which is the maximum voltage available from the thermoelectric module at any one time while current is equal to 0, while short-circuit current is the maximum current that is available while voltage is equal to 0 [72].

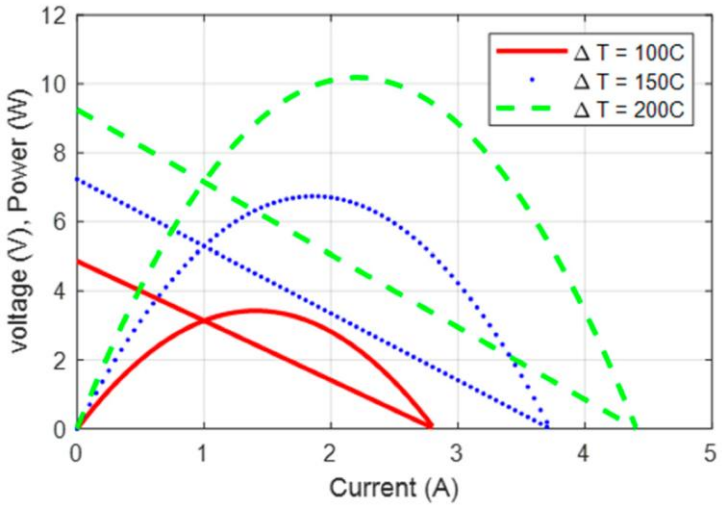

Figure 6. Power characteristics of thermoelectric module [72].

Figure 6 depicts the power characteristics of a thermoelectric moule, it can be seen that the power vs current curve is typically an inverse quadratic relationship, while the voltage vs current is linear, the maximum power output therefore occurs at 50% open-circuit voltage for thermoelectric modules as this is where the product of voltage and current produces the most

power [72]. Maximum Power Point Tracking (MPPT) is also important to outline. MPPT is the process by which an energy harvesting boards optimizes the power harvested from thermoelectric modules by ensuring 50% open-circuit voltage is present at all times using a boost converter [72]. MPPT increases the efficiency of TEG's by ensuring maximum power is being harvested, something which could be essential in applying TEG's to manufacturing waste heat processes which do not release substantial amounts of heat.

2.4 Manufacturing Waste Heat

The ever-increasing price of fossil fuels has motivated the manufacturing industry to see waste heat as more than just a by-product of manufacturing processes. Waste heat is readily available and created in many processes such as brewing in a brewery, steelworks and silicone casting. Manufacturers are looking towards new innovative ways of harvesting waste heat before it is lost forever, such as by using thermoelectrics. Thermoelectrics can convert waste heat into electricity, something that manufacturers can utilize to power IoT sensor networks or other machinery such as actuators/fans.

Waste heat potential was discovered by Cook (1971) who determined that approximately 50% of the US energy consumption was lost as waste heat [73]. This highlighted the need to research and understand the potentials surrounding waste heat. Today manufacturing waste heat accounts for approximately 10-50% of total sector fuel consumption depending on the particular manufacturing sector [74], this truly highlights the need for implementing energy harvesting technologies to recapture the waste heat before it is lost forever.

2.4.1 Benefits of Waste Heat Harvesting

The benefits of harvesting waste heat are as follows:

- Provide electricity, steam, space heating, and hot water.
- Recycle energy to use in other processes.
- Reduce the impact on the environment.
- Increase manufacturing efficiency and reduce manufacturing costs.

2.4.2 Managing Waste Heat

Unlike the general waste management principle of ‘‘Reduce, Recycle and Reuse”, waste heat management should follow the principle of ‘‘Reduce, Recycle, and Recover” as shown in Figure 7 [74].

Firstly, in order to manage waste heat, we must minimize it by improving the efficiencies of manufacturing processes, secondly, we must recycle the waste heat within the manufacturing processes, lastly, we must recover the waste heat to generate electricity, create steam etc.

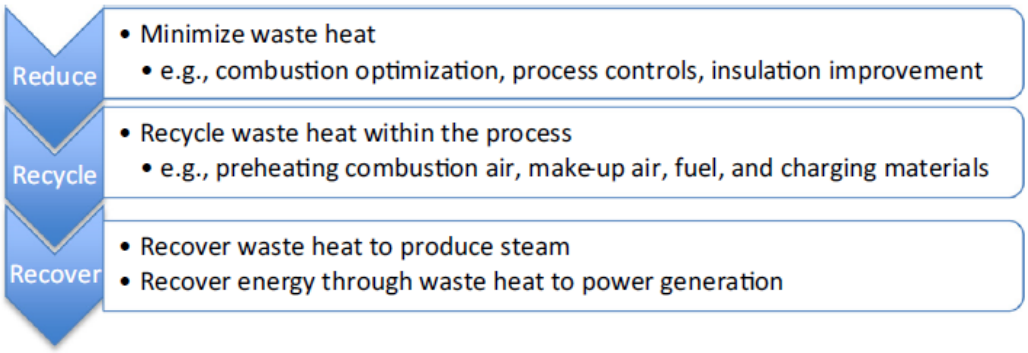

Figure 7. Managing waste heat [74].

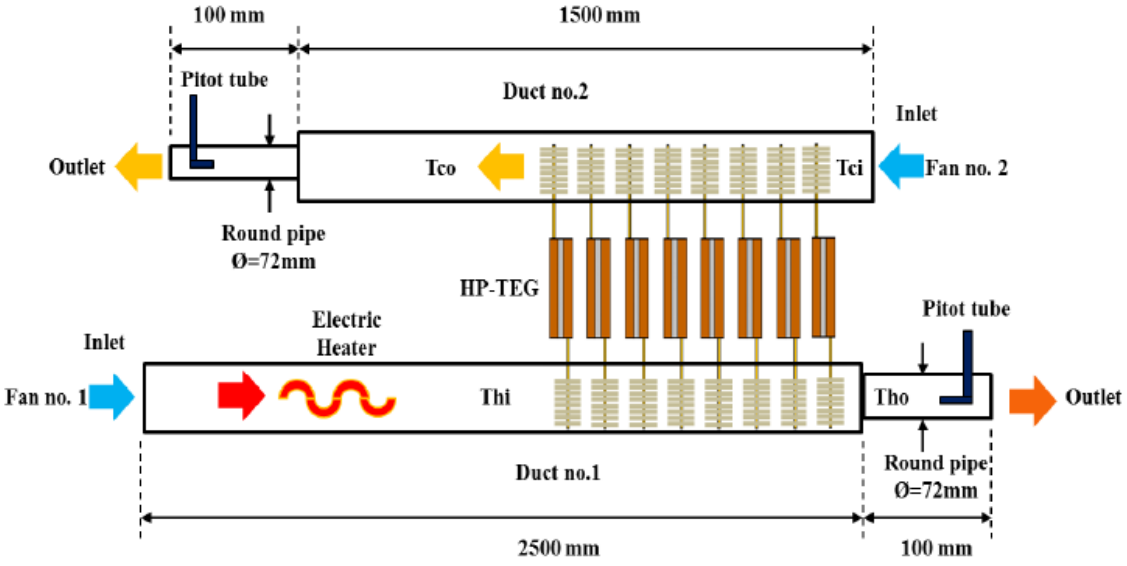

Figure 8. Heat-pipe TEG for crossflow application [75].

Thermoelectrics can manage waste heat by recycling and/or recovering it. A TEG can be implemented similar to Figure 8, where electricity can be generated, and waste heat recycled into another process, when a temperature difference is present across 2 manufacturing process ducts.

2.5 Thermoelectric Generator Systems

2.5.1 Steelworks

Kuroki et al. (2014) [76] explored the potential for manufacturing waste heat recovery via the use of thermoelectrics and steelworks by verifying the pre-existing TEG installed within JFE steel corporation's steel casting line, as depicted in Figure 9. The verification of the system was required to ensure the system was producing optimal power output and therefore performing as expected. The verification provides an indication of the W/m^2 achievable for the ΔT range of the JFE system. The TEG system harvested waste heat from the molten steel products and was suspended 2 m above the casting carousel as shown. The cross-sectional harvesting area of the system was 2 m x 4 m, or 8 m^2.

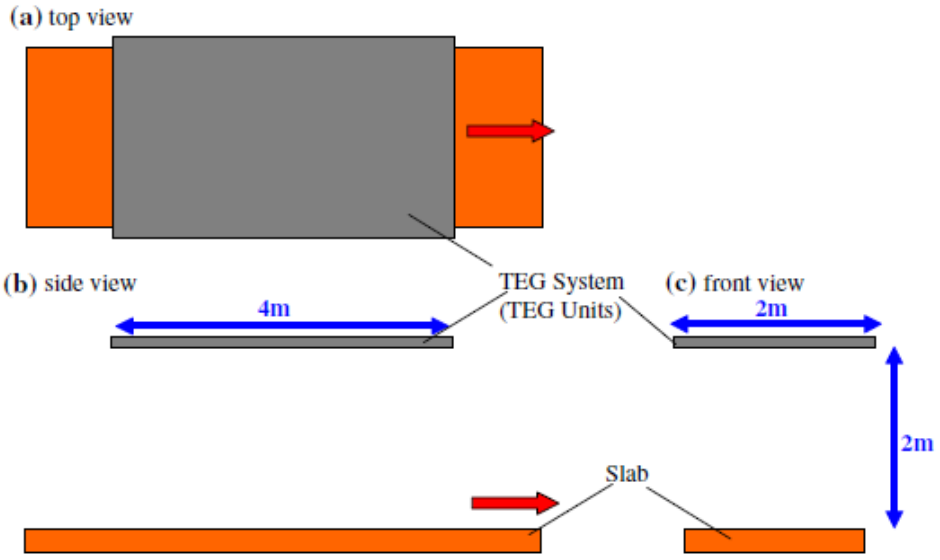

Figure 9. Steelworks TEG [76].

The maximum experimental output achieved from the JFE system was approximately 9 kW with a slab width of 1.7 m and temperature of 1,188 K or thermoelectric hot-side module temperature of approximately 480 K, therefore the thermoelectric modules were operating

below their 553 K threshold, indicating that more power output may be able to be achieved with higher slab temperatures or reduced TEG suspension distance.

This system truly highlights the huge potential for power generation within manufacturing processes due to the impressive harvestable power of 9 kW.

2.5.2 Silicon Casting

Borset et al. (2017) [77] explored the potential for industrial waste heat recovery via the use of thermoelectrics and silicon casting, providing an indication of the W/m^2 achievable for the ΔT range of the system. The TEG system was developed, as depicted in Figure 10, and implemented within a silicone casting factory. The system harvested waste heat from molten casted silicon and was fixed to the shielding wall as shown. The effective harvesting cross-sectional area was equivalent to 0.5 x 0.5 m or 0.25 m^2.

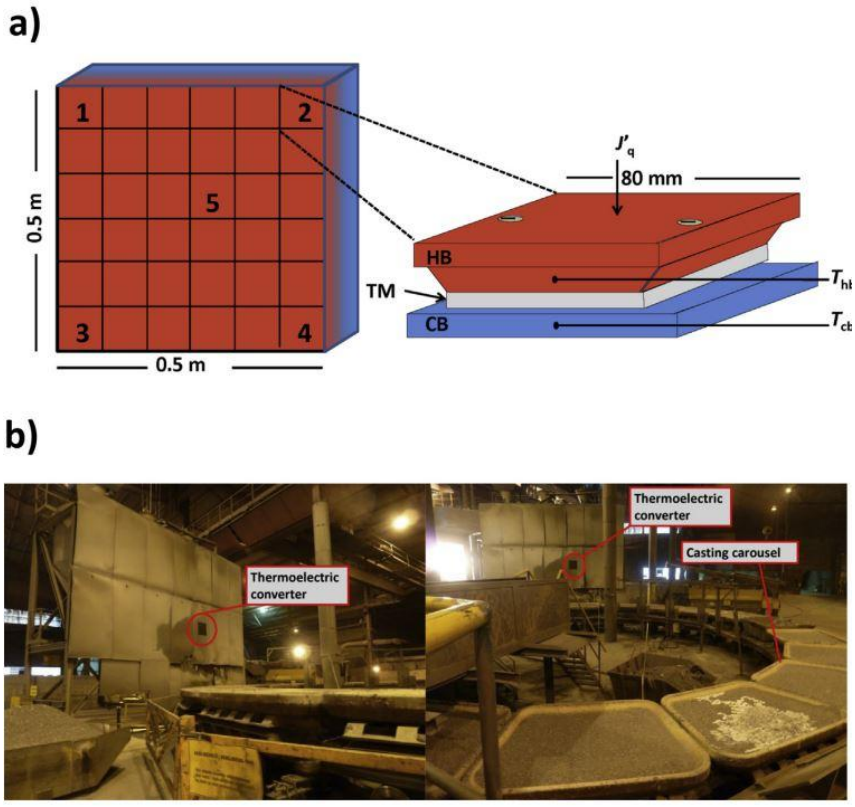

Figure 10. Silicon casting TEG [77].

Borset et al. (2017) determined the maximum experimental power output to be 40.5 W for a temperature difference of 100 K. It was determined that an increase in power generation can be achieved if cooling efficiency and radiated properties are increased.

The system developed by Borset et al. (2017) [77] highlights the possibility to harvest radiated waste heat via thermoelectric.

2.5.3 Air Duct

Remeli (2015) [75] developed a viable heat pipe TEG (HP-TEG) system to explore the potential of manufacturing waste heat recovery via the use of thermoelectrics and heat pipes. The system consisted of thermoelectric modules sandwiched between two heat pipe heatsinks as depicted in Figure 11.

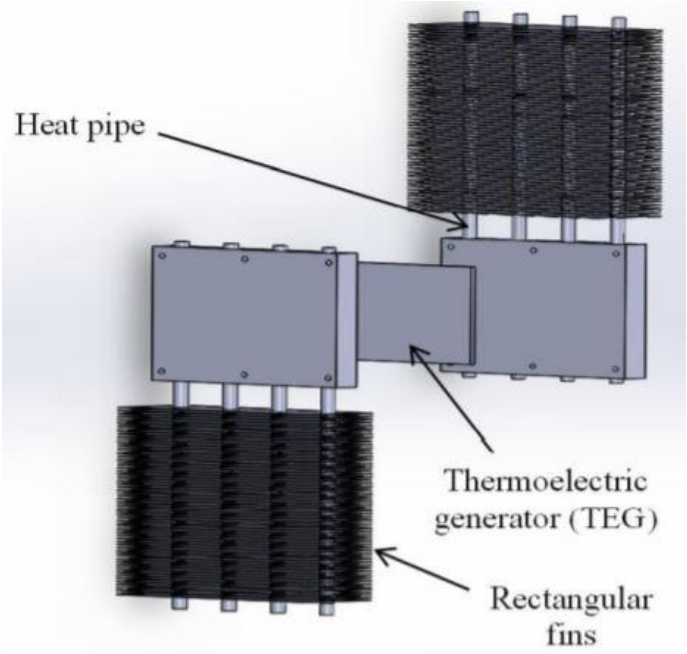

Figure 11. Heat-pipe TEG [75].

The TEG was placed in a U duct, as depicted in Figure 12. Heat-pipe TEG schematic [75]., and contained 8 HP-TEG units, with effective cross sectional harvesting area of 8 x 0.12 x 0.12 m or 0.115 m^2, placed in series to provide increased power generation and waste heat recovery. Remeli (2015) determined the maximum experimental heat transfer rate was 1079 W when air face velocity was ≈ 1.1 m/s. Heat transfer rate could be increased if air velocity is further decreased, however this led to operating temperatures above thermoelectric module thresholds.

The maximum power generated from the experimental system was ≈ 7 W at an air face velocity of ≈ 1.1 m/s.

The experimental system was then tested within a crossflow application, as depicted in Figure 8, to accurately resemble an industrial waste heat application where hot and cold air are normally separated, thus analysing waste heat recyclability. The maximum heat transfer rate of the HP-TEG system was 900 W. The maximum power generated from the system was ≈ 4.4 W at cold-side air face velocity of ≈ 1.8 m/s. The crossflow system provided less power generation due to less heat transfer rate resulting from experimental setup, therefore power generation can be increased with further experimental improvements.

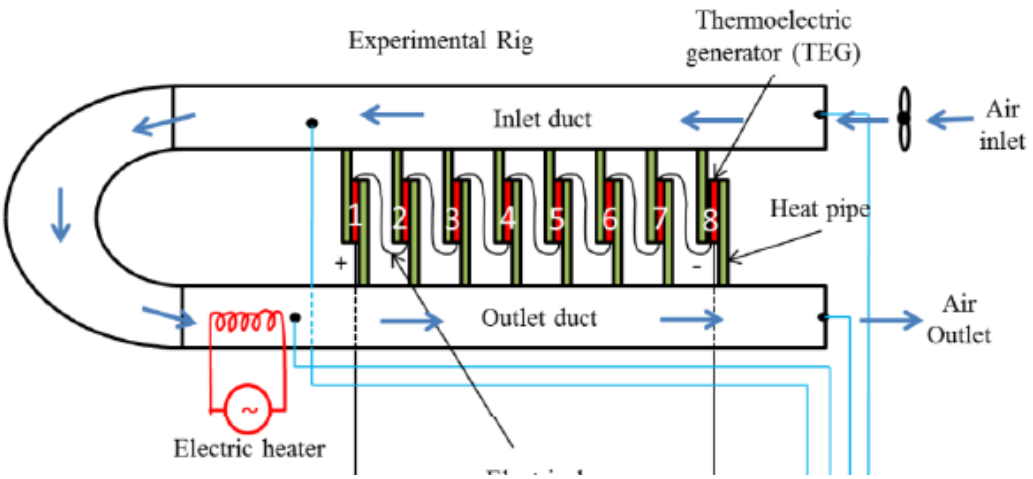

Figure 12. Heat-pipe TEG schematic [75].

The power required to power the system fans was recorded to be less than 1.6 W, therefore the HP-TEG system can be completely passive as the power generated from the system is uniformly larger than the fan power.

This system firstly demonstrates the effectiveness of heat-pipes within a TEG and secondly demonstrates that a TEG can be a viable method of recycling waste heat into other manufacturing processes.

2.5.4 Carburizing Furnace

Kaibe et al. (2012) [78] field tested the TEG system that was installed above a carburizing furnace, as depicted in Figure 13, to harvest waste heat from the exhaust flame. The exhaust flame was directly below the hot-side face of the TEG and allowed for a hot-side temperate of up to 280 °C, while the cold-side temperature was consistent at 30 °C using water cooling. The TEG was able to generate 214 W with a cross-sectional area equivalent to 0.12 m^2, which equals 1783 w/m^2. This highlights the effectiveness of implementing a TEG using an open flame as a heat source.

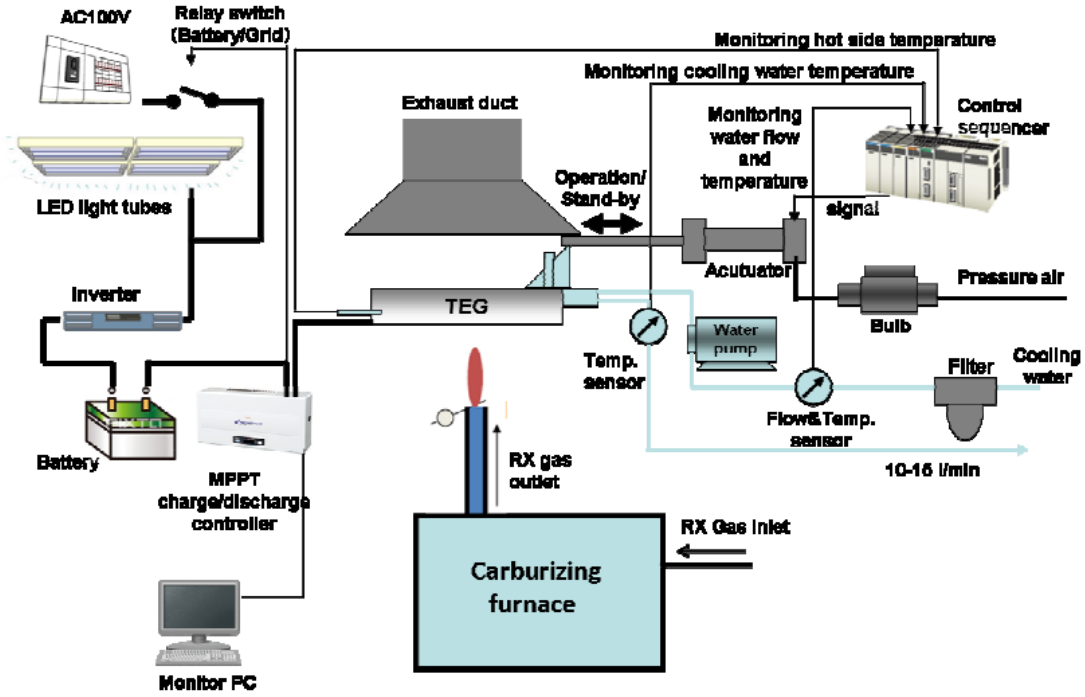

Figure 13. Carburizing furnace TEG [78].

The TEG was used to power LED lights inside the factory by direct power and via charging batteries connected to the system with 180 W being directed to battery charging.

The field-tested system highlights the effectiveness of harvesting waste heat via an open flame manufacturing process and thermoelectrics due to the impressive 1783 w/m^2 achieved.

2.5.5 Combustion Chamber

Aranguren et al. (2015) [79] developed a TEG, as depicted in Figure 14, that utilised the temperature of exhaust gases form a combustion chamber to harvest waste heat. The system was capable of producing 21.56 W with an effective cross-sectional area of 0.25 m^2 which equals 85.04 W/m^2. The system achieves this buy extending the TEG along the length of the exhaust channel and by utilizing both heat fins and heat-pipes.

The application of the system demonstrates the capabilities that thermoelectric energy harvesting has within manufacturing industries that use combustion aa a means for manufacturing, while also demonstrating a system that can easily be scalable.

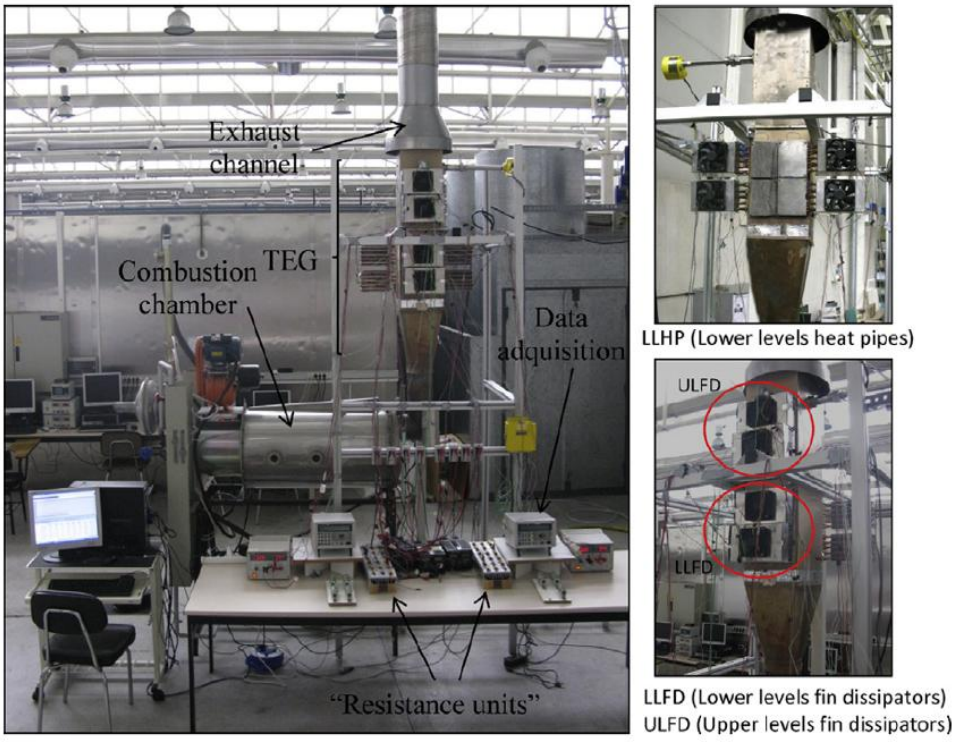

Figure 14. Combustion chamber TEG [79].

2.5.6 Cement Kiln

Mirhosseini at al. (2019) [80] developed a mathematical model of a proposed TEG system for a cement kiln. The system was designed in the shape of an arc to sit around the circular kiln, as depicted in Figure 15. Various parameters of the system were analysed such as, leg length, fill factor, air temperature, and air velocity, to determine optimal power output of the system.

The total power achieved theoretically by the system was equivalent to 453.28 W with a cross-sectional area of 4.28 m^2, which is equivalent to 105.91 W/m^2. The paper highlights the necessity of analysing the system before manufacture using either a mathematical model or FEA software to determine the best possible parameters for maximum power output.

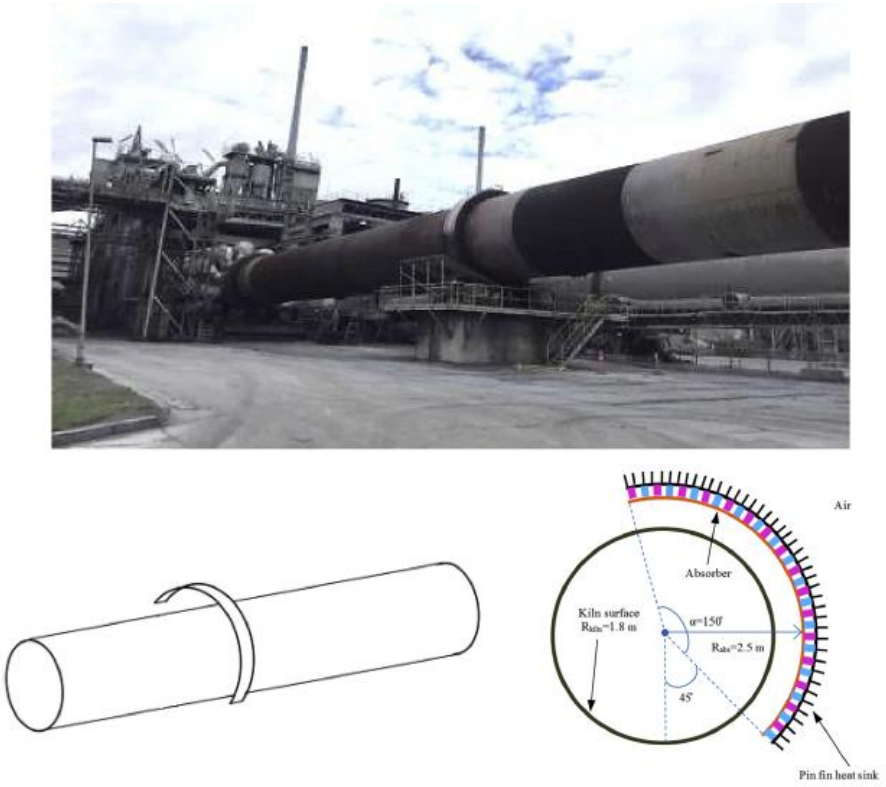

Figure 15. Cement kiln TEG [80].

It is also interesting that the system design implemented some sort of custom cylindrical thermoelectric modules instead of typical off-the-shelf modules, with the latter being the less expensive option for initial implementation.

2.5.7 Turbines

Turbines are widely used in wind power, hydro power, heat engines etc. Their wide availability and excessive waste heat have led to the search for ways to harvest this heat for powering other devices. Thermoelectrics has been researched with the intention of demonstrating feasibility with regards to turbine waste heat energy harvesting for wireless IoT sensors.

Wu et al. (2018) [81] investigated the feasibility of thermoelectrics to harvest waste heat energy from turbines for powering a sensing/monitoring system. The created TEG as depicted in Figure 16, was capable of producing approximately 0.92 W at a hot-side module temperature of 325 °C, which is more than enough to power a few wireless sensors inside the turbine [81]. The energy conversion efficiency of the system, however, was 0.94%, highlighting that future research into thermoelectrics and turbines will most likely increase efficiency and allow more waste heat to be harvested.

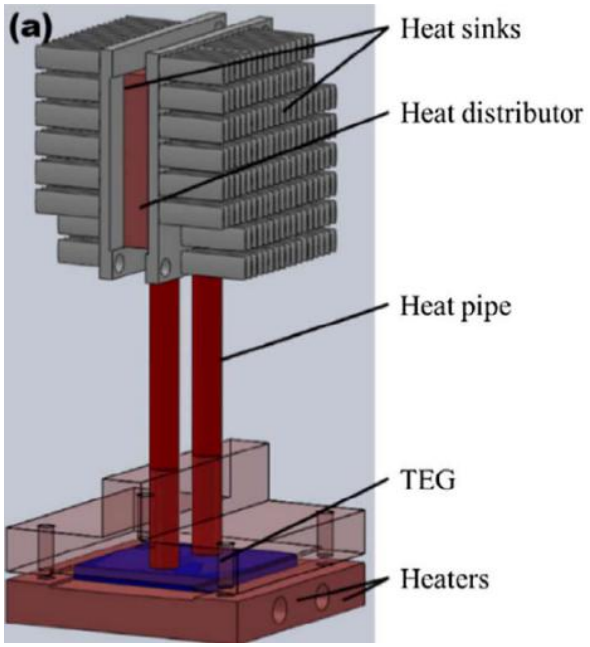

Figure 16. Turbine TEG [81].

2.5.8 Nuclear Power Plants

Nuclear power plants are a consistent safety concern for workers due to nuclear radiation that can severely impact human anatomy if exposed, therefore research into ways of reducing human interactions with radiation via monitoring sensors have been investigated such as by using thermoelectrics to prolong the uptime of wireless sensors. Thermoelectrics can harvest energy from nuclear power plants by using the waste heat from coolant system piping which can then be used to power safety monitoring systems etc.

Chen et al. (2016) [82] investigated the feasibility of thermoelectrics to harvest waste heat energy from nuclear power plants for powering plant safety wireless sensors. The designed

TEG, as depicted in Figure 17, was capable of producing 3.0 W at 340 °C hot-side temperature. The designed electrical components, including the sensors, wireless communication chip, management circuit, and micro-controller, consumed less than 1.0 W during operation, therefore they were entirely powered by the thermoelectric generator. The biggest issue with nuclear power plants is nuclear radiation and its ability to destroy electronics, therefore future research is required to improve the lifecycle of electronic components to further increase feasibility.

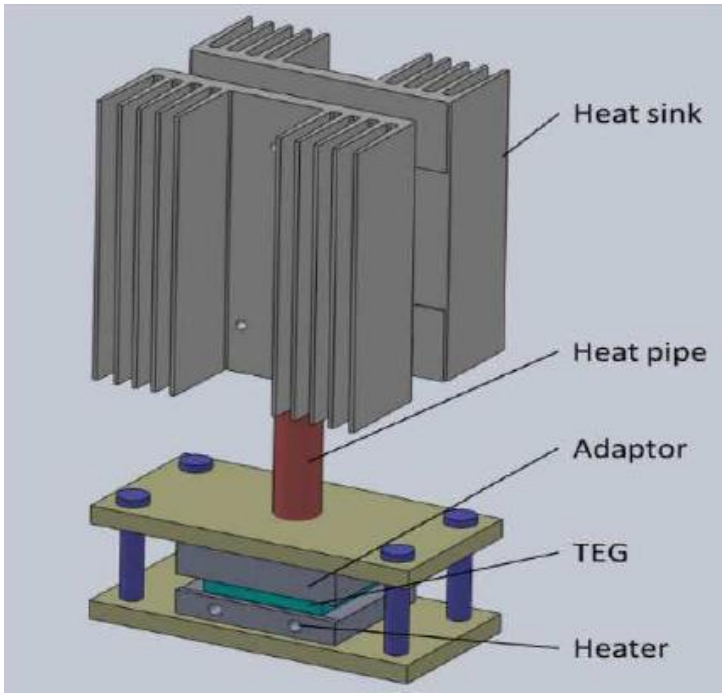

Figure 17. Nuclear power plant TEG [82].

2.5.9 Central Processing Unit (CPU)

Ma and Lui (2007) [83] developed a completely passive CPU cooling system, as depicted in Figure 18, that used liquid gallium metal and a MagnetoFluidDynamic (MFD) pump that was powered by a TEG which utilized the temperature difference between the hot CPU surface and cool surrounding ambient air. The system featured 2 thermoelectric modules stacked vertically with a copper plate in between to double the effective working area. The TEG was capable of producing 100 mW with a temperature delta of 20 ℃ and effective cross-section of 2 x 40 x 40 mm which was adequate to power the MFD pump, thus no other external power inputs were required.

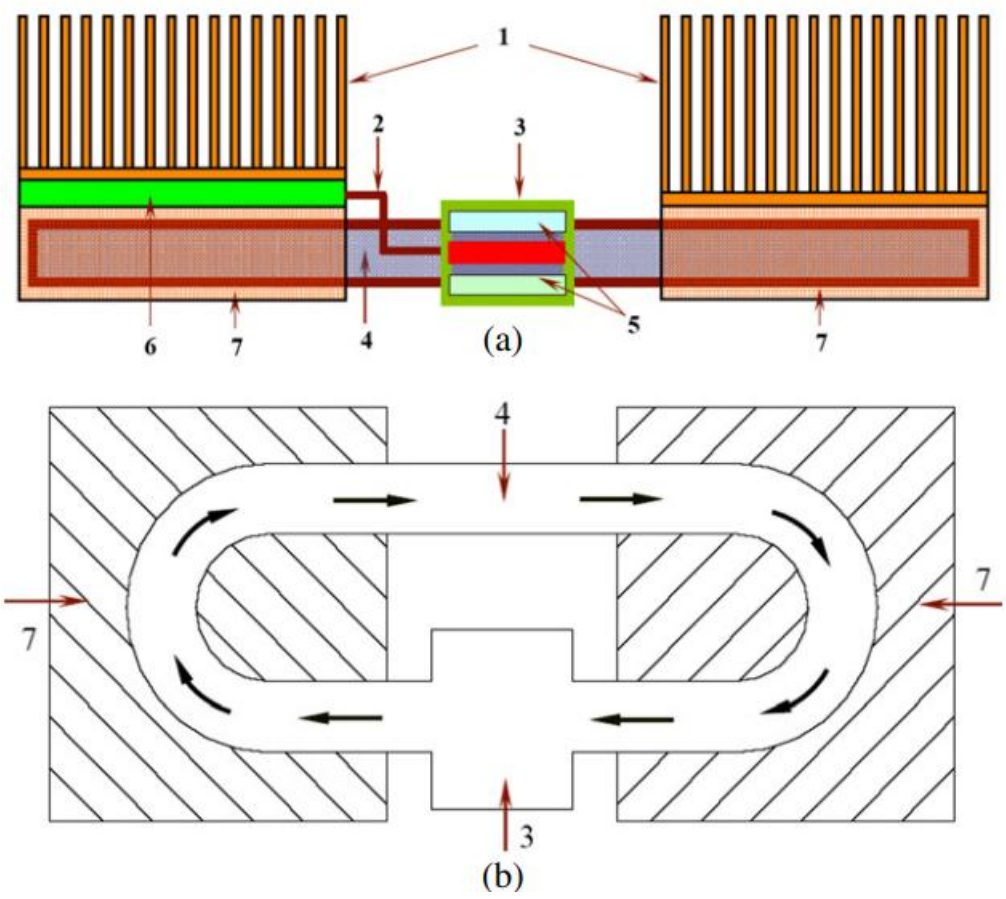

Figure 18. CPU TEG [83].

2.5.10 Steam Pipe

Iezzi et al. (2017) [84] developed a flexible TEG that fit around a steam pipe to generate electricity for a WSN [Figure 19]. The system was capable of producing 308 μW of power at a temperature difference of 127 °C with an effective cross-section of approximately 12 x 150 x 60 mm. The power generated was only sufficient to power a temperature sensing circuit for 10 min after charging for 4 hours, indicating that further improvements are required, however the flexible nature of the TEG demonstrates that any shaped application can be suited to thermoelectrics.

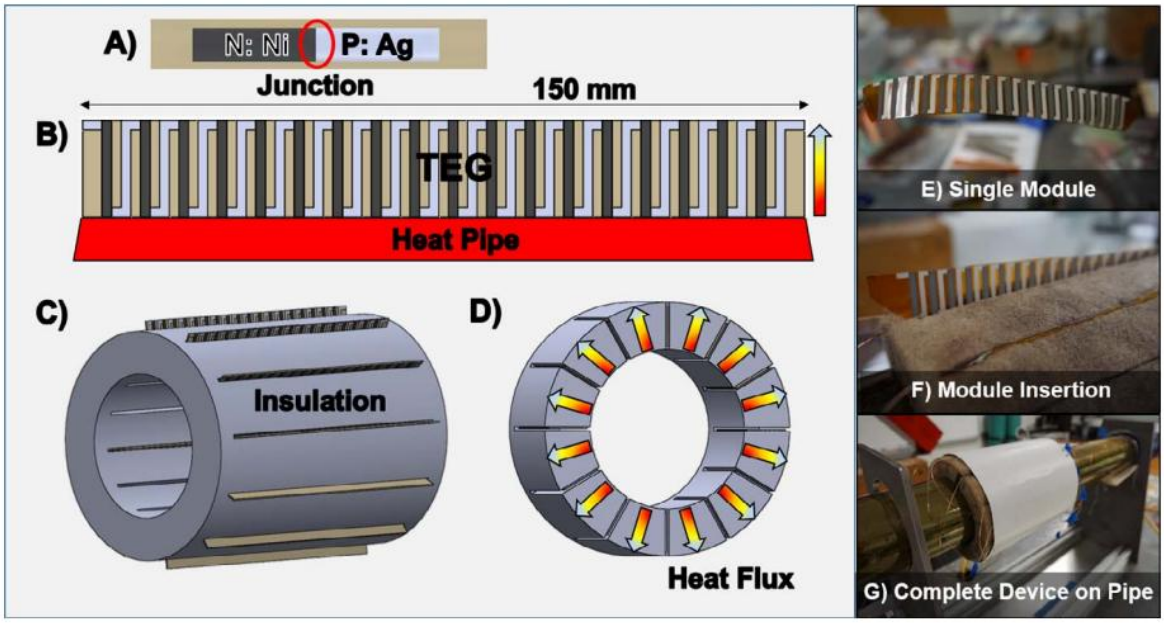

Figure 19. Steam pipe TEG [84].

2.5.11 Heat Exchanger

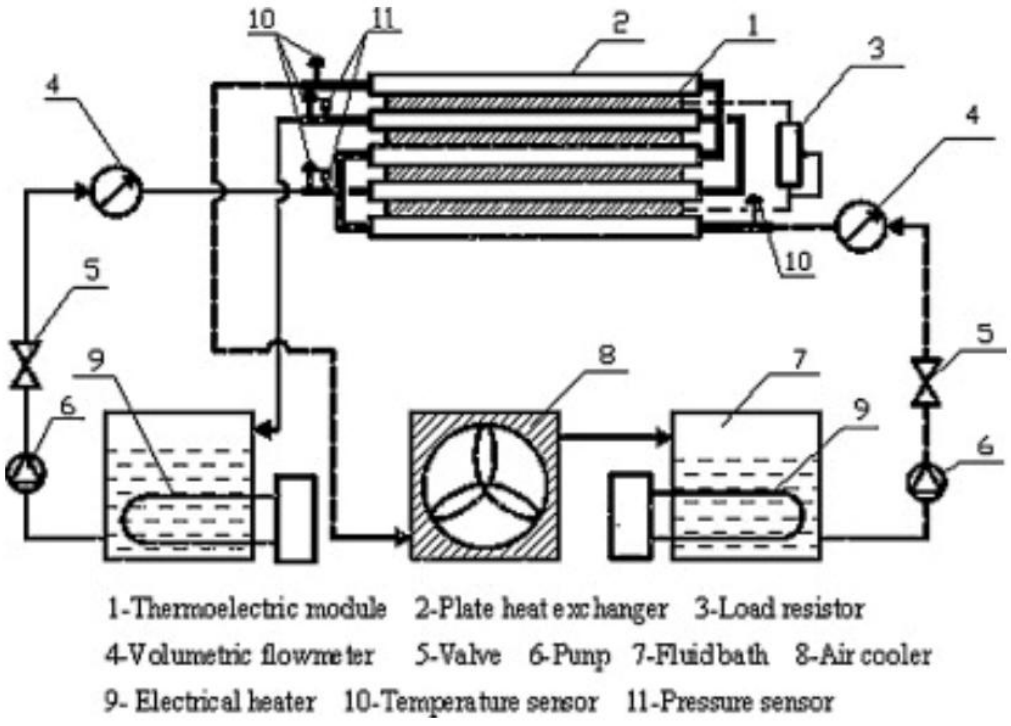

Figure 20. Heat exchanger TEG [85].

Niu et al. (2009) [85] experimentally analysed the potential of a heat exchanger TEG by developing the system in Figure 20 which contained 56 BiTe thermoelectric modules with cross sections of 40 mm × 40 mm, the system allowed for the control of two inlet fluid temperatures which were adjusted to replicate both hot and cold fluids simultaneously to represent applications that can be found in manufacturing processes. The maximum power generated by the system was equivalent to 146.5 W at a hot and cold inlet temperature of 150 ℃ and 30 ℃ respectively, this resulted in a conversion efficiency of 4.44%.

2.5.12 Stove Powered

Almost 3 billion people rely on stoves for cooking, heating, and lighting [86], this has led to research into investigating the feasibility of harvesting waste heat emitted from stoves through the use of thermoelectrics and air/water convection, such as [87–93]. It has been determined that thermoelectrics can feasibly generate electricity from stove waste heat which can then be used to power a fan for an exhaust, a light, a radio, or even charge a mobile phone [86].

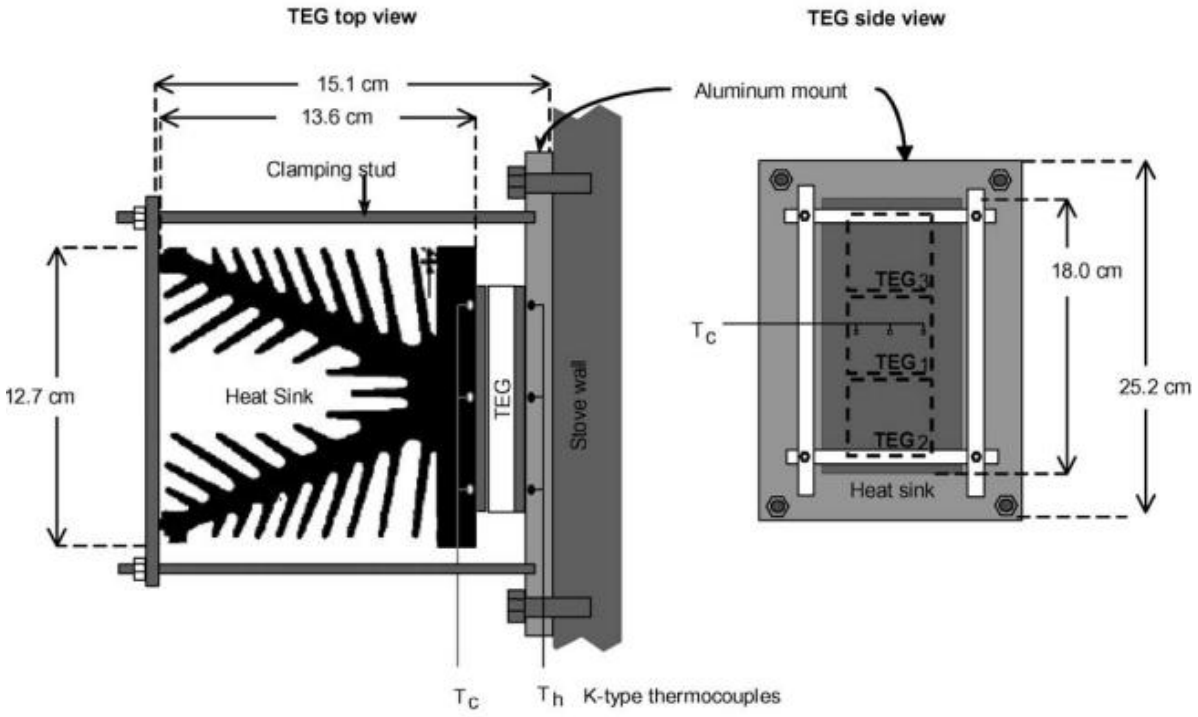

Figure 21. Stove powered TEG [88].

In [87–93] stove powered TEGs, such as that depicted in Figure 21, were investigated to determine their power output. The power density of the aforementioned systems can be seen graphed in Section 2.5.17.

2.5.13 Wearables

Thermoelectrics has been researched with regards to applications in fields outside of manufacturing, such as with creating new wearable devices that can utilize heat generated by the human body in conjunction with surrounding ambient temperatures to harvest energy and generate electricity. The biggest drawback of thermoelectric wearables is their minimal power output due to the relatively small temperature deltas.

The conversion of body heat into electricity using thermoelectrics is useful for self-powered wearable electronics such as medical sensors and smart watches [94]. Kim et al. (2014) [94] researched the feasibility of thermoelectrics to power wearable mobile devices by creating a flexible glass fabric-based TEG, as depicted in Figure 22, that was thin, lightweight, and flexible. The generator achieved a power density of 28 mW g^{-1} at a $\Delta T = 50$ K, this is several tens of times higher than that of previous systems and truly highlights the exponential increase of thermoelectric efficiency resulting from research in recent years.

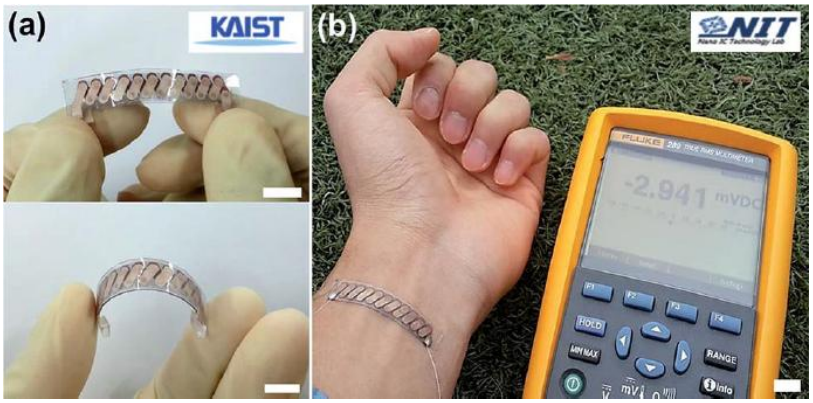

Figure 22. Wearable TEG [94].

Torfs et al. (2007) [95] developed a fully autonomous wearable TEG that resembled a watch, as depicted in Figure 23. The sensor portion of the system measured a person's blood oxygen level and required 89 µW of input power to counteract its average power consumption of 62 µW, however the custom BiTe module. which had an effective cross-section of 38 x 34 mm,

was able to provide more than 100 μW at a 15 °C temperature delta, thus producing a TEG with a sensor system that was fully autonomous.

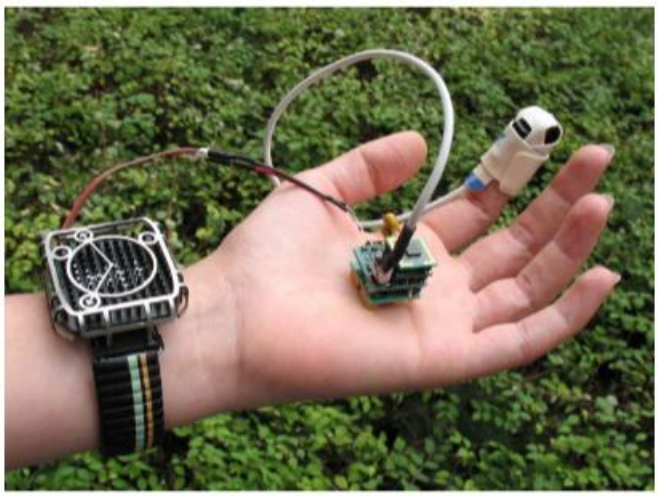

Figure 23. Autonomous wearable TEG [95].

2.5.14 Hydrothermal

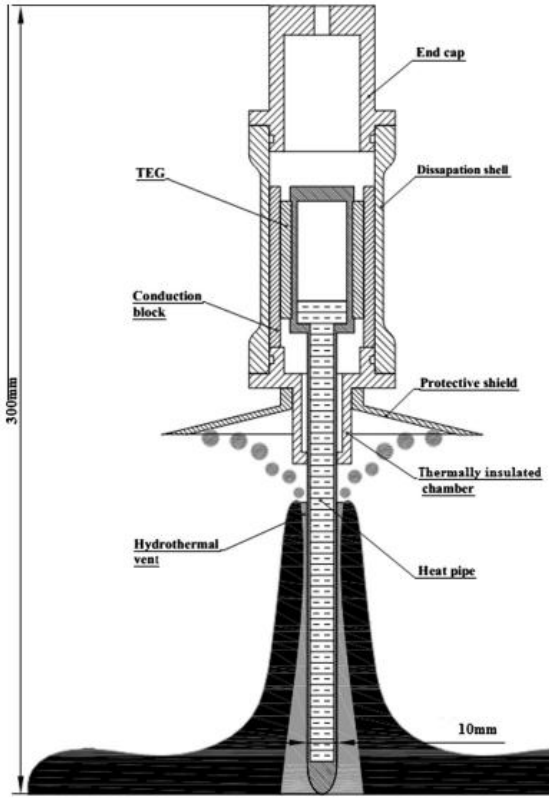

Figure 24. Geothermal TEG [96].

Xie et al. (2016) [96] implemented a TEG within a hydrothermal vent [Figure 24] at 2765 m below the ocean's surface to harvest waste heat from geothermal reactions using thermoelectrics. The TEG consisted of a heat pipe that transferred the heat to 4 modules 20 mm x 40 mm in cross-sectional area. The system generated 3.9 W to power an LED lamp and a data logger with a temperature delta of 127 °C that was present between the heat pipe and the ocean water-cooled dissipation shell.

In reference [97] another geothermal TEG was developed to research the feasibility of thermoelectrics to harvest energy from geothermal anomalies. The developed system is depicted in Figure 25, it contained a hot-side heat exchanger which was connected directly to the borehole and the thermoelectric modules, a cold-side heat exchanger was also created and connected to the modules to provide the temperature delta required to generate electricity. The TEG was capable of producing a maximum power output of 36 W (4.5 W per module), or 286.94 kWh/yr. This represents a substantial amount of energy that demonstrates thermoelectric's feasibility as a technology that may provide larger renewable energy installations.

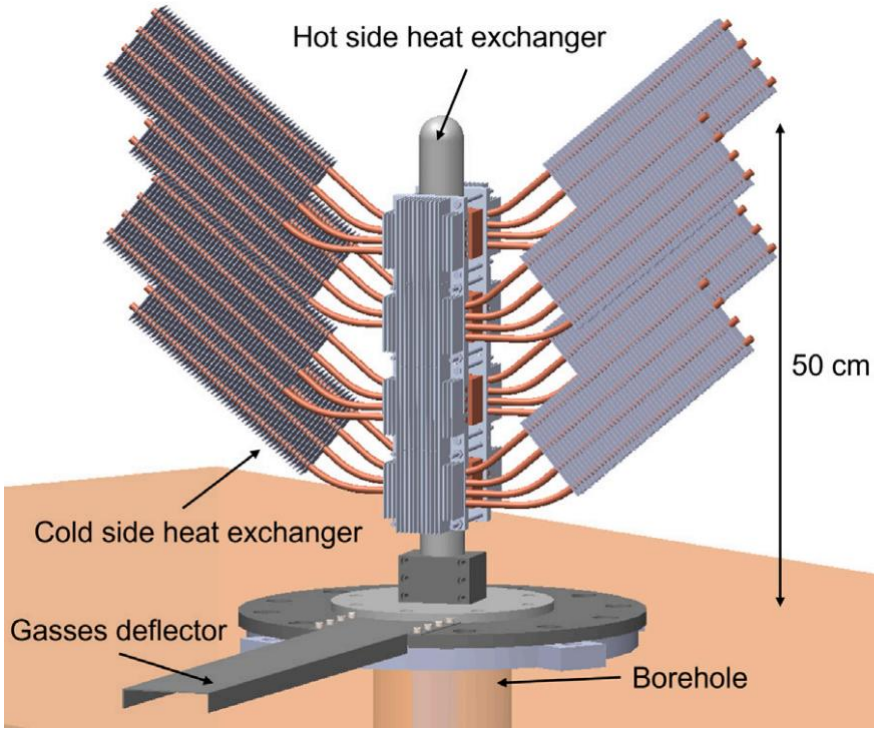

Figure 25. Geothermal anomalies TEG [97].

2.5.15 Aviation

The aviation industry has large potential for thermoelectric energy harvesting due to the cold ambient air at cruising altitude, this provides a large temperature delta that can be investigated with the intention of generating adequate electricity for IoT monitoring sensors. Autonomous wireless sensors are essential to reduce maintenance costs within the aviation sector as they can provide the means for offsite maintenance checks. Thermoelectrics can increase the ease of transitioning to such sensors by providing a passive means for power through energy harvesting, this can possibly remove the need for cabling and battery recharge/replacement burdens.

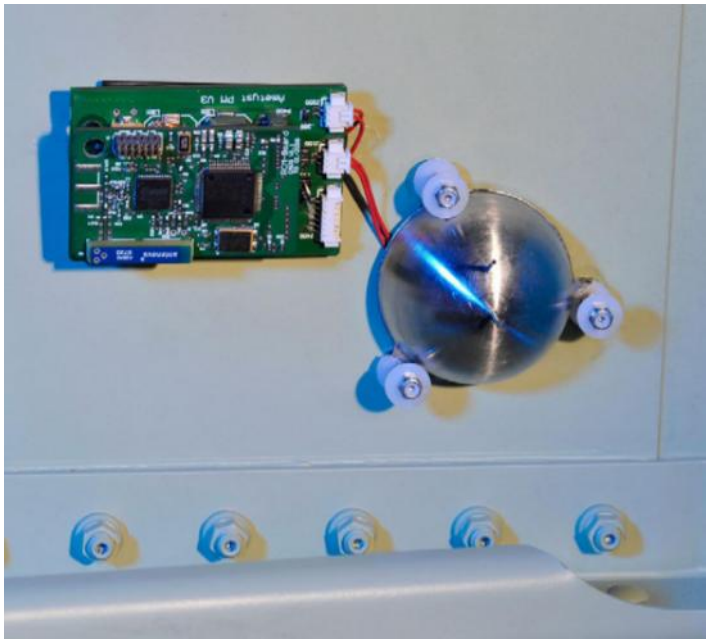

Figure 26. Aeronautical TEG [98].

Samson et al. (2011) [98] investigated the feasibility of thermoelectrics to power autonomous wireless sensors in aviation by creating a new TEG, as depicted in Figure 26, that increased energy output by 14% and overall system efficiency by approximately 50% when compared with a pre-existing system. The total energy generated by the system over 6000 seconds was equivalent to 26 J. The increase in system efficiency highlights the effectiveness of research into thermoelectrics and strengthens the feasibility of energy harvesting using thermoelectrics in aviation.

2.5.16 Brewery

Benday et al. (2017) [99] explored the potential for industrial waste heat recovery via the use of thermoelectrics and a brewery by recording real-time hot-side temperature data from a brewery's steam trap at the University of California and determining the effective power output. The power output results were then input into an economic model to calculate the Net Present Value (NPV) and therefore determine the TEG's feasibility.

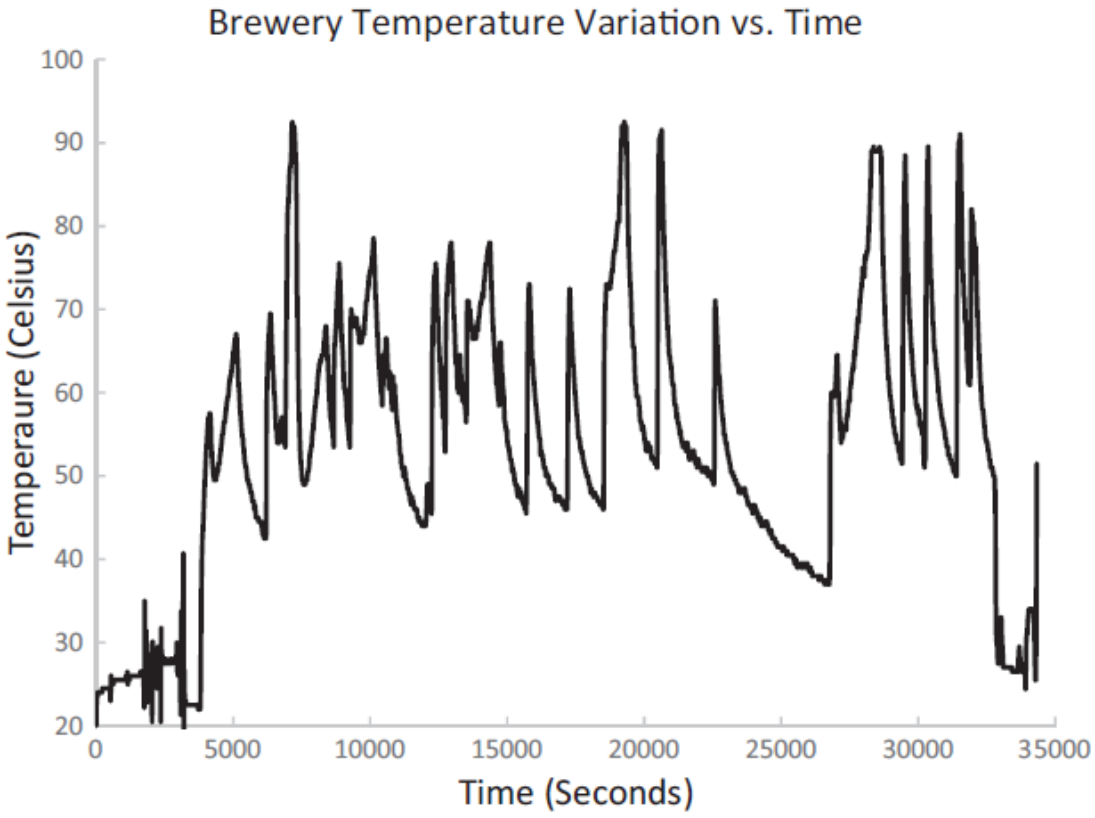

Figure 27. Brewery temperature vs time [99].

Figure 27 contains the measured steam trap brewing temperatures throughout a single brewing cycle measured every 15 seconds. It can be seen that the data contains short temperature spikes resulting from cycle-based steam heating which allows the brewing kettle to reach optimal temperatures efficiently, this result subset was of importance as it emphasises the vast temperature differences that may affect a TEG's performance, thus it is of importance to analyse such characteristics when determining a systems feasibility.

4 cutting edge materials were analysed and BiSbTe resulted in the highest power output (526 W/m^2) since it had the highest figure of merit zT in the working temperature range and a very low L_{opt}, where L_{opt} is a materials optimal length to hold a temperature gradient.

It was determined that the NPV of a TEG system made up of BiSbTe thermoelectric modules was positive after 25 years, however improvements to the TEG system can be made to improve power output and thus NPV by identifying higher temperature heat sources, optimizing the choice of heat exchanger to eliminate excess costs, and identifying industries for investment with lower cost of capital [99].

2.5.17 Power Density

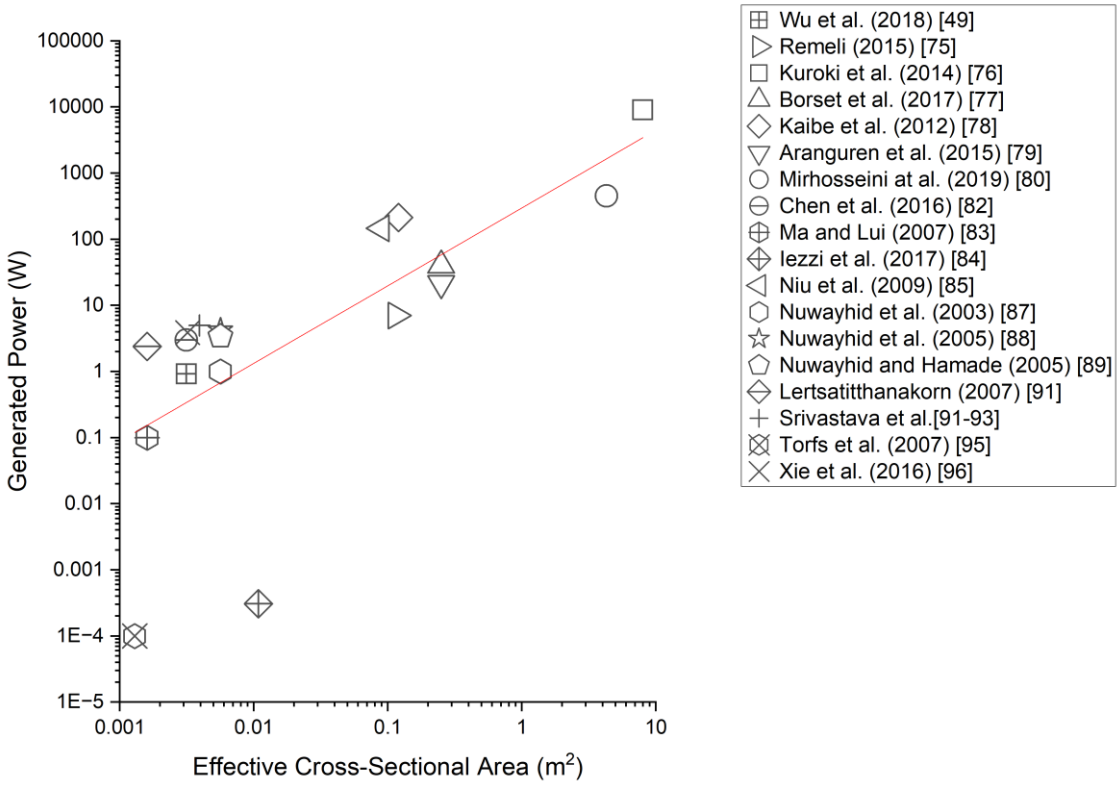

Figure 28. Generated power versus effective cross-sectional area for TEG systems reported in the scientific literature [49, 75–80, 82–85, 87–93, 95, 96].

Figure 28 contains the power density results of 18 TEG systems reported in the literature. It is evident from Figure 28 that multiple TEG systems have been able to achieve several Watts of generated power with an active cross-sectional area similar to what could realistically be

achieved via harvesting within a brewery. Assuming such a power output could be achieved, it is likely that a developed TEG system could provide the energy required to create a network of wireless IoT-enabled sensors to monitor CO_2 in various locations in parallel with a long battery life.

2.6 Summary and Research Questions

In summary, the importance of monitoring IAQ has been discussed with specificity to CO_2 due to it being a proxy for IAQ and with the potential for it to be abundant in workplaces such as breweries. IoT sensors were explored, with respect to specific wireless protocols such as Wi-Fi and LoRa, while also outlining specific applications to create an understanding of how to reduce the power usage of current IAQ monitoring systems. Energy harvesting was then discussed with emphasis on thermoelectrics, to create the foundation for developing an effective TEG that can efficiently power wireless IoT sensor nodes. Manufacturing waste heat was subsequently explored, along with its benefits and steps to manage it. This outlined the need for energy harvesting technologies in the manufacturing industry. Lastly, existing TEG systems were discussed to create a better understanding of previous work.

Investigating previous literature indicates that there is indeed a gap that can be addressed by this research project. The research questions that will be answered are as follows:

1. Is current CO_2 monitoring sufficient to inform workplaces (such as breweries) when potentially dangerous levels are reached throughout the workplace?
2. If not, can a network of wireless IoT-enabled sensors be created to monitor CO_2 in various locations, in parallel with low power consumption and long battery life?
3. If battery life remains an issue, can thermoelectric energy harvesting be used to monitor CO_2 in parallel with a long battery life, thus removing the battery recharge/replacement burden of IoT technology?

3. Methodology

This chapter contains the methodology of the practical experiments undertaken in this research project. Section 3.1 contains the methodology investigating the application of the end research project system with emphasis on answering research question 1. Section 3.2 outlines the procedure used for sensor power testing and optimizations with the intention of answering research question 2. Section 3.3 describes the methodology utilized to develop a TEG that can address research question 3.

3.1 CO_2 Monitoring Inside a Brewery Using Wireless IoT Sensors

A working brewery in Sydney, Australia was selected as the use case to investigate the dynamic concentration of CO_2 over the course of various working cycles during a period of two months. The brewery produces approximately 1.3 million litres of beer annually, is approximately 900 m^2 in area across 2 levels, has 10 fermentation tanks, 3 bright beer tanks, and 2 water tanks, ranging from 4000–12,000 L. As shown in Figure 29, the brewery top floor contains all the fermentation and brewing infrastructure, while the bottom floor contains the office, canning line and bar/dining area. The brewery has some permanent staff supported by a casual workforce of approximately 50 employees, with a maximum of 5 workers working on the top floor, 5 in the canning line, and 3 in the office, at any one time. The main ventilation point of the brewery is the large roller door at the bottom of the ramp and just outside the office. The brewery is equipped with the hard-wired CO_2 monitoring system shown in Figure 1.

3.1.1 Wi-Fi Wireless IoT CO_2 Monitoring System

The developed wireless Wi-Fi IoT CO_2 monitoring system consisted of the physical sensor nodes [Figure 30] and the backend infrastructure [Figure 31]. The sensor portion consisted of the following:

1. 4 lithium ion 18650 batteries (14,000 mAh total) connected in series.
2. Sparkfun ESP32 Thing board which received and transmitted CO_2 data over Wi-Fi.
3. Adafruit SCD-30 CO_2 sensor which can measure CO_2 (ppm) in the range of 400 to 10,000 ppm with a resolution of ± (30 ppm + 3%) ppm, it can also measure air temperature (°C) with an accuracy of ± (0.4 °C + 0.023 x (T- 25 °C)) @ 0 - 50 °C and humidity (%) with a resolution of ± 3% @ 25 °C.

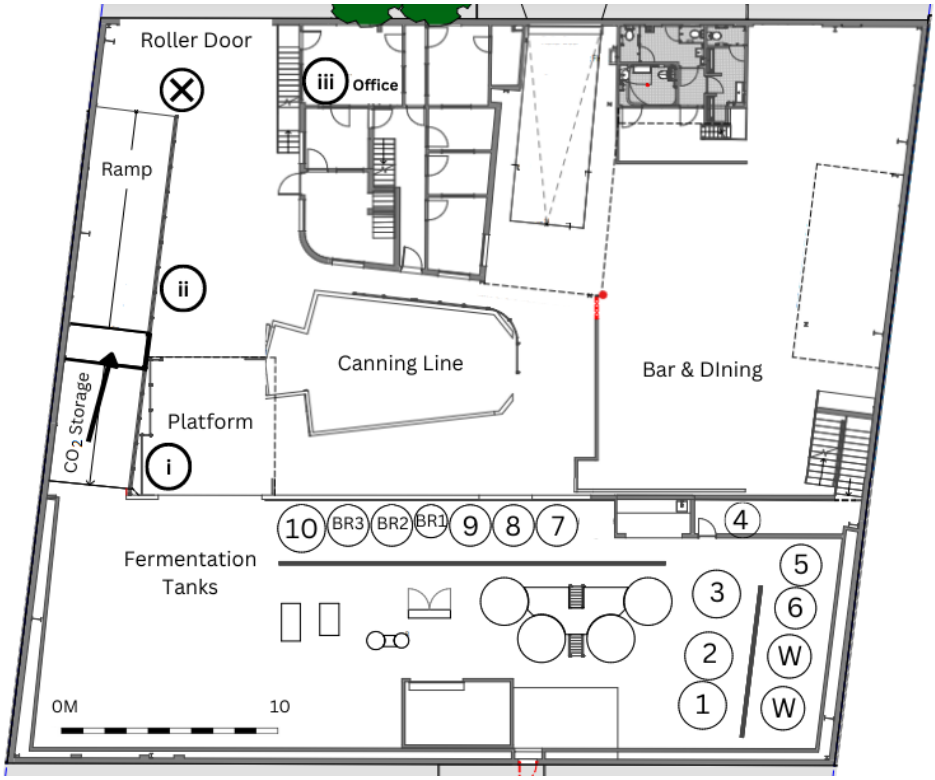

Figure 29. A floorplan of the brewery. Sensor positions, X: hardwired. i: Node 1, ii: Node 2, iii: Node 3, W: water tanks, BR1-3: bright beer tank, numbers 1-10 indicate the fermentation tank numbers, the arrow indicates the CO_2 storage.

The procedure for the developed wireless Wi-Fi IoT CO_2 monitoring system was as follows:

1. Arduino IDE was used to program (code in Appendix) and connect the ESP32 boards to the Wi-Fi access point, which was the primary network connection.
2. Once connected to the local Wi-Fi network, the sensor nodes were then connected to a Mosquito MQTT Broker instance running on a Raspberry PI under Rasbian OS.
3. The nodes then uploaded CO_2 data every 30 s by publishing to the broker.

Running simultaneously on the Raspberry PI were instances of Node-Red 3.0 and InfluxDB 2.0. Node-Red was used to subscribe to the MQTT topics and add any extra tags required to the data before it was written to InfluxDB. Each node was given a unique field name in the database and tags were added as needed to provide metadata. InfluxDB 2.0 allowed the use of the new graphical user interface previously named Chronograf to integrate the data and find patterns in the CO_2 levels.

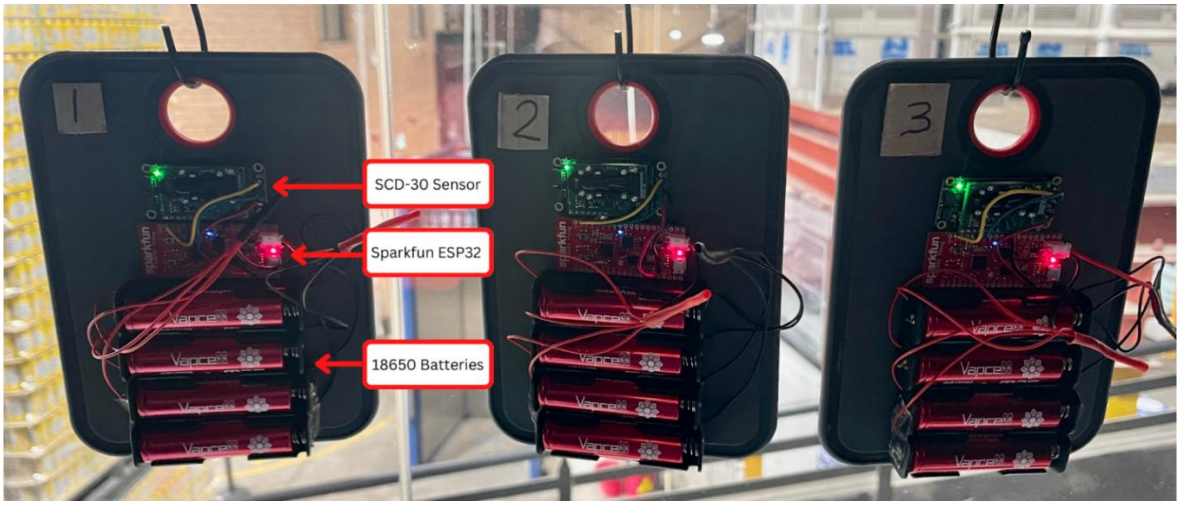

Figure 30. IoT CO_2 sensor nodes 1-3.

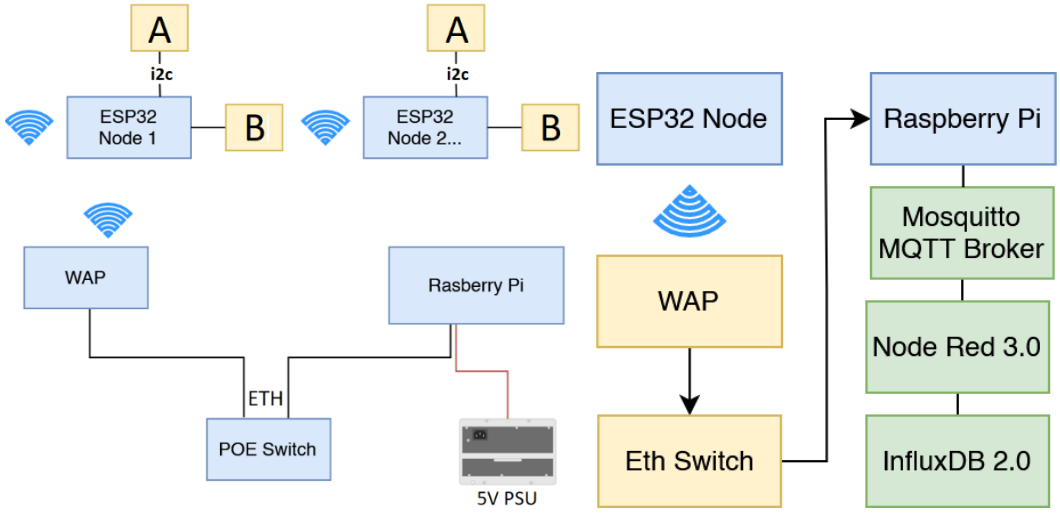

Figure 31. Digital architecture for the sensor network, A: SCD-30 sensor, B: 18650 batteries, WAP: wireless access point, POE: power over ethernet, ETH: ethernet.

The wiring arrangement for the CO_2 sensor nodes is shown in Figure 32. The sensor was connected to the ESP32 boards using the i2c protocol, both the SDA and SCL sensor ports were connected to their counterparts on the ESP32 boards, while the 3 Volt and Ground ports were also connected to their counterparts to receive power from the ESP32 board as well.

Three identical wireless Wi-Fi IoT CO_2 monitoring nodes were assembled to monitor the CO_2 levels in three different sections of the brewery's workplace. All 3 sensors were firstly placed in close vicinity of a pre-existing CO_2 monitoring system for calibration. Monitoring all 4 CO_2

values from the 4 nodes using Influxdb allowed for the sensors to be recalibrated using the Arduino code to ensure all measured values were consistent.

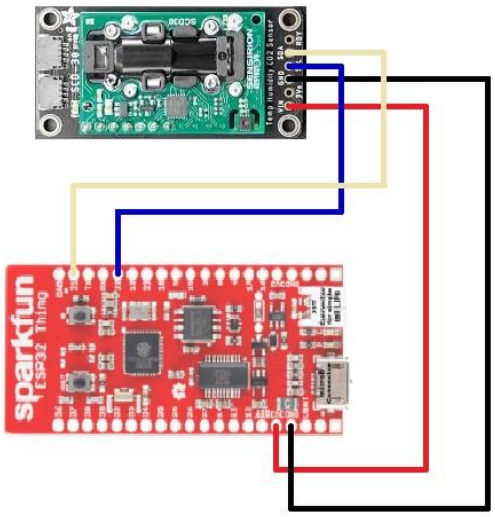

Figure 32. Node wiring arrangement: yellow: SDA, blue: SCL, red: 3V3, black: Ground.

3.1.2 Brewery CO_2 Field Testing

Node 1 was then placed near the fermentation tanks as this location was where CO_2 venting occurred, while Node 2 was placed near the canning line as this was directly below the fermentation tanks and was a suspected location for CO_2 since it is denser than air and might sink to this location once released. It is also in close proximity to the bay where CO_2 for carbonation is stored. Finally, Node 3 was placed in the office area. Figure 29 depicts the precise location of the nodes and hard-wired alarm.

An additional manual data stream was created primarily to determine when the brewery was venting CO_2. A venting sheet was created and printed for the staff to take note whenever venting occurred. The sheet recorded when (date/time) venting occurred, venting duration, the fermentation tank number and any additional comments.

The bright beer tanks (BR1-3) are vessels that contain beer that is ready for packaging and that has already been carbonated. In the case of bright beer tank venting, the vent is done after the beer is transferred out of the tank to packaging (canning) and is done to remove excess CO_2 in

the tank. Similarly, when the carbonation CO_2 storage tank was refilled by a commercial supplier, was also manually recorded.

The influx database was observed at the end of every working day to determine any CO_2 trends that may have resulted from venting. The following day, the database information was compared to the manual data stream to analyse the impact of the venting and to draw conclusions.

Finally, observation sessions were undertaken in the brewery to record numbers and movements of workers throughout the brewery space.

3.2 Sensor Power Testing

3 sensor node configurations were tested in conjunction with the Keithley 2460 source meter as the power source, with 2 using the LoRa protocol and 1 using Wi-Fi [Figure 33]. Both LoRa sensor nodes measured the CO_2 (ppm) concentration in ambient using either the Adafruit SCD-30 or Cozir LP3 sensor. The Grasshopper LoRaWAN board was connected directly to the Adafruit SCD-30 or Cozir LP3 sensor via the i2c and UART protocols respectively to receive and transmit CO_2 (ppm) data directly to TTN via a Dragino LoRaWAN gateway [Figure 34]. 2 different sensors were necessary to highlight the differences between conventional CO_2 sensors and new innovative low powered sensors. The Adafruit SCD-30 and Cozir LP3 sensor have an accuracy of ±(30 ppm + 3%) and maximum measurement capability of 10,000 ppm. The LP3 sensor is stated to use new LED sensing as opposed to conventional, more power intensive, methods. Finally, Arduino IDE was used to edit the code onboard the grasshopper board to adjust connection info and conditions such as DR, TX, and message interval.

The Wi-Fi sensor node also measured CO_2 (ppm) concentration in ambient using the Cozir LP3 sensor. The sensor was connected directly via UART to the Sparkfun ESP32 Thing board which was used to receive and transmit CO_2 (ppm) data via a Wi-Fi router to an MQTT broker that was running on a computer connected to the same local network. Arduino IDE was also used to adjust connection info and conditions such as the message interval. The Wi-Fi sensor node was necessary to highlight the advantages and disadvantages of using LoRa as opposed to conventional methods already popular in the IoT space.

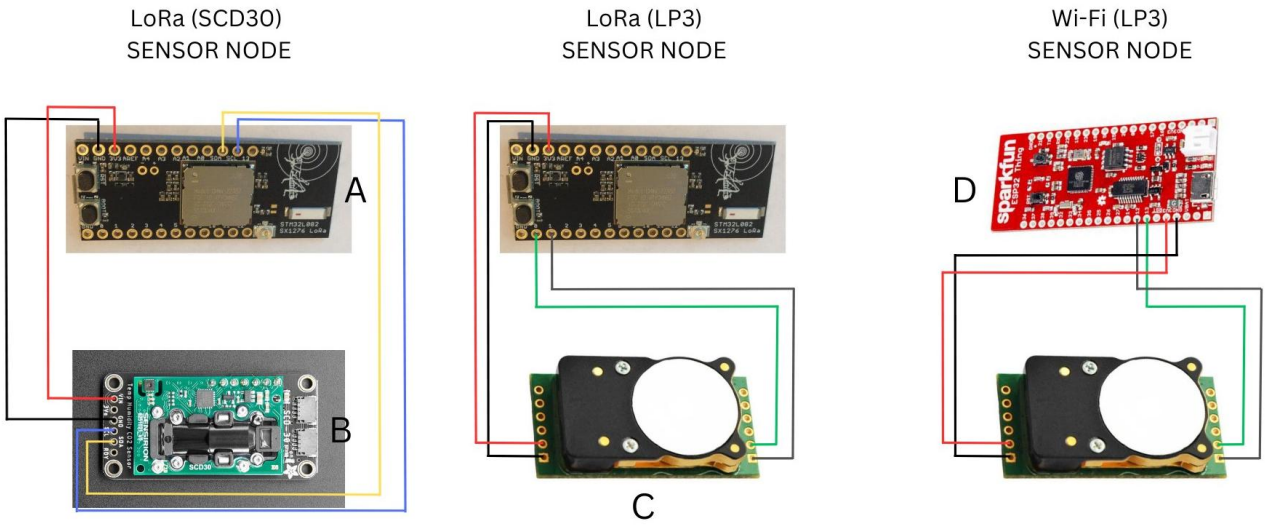

Figure 33. LoRa and Wi-Fi sensor nodes, A: Grasshopper LoRaWAN, B: Adafruit SCD-30, C: Cozir LP3, D: Sparkfun ESP32 Thing, black: GND, red: 3V Input, yellow/blue: i2c, green/grey: UART.

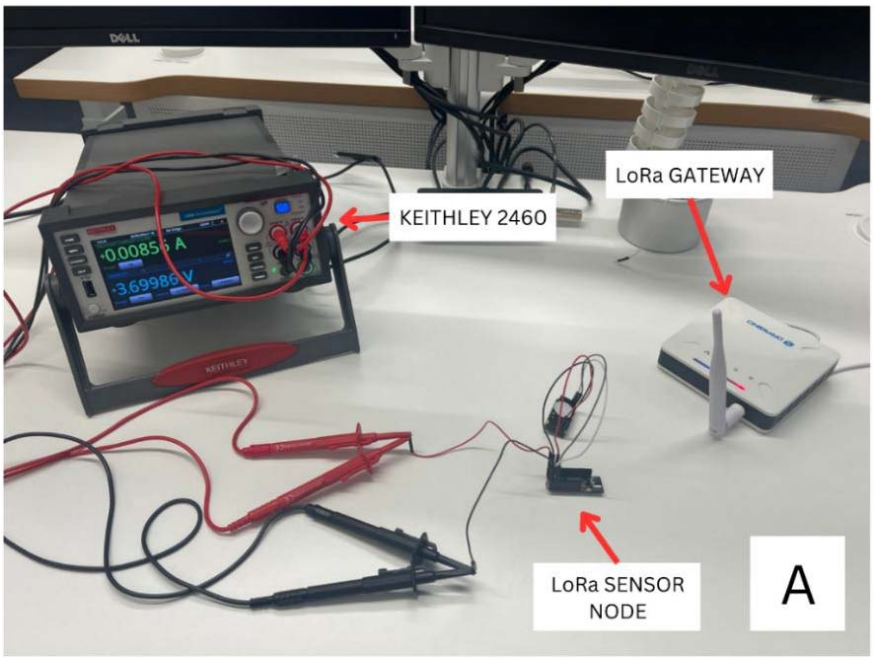

Figure 34. Keithley 2460 + LoRa (LP3) sensor node experimental setup.

3.2.1 Minimizing Power Draw - Data Rate, Transmission Power, Arduino IDE Coding Optimization

3.2.1.1 Data Rate

The first experiment consisted of testing the data rate of the LoRaWAN connection for the LoRa sensor node (LP3) to assess its impact on the overall current consumption. The method of testing the data rate consisted of specifying lora.setDataRate = DR(DR) in the Arduino Code. Firstly, lora.setDataRate = DR(0) was set, the sensor node was then powered on and the current draw (mA) was measured over 10 minutes (3 trials) with the Keithley 2460 source meter as a power source [Figure 34] ensuring the sensor node was connected to the TTN and sending CO_2 (ppm) data payloads. The data rate was then increased by 1 and the sensor node was retested up to DR(5).

It should be noted that the grasshopper board is capable of DR(6), however this option led to inconsistent results in testing which was most likely due to the difference in bandwidth moving from DR(5), therefore it was omitted.

3.2.1.2 Transmission Power

The second experiment tested the transmission power of the LoRaWAN connection for the LoRa sensor node (LP3) to assess its impact on the overall current consumption. Testing the transmission power consisted of specifying lora.setPower(dBi) in the Arduino Code. Firstly, the minimum TX power of lora.setPower(10) was set, the sensor node was then powered on and the current draw (mA) was measured over 10 minutes (3 trials) with the Keithley 2460 source meter as a power source ensuring the sensor node was connected to the TTN and sending CO_2 (ppm) data payloads. The transmission power was then increased by increments of 4 and the sensor node was retested until the maximum value of TX(30) was achieved.

3.2.1.3 Arduino Code Optimizations

Coding with Arduino IDE sometimes requires optimization to ensure the code is the most efficient when it comes to the particular use case due to the initial code, in most cases, being only a template that can be used for multiple use cases, therefore it may not always be the most efficient. The next task involved experimenting with the Arduino code to ensure it was the

most efficient at sending and receiving LoRa packets to the TTN. This included removing loops/terms that could cause the board to use more current, for example, an if-loop that was contained within the void loop of the Arduino code would need to run at every void loop start and would therefore consume more current.

3.2.2 LoRa, Wi-Fi Power Comparison - Sensor Frequency, Obstacle & Distance Testing

The next experiment included varying the sensor measurement frequency of all 3 sensor nodes to analyse if it had any impact on overall current consumption. The experiment consisted of specifying the sensor CO_2 (ppm) measurement frequency within the Arduino code for the Wi-Fi and LoRa sensor nodes by varying delay(x) in the void loop, where x is the approximate amount of time between transitions in ms. For testing, sensor measurement frequency was firstly set to 7 seconds (3 trials), the sensor node was then powered on and connected, current draw (mA) was then measured over 10 minutes for all 3 sensor nodes using the Keithley 2460 as a power source. The sensor measurement frequency was then increased to 15, 30, 60, and 120 seconds for consecutive tests.

Next the propagation capabilities of both LoRa and Wi-Fi were analysed to determine the effect that various building materials had on average current draw. The University of Technology Sydney's (UTS) Tech Lab was used to aid with testing, a floorplan of the lab is depicted in Figure 35. The sensor nodes were placed at Point A where earlier tests had taken place while both the LoRa gateway and a Wi-Fi mobile hotspot were placed at various points within the Lab as shown in both Figure 35 and Figure 36. Point B was located 15 m from Point A and was chosen on the basis that it was fully enclosed which is required when testing signal propagation without reflection. Point C was located 16 m from Point A and was at the midpoint of the lab area, Point D was 40 m away from Point A and was the point furthest within line of sight, Point E was 36 m from Point A and was the furthest point the Wi-Fi signal could reach, and finally, the hallway was 52 m from Point A and was the furthest the LoRa signal could reach.

Point B was fully enclosed as shown on the floor plan and contained potential interference materials such as metal from the computers on the tables and wood/metal that was used to make the walls, Point C contained potential interference materials such as glass that was used for the staircase exit and glass/wood/metal that was used for the walls in the adjacent room, Point D

was in line of sight and therefore contained a path free of obstructions, and finally, Point E/Hallway contained potential interference materials such as glass/metal/wood that were used to make up the walls of the adjacent meeting rooms, with some metal obstructions in between.

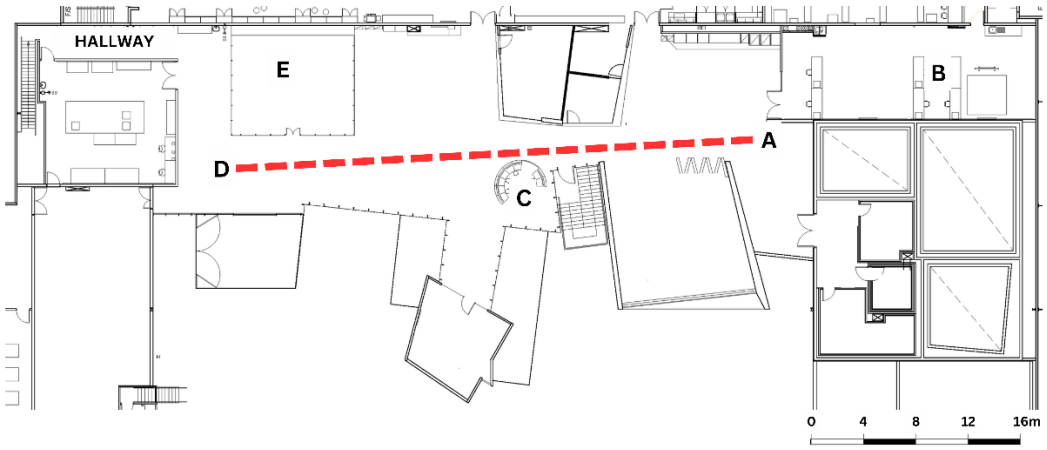

Figure 35. UTS tech lab floor plan, A: Point A, B: Point B, C: Point C, D: Point D, E: Point E, dashed line: line of sight.

Figure 36. Gateway/hotspot placement, B: robotics lab, C: couch, D: 45 m line of sight, E: brewery, red box: approximate sensor node position.

Testing the effect of various locations was done by firstly placing the gateway/hotspot at each point for 5 minutes (3 trials), the sensor node at Point A was then powered on and the current draw (mA) was measured using the Keithley 2460 as a power source. It should be noted the

Hallway location was only tested using the LoRa signal as this was the furthest the signal could reach while the Wi-Fi signal could only reach Point E.

3.2.3 Sensor Battery Life

Battery life simulation can help create a visual representation of the practical differences between wireless protocols for IoT sensor technologies by estimating potential battery life and the severity of the battery recharge/replacement burden.

The last experiment consisted of simulating the battery life of both the Wi-Fi (LP3) and LoRa (LP3) sensor nodes by using the Keithley 2281S battery simulator [Figure 37]. The battery used for creating the simulation was the T-Power 3.7 V Lithium-ion AA with a capacity of 1,000 mAh. The battery simulation procedure was as follows:

1. The battery was firstly connected to the Keithley 2281S and discharged until empty (3.3 V and 4 mA).
2. Once discharged the battery was charged until full (4.2 V and 4 mA) to form the basis for generating the battery model, the battery model was then generated using the charging characteristics recorded from the aforementioned charging cycle.
3. The battery simulation was then performed using the battery model generated.

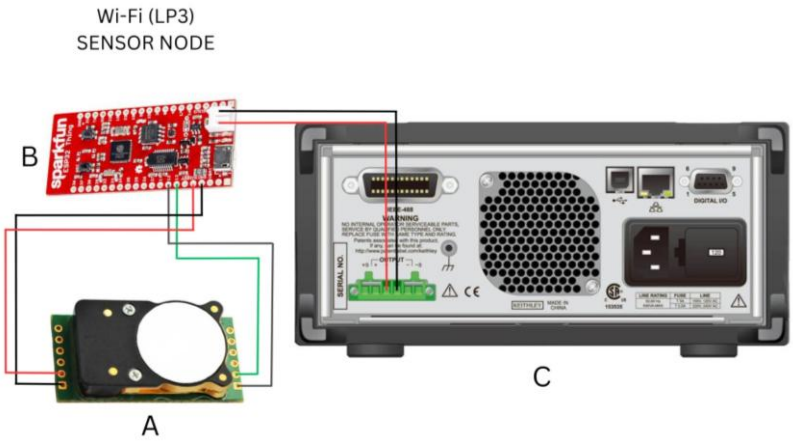

Figure 37. Keithley 2281S + Wi-Fi (LP3) sensor node experimental setup, A: Cozir LP3, B: Sparkfun ESP32 Thing, C: Keithley 2281S, black: GND, red: 3V Input, green/grey: UART.

The generated battery model in the form of State-of-Charge (SOC) vs Voltage is depicted in Figure 38 with the battery capacity for the voltage range equalling 947 mAh.

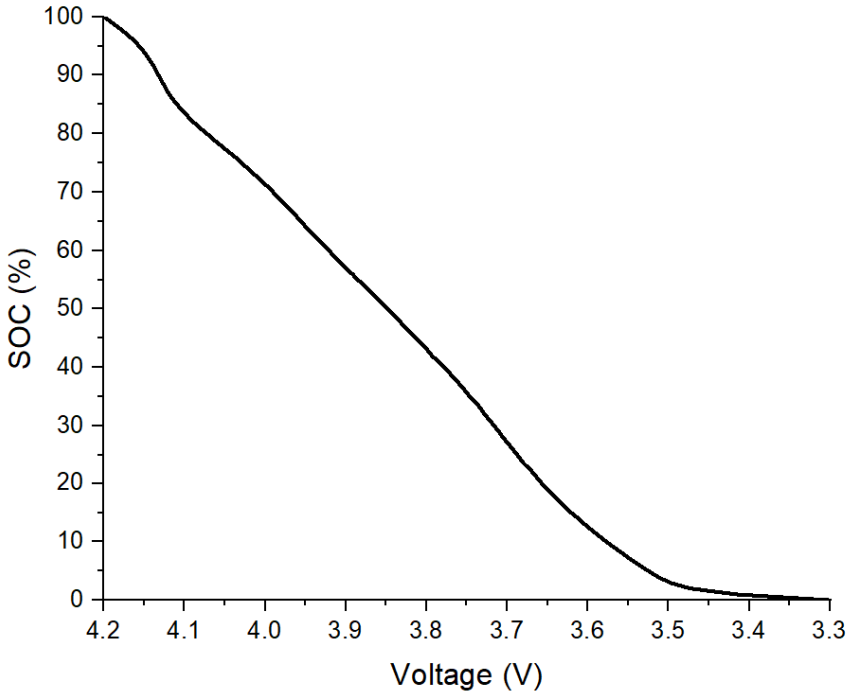

Figure 38. Generated battery model.

The battery life simulation tests procedure was as follows:

1. Firstly, the Wi-Fi (LP3) sensor node was connected to the Keithley 2281S through the boards + and - ports [Figure 37] as to simulate a battery connected.
2. The battery model was then used to simulate a running battery with the sensor in full operation until the battery state of charge (SOC) was 0%, this gave an indication of overall battery life.
3. The test was then replicated for the LoRa (LP3) sensor node with the simulator being attached to the V_{in} and Ground ports of board.

3.3 Developing a TEG

The first step with regards to developing the TEG system was the identification of a heat source that could provide the heat required to generate electricity from the thermoelectric module. The source of the waste heat was identified in an operational Australian brewery and is depicted in Figure 39. The source was a hot pipe outlet from one of two Simons boilers (Figure 40). The boilers are used to generate superheated steam for several brewing processes. Both boilers were rated at 500 kW, used natural gas as their fuel source, and had a capacity of 891 L.

Figure 39. Hot pipe (dark pipe, running horizontally) used as the waste heat source within a working brewery.

Figure 40. Two Simons 500 kW boilers within a working brewery.

Such boilers are common in breweries, due to their necessity in several steps of the brewing process. The steam created from the boilers is used in mashing and wort boiling, to generate hot water; wort cooling, to reheat the returned water; and kegging, to sanitize the kegs. It is therefore evident that the boilers are essential to the brewing process and their presence will be common to almost all working breweries.

In an initial experiment, the hot pipe temperature was determined to enable a prediction of the power output of the final system. This was done by monitoring the temperature of the pipe using a K-type thermocouple connected to a Picologger and PC. Temperature was monitored for a period of 24 h including times when the boiler was operational and non-operational.

3.3.1 TEG Design

3.3.1.1 Heat-Exchange Coupling, Thermoelectric Generator and Heat Sink

Coupling of the TEG (Figure 41) was required to enable the waste heat to pass from the round hot pipe through the planar TEG, providing means for electricity generation. The coupling was designed in SolidWorks to fit around the boilers 2-inch outlet pipe. It was machined using a CNC from aluminium, chosen as it is a low-cost material with high thermal conductivity. The contact surfaces of the coupling were polished and had thermal paste applied to reduce thermal resistance at each interface. The module chosen was the GM250-127-28-10 due it having the largest matched power output (28.3 W) of off-the-shelf thermoelectric modules, according to its datasheet. The thermoelectric module had an effective cross-section of 62 mm x 62 mm and a similarly sized square indentation was designed on the coupling to prevent the module from sliding laterally across the faces. The entire coupling design was intended to clamp around the pipe using a hinge and bolt design, while the heatsink was intended to be applied to the coupling via two M5 screws, as shown in Figure 42.

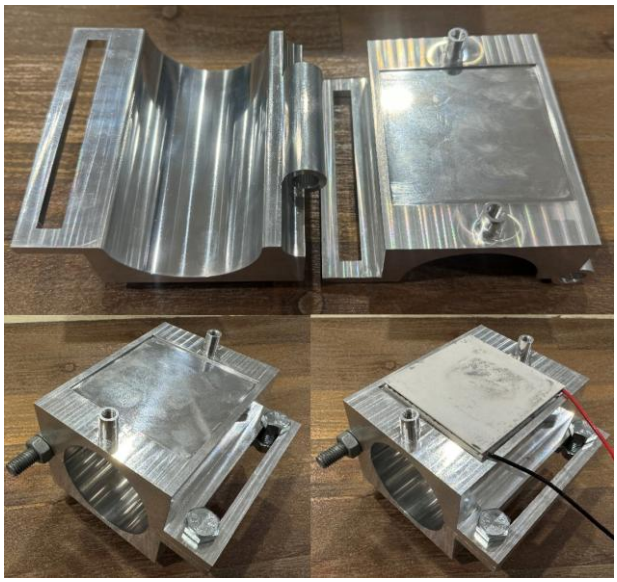

Figure 41. Coupling to enable heat transfer from the hot pipe into the TEG.

Lab experiments were subsequently conducted using a hotplate (150 °C) in contact with the hot-side of the TEG and a range of different heat sinks on the cold-side. The Noctua NHP1 [Figure 42] was eventually chosen as it produced the lowest cold-side temperature of approximately 90 °C. Further results of these tests are presented in the results section (Section 4.3.1). The heatsink was constructed out of aluminium and contained six aluminium heat pipes to provide improved cooling performance.

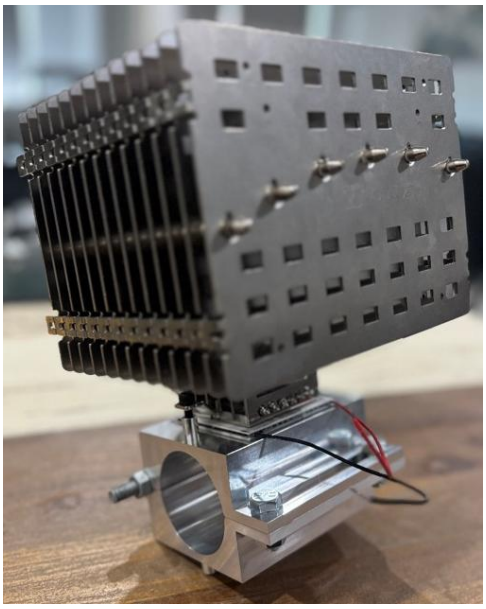

Figure 42. Thermoelectric system, including the heatsink, a Noctua NHP1.

3.3.1.2 LoRa Wireless IoT Sensor Node

The LoRa (AH1) wireless IoT sensor node depicted in Figure 43, contained the Cozir AH-1 CO_2 sensor to measure CO_2 concentrations within the brewery for IAQ monitoring. It also contained a grasshopper LoRaWAN board in order to transmit CO_2 data to a LoRaWAN gateway. A 1,000 mAh Li-ion rechargeable battery was used to power the grasshopper board. The battery was connected to a Steval ISV019V1 harvesting board, which captured electricity from the TEG to charge it via maximum power point tracking, to ensure maximum power was being harvested from the TEG at all times.

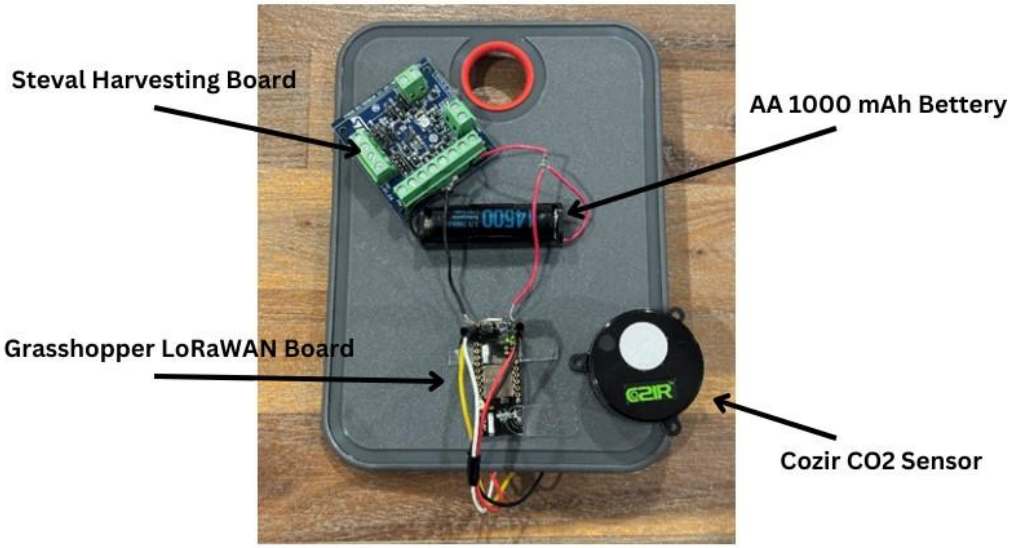

Figure 43. LoRa (AH1) wireless IoT CO_2 sensor node and its components

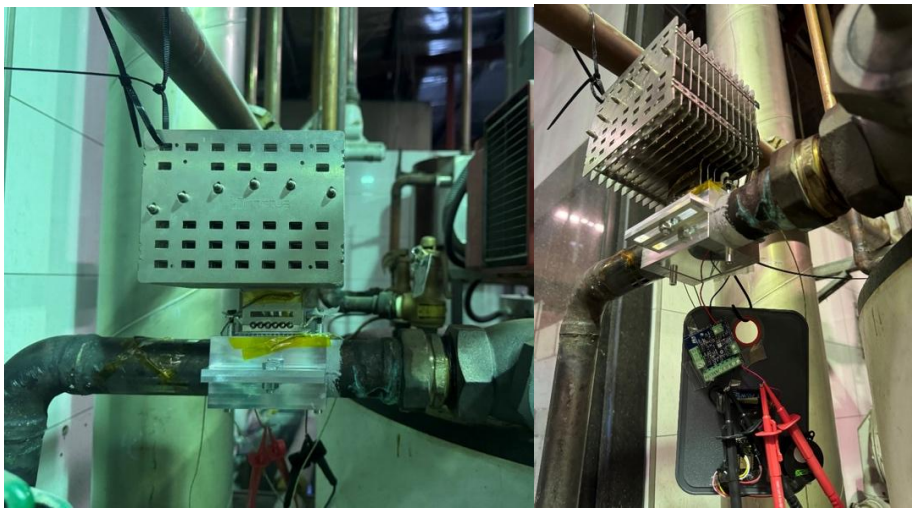

Figure 44. Developed thermoelectric system applied to a hot pipe (left) with the sensor node suspended below (right).

The installed TEG and LoRa (AH1) wireless IoT sensor node is shown in Figure 44, with the wiring schematic of the system outlined in Figure 45. The TEG was attached to the pipe via the clamping design with a bolt to secure it in place. Thermal paste was applied between the pipe and TEG to provide optimal heat transfer. The entire LoRa (AH1) sensor node was connected to the thermoelectric module as shown in the schematic to allow the battery to be recharged via the TEG. It is noteworthy that the entire sensor node could be removed from the system by disconnecting the module wires from the energy harvesting board. The sensor node

would then continue to run on its own battery uninterrupted, allowing it to monitor CO_2 levels anywhere in the brewery and to transmit that data wherever LoRa signal from the gateway is present.

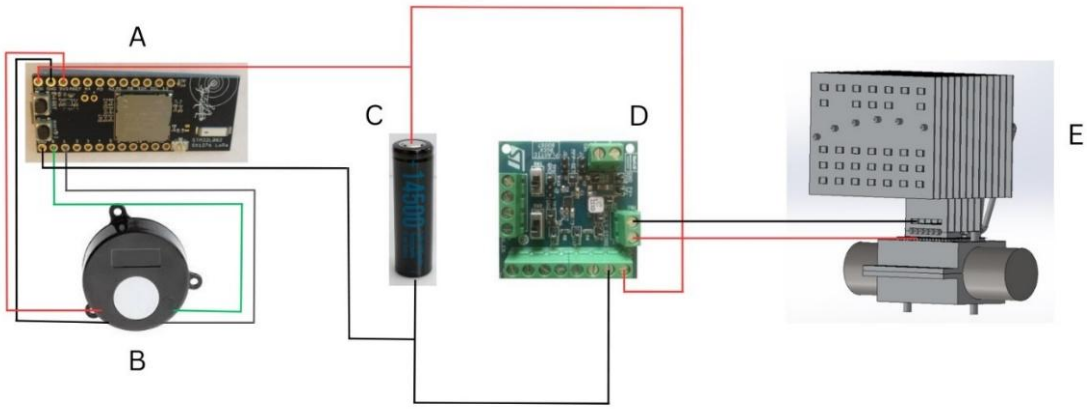

Figure 45. Wiring schematic of TEG and LoRa (AH1) sensor node, A: LoRa Grasshopper, B: Cozir AH-1, C: 1,000 mAh battery, D: STEVAL-ISV019V1, E: TEG, red: positive, black: negative, others: TX/RX.

3.3.2 System Characterisation

3.3.2.1 Temperature, Open-Circuit Voltage and Power Measurements

A Keithley 2460 source meter was connected to the thermoelectric module to monitor open-circuit voltage every 1 s. K-type thermocouples, connected to the Picologger, were used to monitor temperatures every 1 s throughout all experiments on the pipe, hot-side of the TEG, cold-side of the TEG, and the brewery ambient in proximity to the boilers.

The Keithley 2460 was also used to create a current-voltage (IV) curve of the thermoelectric module every 15-30 min, which was required to determine the maximum matched power generated by the TEG. An IV curve for a thermoelectric module takes the shape of a quadratic curve with the maximum power in the middle, which is often referred to as the maximum matched power output.

3.3.2.2 Battery Voltage and State-of-charge

In order to test the TEG's feasibility, battery voltage and SOC experiments were run for a time-period of approximately 768 hours (32 days) with some data missing on day 16 and days 20-24. The boiler schedule for the time-period where experiments were run, is present in Table 5. For this time-period, the boilers were active from 3-5 times per week for approximately 4-10 hours per day.

Table 5. Boiler schedule over a 768-hour time-period.

Date	Boiler	Time	Week 1	Date	Boiler	Time	Week 3
Day 1	yes	8h	Mon	Day 15	yes	4h	Mon
Day 2	no		Tues	Day 16	Yes	10h	Tues
Day 3	no		Wed	Day 17	yes	8h	Wed
Day 4	yes	8h	Thur	Day 18	yes	8h	Thur
Day 5	yes	8h	Fri	Day 19	yes	7h	Fri
Day 6	no		Sat	Day 20			Sat
Day 7	no		Sun	Day 21			Sun
Date	**Boiler**	**Time**	**Week 2**	**Date**	**Boiler**	**Time**	**Week 4**
Day 8	yes	5h	Mon	Day 22			Mon
Day 9	yes	7h	Tues	Day 23			Tues
Day 10	yes	8h	Wed	Day 24			Wed
Day 11	Yes	9h	Thur	Day 25	yes	8h	Thur
Day 12	no		Fri	Day 26	yes	7h	Fri
Day 13	no		Sat	Day 27	no		Sat
Day 14	no		Sun	Day 28	no		Sun
				Date	**Boiler**	**Time**	**Week 5**
				Day 29	yes	8h	Mon
				Day 30	yes	8h	Tues
				Day 31	yes	9h	Wed
				Day 32	yes	8h	Thur

A Keithley 2460 was connected to the battery of the LoRa (AH1) sensor node to monitor battery voltage throughout testing. Battery voltage was used to provide insight into whether the battery was being charged or discharged over time. The maximum voltage of the Li-ion battery was approximately 4.2 V, while the minimum for this application was considered as 3.3 V, due to the grasshopper board specifications.

The SOC of the battery was determined by using the battery model in Figure 38. This provided a means to directly convert measured battery voltage to SOC.

3.3.2.3 Carbon Dioxide Monitoring

The CO_2 levels in proximity to the brewery's boilers were monitored throughout experimentation. CO_2 was recorded with a measurement frequency of 7 s and data was transmitted via LoRa at an interval of 7 s. This was to provide evidence that the LoRa (AH1) sensor node was active and transmitting readings throughout the test-period. It is interesting to note that the sensor was able to operate throughout the entire 768 h test and was unaffected by a mains power interruption at the brewery, which disrupted the other data collection during day 16 and days 20-24.

4. Results & Discussion

This section contains the results and discussion of the research project. Section 4.1 contains those pertaining to the application of measuring CO_2 levels within a brewery to address research question one, while Section 4.2 addresses research question two by assessing power requirements of CO_2 sensing and attempting to reduce the power burden. Section 4.3 provides the results and discussion related to a developed thermoelectric recovery system to address research question three.

4.1 CO_2 Monitoring Inside a Brewery Using Wireless IoT Sensors

This section will address research question 1, namely "Is current CO_2 monitoring sufficient to inform workplaces (such as breweries) when potentially dangerous levels exist anywhere throughout the workplace?" This research question will be addressed by measuring the CO_2 levels inside an Australian brewery in 3 locations. These locations are (i) the fermentation tanks (Node 1), (ii) the canning line (Node 2), and (iii) the office (Node 3).

A 10-day set of venting events within the brewery, that occurred while experimentally monitoring CO_2 values, is summarized in Table 6. The CO_2 levels inside the brewery were monitored using the wireless Wi-Fi IoT sensor nodes as described in Section 3.1.1 with a sampling rate of 30 seconds. This 10-day subset should create a good understanding of how the brewery will function throughout the year as the 10-days was subject to a brewing schedule that is typical for the entire year.

Shown in Table 6 is the approximate venting time as recorded by the brewery staff along with the duration of the event. Vents occurred for approximately 30 min, unless otherwise stated. This was the case in all but a few instances. The time the venting event occurred were found to vary by as much as ± 60 min relative to the time recorded, due to the brewery workers entering venting data without complete accuracy, from the approximation of times and/or entering vents from an earlier day and attributing an approximate timeframe. Also included is the tank number that was vented, with all locations outlined on the brewery floorplan as described in Section 3.1.1. It should be noted that 'BR' stands for the *Bright Beer* tank, while 'Stored CO_2' refers to venting which occurred while filling the storage containers.

Table 6. A 10-day subset of CO_2 venting events within the brewery. Vents occurred for a duration of approximately 30 min, unless otherwise stated.

Venting Day		**Vent Time (Duration)**	**Tank Number**
1	a	2 pm	6
	b	7 pm	BR2
2	a	2 pm	4
	b	4 pm (Not recorded)	BR1
3	a	2 pm	1
4	a	2 pm	8
5	a	10 am	9
	b	2 pm	Stored CO_2
6	a	9 am	Stored CO_2
	b	12 pm	3
7	a	11 am	5
8	a	11 am (60 min)	Stored CO_2
	b	12 pm	2
9	a	12 pm	7
	b	1 pm	10
10	a	9 am (45 min)	Stored CO_2
	b	11 am	8

4.1.1 CO_2 Concentrations

It is firstly important to determine the baseline CO_2 concentration within the brewery for all 3 locations to aid with the analysis of trends which may have arisen from venting in latter parts of this report. There is some minimal degree of uncertainty in the results measured due to the

accuracy of the sensors being ± (30 ppm + 3%) ppm. Figure 46 depicts the baseline CO_2 concentration versus time for all 3 nodes recorded on a non-working day where no vents took place. It should be noted that due to the fact that it was a non-working day, it was difficult to reconnect disconnected nodes, therefore a longer time period was unachievable, while also in this instance, Node 3 had some missing data before 5 PM.

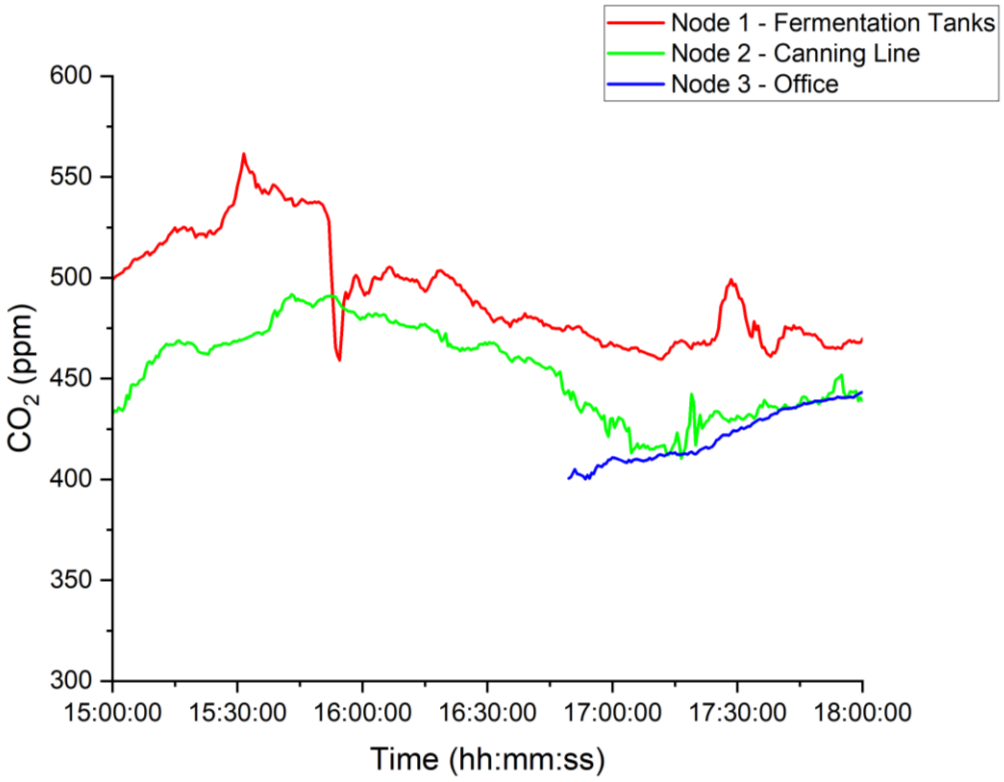

Figure 46. Baseline CO_2 measured versus time for non-working day at the fermentation tank's (Node 1), canning line (Node 2) and office (Node 3) locations.

It can be seen from Figure 46 that throughout the 3-hour time-period the baseline concentration of Node 1 resided in the range of 460 - 570 ppm, while Node 2 and 3 were slightly lower, in the range 420 - 480 ppm, and 410 – 450 ppm, respectively. These values are in line with what might be expected. It can also be seen that both Node 1 and Node 2 share similar trends throughout the time-period, with Node 3 following closely for the period where data was recorded. Small fluctuations above and below the baseline can be attributed to the fact that the brewery still had some activity from the bar portion being open for customers, this firstly would allow some CO_2 to enter the brewery from the respiratory action of people within the vicinity while also allowing some air circulation from open doors etc. It is interesting that the CO_2

concentration within the fermentation location appear to be approximately 50 ppm on average larger than both the canning line and the office locations. This is within the margin of error of the sensors, however this could also be attributed to the top floor of the brewery, where the fermentation tanks were located, having either less ventilation of normalized air and/or some CO_2 being slowly emitted from fermenting apparatus.

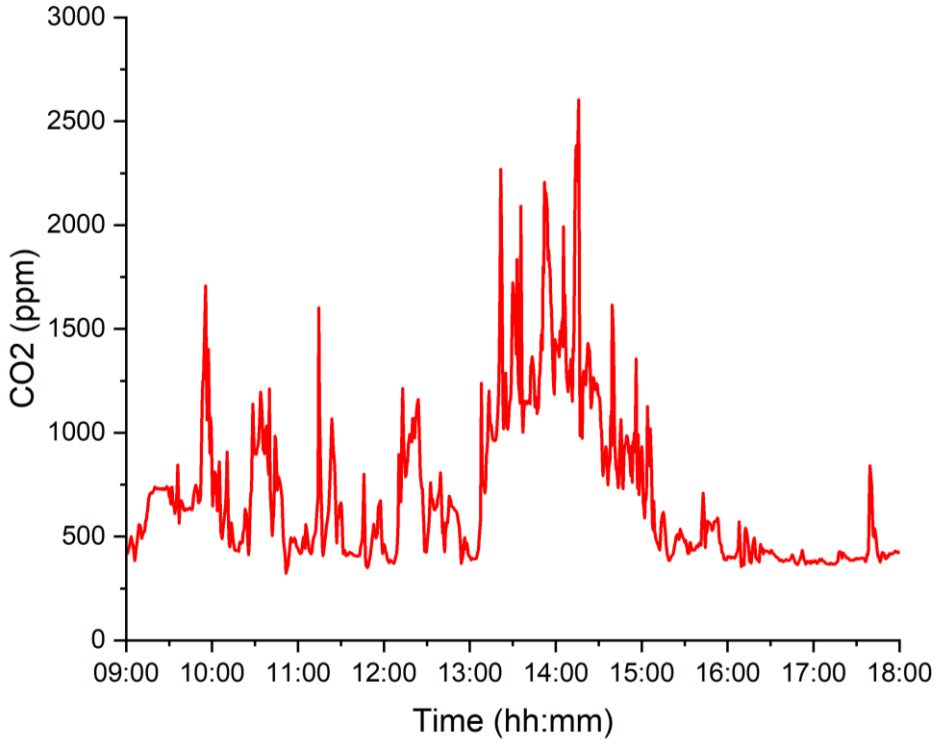

Figure 47. CO_2 measured versus time for venting event 1a at the fermentation tanks location (Node 1).

It is important to now analyse the particular trends with regards to the CO_2 concentration in the brewery and compare them with the venting events and baseline concentrations to determine if venting raised the CO_2 level within the brewery, thus creating potentially unsafe environments. The CO_2 values recorded within the brewery at Node 1 during venting event 1a are depicted in Figure 47. It can be seen from Figure 47 that there is a large increase in CO_2 concentration close to the brewery's fermentation tanks, starting at approximately 1:30 pm, this was likely due to venting event 1a taking place at that time, raising CO_2 levels above the baseline concentration and more importantly above the safe limit of 1,000 ppm for approximately 2 hours due to the venting of CO_2 from fermentation tank number 6. It should be noted that in

Table 6 it is stated that the venting event 1a occurred at 2 PM, however from Figure 47 it can be seen that the CO_2 levels spiked at 1:30 PM, this is within the 60 minute timeframe aforementioned.

Similar increases in CO_2 concentrations above baseline concentrations occur across the majority of venting events with more examples shown in Figure 48, Figure 49, and Figure 50Figure 51, this strengthens the relationship that venting does indeed increase the indoor CO_2 concentrations above the baseline creating potential unsafe working environments.

It is also important to compare 3 locations side-by-side to discuss if the CO_2 concentration is increasing/decreasing uniformly throughout the brewery as a result of venting events. Figure 48 contains the CO_2 values recorded within the brewery at the fermentation tanks (Node 1), canning line (Node 2) and office (Node 3) locations for venting day 6. It can immediately be seen when analysing Figure 48 that there was a large spike in CO_2 concentration for all 3 locations, raising the CO_2 concentration above baseline levels, beginning at approximately 8:30am. This increase was a result of CO_2 venting that took place during venting event 6a which was recorded in Table 6 to have occurred at 9 am, however it appears to have occurred at 8:30 am which is within the 60 min tolerance. This venting event was a stored CO_2 top-up that resulted in dramatically increased CO_2 concentration in all 3 locations, however it appears to have had a larger impact on the CO_2 concentration within the first-floor areas, the office and canning line locations. This was expected, due to both nodes being located on the bottom floor of the brewery where the CO_2 storage tanks are held, however what was not expected was the large overall increase in CO_2 concentration, or the difference between the two. Venting event 6b seems to have had no considerable influence on CO_2 concentrations within the brewery, this could be due to tank 3's location being further away from all 3 nodes when compared with the CO_2 storage tanks, however results recorded from tanks in close proximity to tank 3, do in fact result in increased CO_2 recordings above baseline readings as will be outlined later, therefore tank 3's little effect on CO_2 concentrations was most likely due to inconsistencies in vented CO_2 volume and/or air flow within the brewery that will be discussed later.

The CO_2 concentration in the office exceeded 13,000 ppm while remaining above 4,000 ppm for approximately 1.5 hours, while the CO_2 concentration in the canning line appeared to increase at roughly the same time reaching above 4,000 ppm for almost 30 minutes, and finally

the CO_2 concentration in the fermentation tanks location appeared to increase approximately 10 minutes after the venting event to reach above 2,000 ppm for approximately 10 minutes.

It is evident that venting event 6a raised CO_2 levels above baseline concentrations to unsafe levels for all 3 locations potentially creating unsafe working environments for employees, however it should also be noted that the office location appeared to reach higher CO_2 concentrations due to being mostly enclosed, resulting in poor ventilation of fresh air, while it also remained higher for longer periods due to the lack of ventilation making it difficult for the CO_2 to be displaced from the area. These differences in CO_2 concentrations detected at different nodes on the same floor can be attributed to differences in ventilation of the different locations. Node 1 appears to respond to the venting event 10 minutes later, this was most likely due to the fermentation tanks being located on the floor above, this would result in the CO_2 taking some time to reach the floor above due to it being denser than air. The differences in recorded CO_2 concentrations of all 3 nodes strengthens the need to have a network of sensors, as a single hardwired sensor will not provide an accurate measure of CO_2 levels in all workspaces.

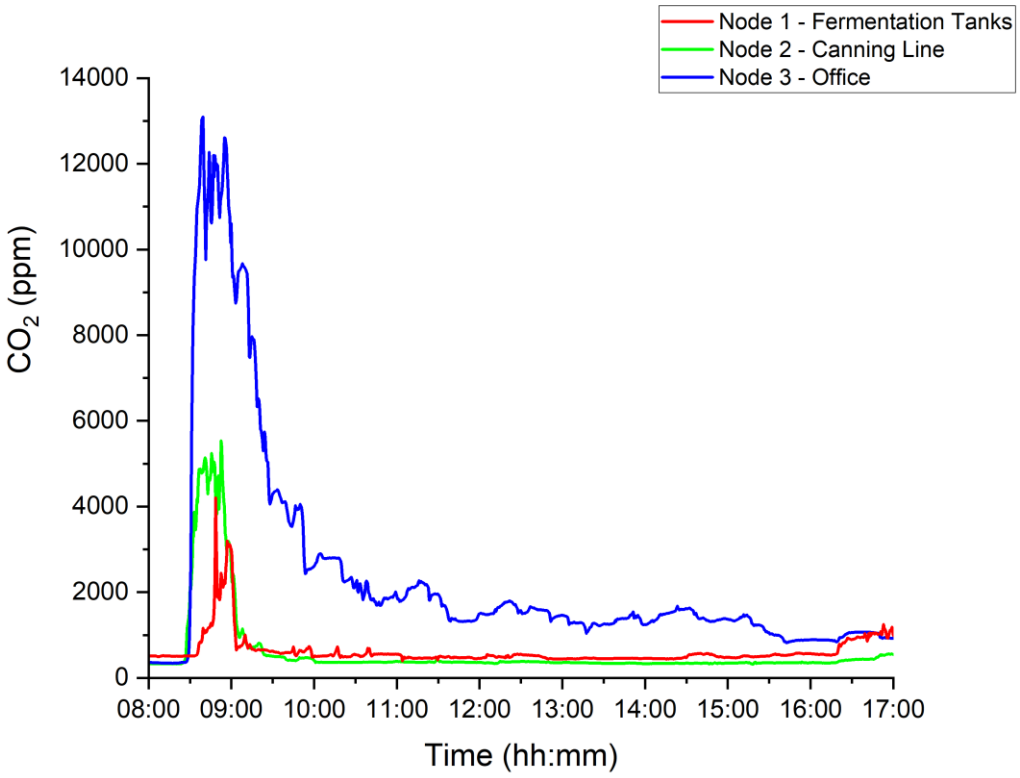

Figure 48. CO_2 measured versus time for venting day 6 at the fermentation tanks (Node 1), canning line (Node 2) and office (Node 3) locations.

It can lastly be seen that the CO_2 concentrations recorded by Nodes 1 and 2 appear to return to baseline concentrations of approximately 500 ppm after 10 AM with Node 1 continuing to have a higher baseline concentration.

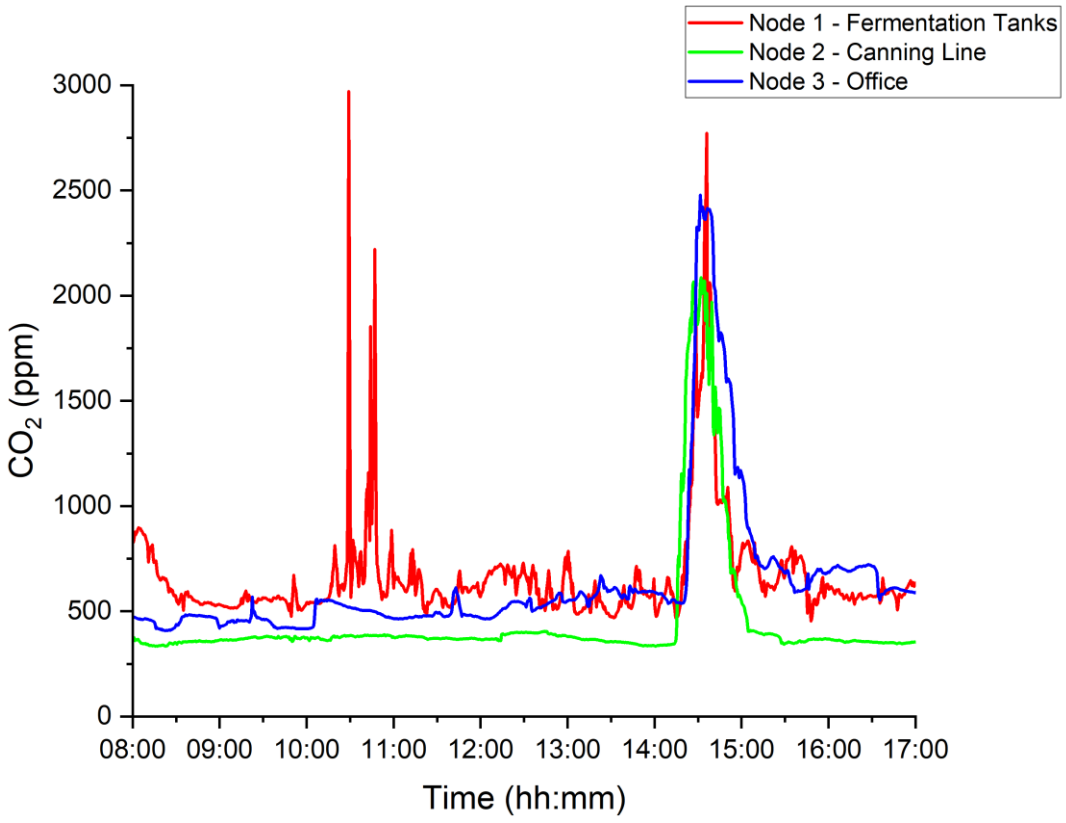

Figure 49. CO_2 measured versus time for venting day 5 at the fermentation tanks (Node 1), canning line (Node 2) and office (Node 3) locations.

In order to provide further evidence of venting raising CO_2 concentrations, the CO_2 values for all 3 nodes against time for venting day 5 is presented in Figure 49. It can be seen that there are 2 series of spikes in CO_2 concentration levels. The first series of spikes occurred at approximately 10:30 am and can be attributed to venting event 5a which consisted of venting one of the upstairs fermentation tanks (Tank 9). Venting event 5a was recorded to have taken places at 10 am in Table 6, however this is within the 60 min tolerance. In this case, only Node 1, which was upstairs, recorded an increase in CO_2 concentrations above the baseline. The second series of spikes, which occurred at approximately 2:30 pm, occurred due to venting event 5b which was recorded to have occurred at 2 pm in Table 6, however this is also within the 60 min tolerance. During this event, all 3 nodes saw an increase in CO_2 concentration above

the baseline, this can be attributed to venting event 5b being a top-up of stored CO_2, therefore it appears that a large volume of vented CO_2 was released resulting in all 3 nodes seeing an increase in CO_2 levels, while venting event 5a most likely was a release of a lesser amount of CO_2, thus resulting in only Node 1 seeing an increase in CO_2 levels. It is also interesting to note that all 3 locations did not see CO_2 levels return to baseline throughout the working day unlike Figure 47 and Figure 48, this was most likely due to the fact that 2 venting events took place throughout the working day with substantial volumes of CO_2 vented and/or worse ventilation throughout the brewery due the roller door not being raised completely. It would be interesting to investigate, in future, the direct relationship between CO_2 levels and how open the roller door is, as this information impacted the results. On the other hand, this finding can also be linked to the need for increased ventilation systems within the brewery, however they are costly, ventilation can also be improved by ensuring the roller door remains fully open, however this is very difficult to enforce without an automatic roller door system which is also costly.

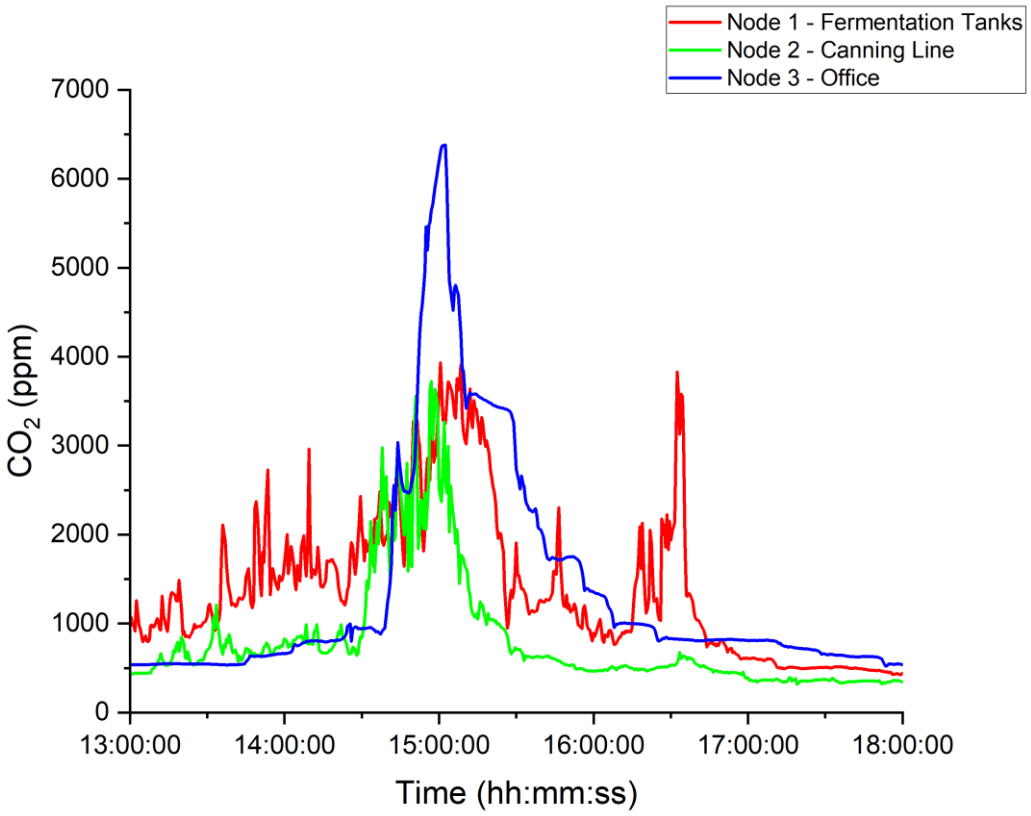

Figure 50 CO_2 measured versus time for venting day 2 at the fermentation tanks (Node 1), canning line (Node 2) and office (Node 3) locations.

In both venting events CO_2 concentrations were increased above baseline concentrations and above safe limits of 1,000 ppm and above 2,500 ppm resulting in the potential creation of unsafe working environments, however as venting event 5a only resulted in Node 1 recording increased CO_2 values, it is furthermore evident that 1 hardwired sensor is not adequate to measure brewery CO_2 levels as the distribution is not uniform.

When comparing venting event 5b with 6a, it can be seen that both venting events are CO_2 top-ups, however both share dissimilar maximum CO_2 concentrations recorded by Nodes 1 - 3. Venting event 6a resulted in CO_2 levels that were at least above 3,000 ppm, while venting event 5b resulted in levels above at least 2,000 ppm, this was most likely due to inconsistencies in the volume of pumped CO_2 in the top-up tanks and/or ventilation within the brewery which will be discussed later. Also comparing Node 1 for both venting events 5b and 6a, it can be seen that the CO_2 values are very similar, however when comparing Node 2/3 it can be seen that CO_2 values are much higher particularly for Node 3. It is therefore evident that even though two venting events on paper may look the same, which may lead to the prediction that both venting events would result in similar CO_2 values, they are in fact very different in this case, therefore CO_2 monitoring is vital in all workspaces.

The CO_2 values for all 3 nodes against time for venting day 2 is now presented in Figure 50 to provide further evidence of venting's direct relation with raising CO_2 concentrations above the baseline in the brewery. From Figure 50 it can be seen that there are 2 regions in which the CO_2 concentrations begin to increase above 3,000 ppm, the first begins at approximately 2:30 PM at can be attributed to venting event 2a (recorded at 2 PM but within 60 min tolerance), and the second begins at approximately 4:20 PM and is most likely the result of venting event 2b (recorded at 4 PM but within 60 min tolerance). It is interesting to note that even venting the bright beer tanks (2b) resulted in increased CO_2 concentrations within the brewery. Comparing venting event 2a with other venting events it can be seen that venting event 2a, 5b and 6a share similarities in which all 3 venting events increased the CO_2 levels in all 3 locations, with Node 1 and Node 2 taking about 1 hour to reduce back to somewhat normal levels and Node 3 in most cases taking longer due to limited ventilation. It would be expected that further similarities would be present, however this was not the case due to reasons that will be discussed later.

Overall, it can be seen from the results, that most venting events directly resulted in some form of increased CO_2 concentration above the baseline, this is concerning as CO_2 concentrations were not only raised above the baseline but also above the safe limit of 1,000 ppm for extended periods in the case of the office location (Node 3). This along with the fact that CO_2 concentrations do not appear to be uniform, strengthen the need for a network of wireless IoT sensors that can uniformly monitor CO_2 elevations throughout the brewery to support safe working environments.

The maximum CO_2 concentration (ppm) recorded by each sensor node for each venting event is presented in Figure 51. The maximum is deduced by inspecting the time-dependent CO_2 concentration for a period of 60 min either side of the nominal vent time, to determine any increase in measured CO_2 as a result of venting relative to the baseline concentration, however, both peak concentration and time to respond following the venting event varied significantly, without clear or explainable correlations. This is apparent in Figure 51, where there is no obvious relationship between one region of the brewery accumulating CO_2 more readily than any other. Likewise, this does not appear to be significantly influenced by which tank is vented. In three cases (7, 8a and 10b), no discernible increase in CO_2 is apparent, however, in the majority of cases, a significant rise in CO_2 is detectable. One might expect that CO_2 would accumulate in one area more than others; however, this seems not to be the case when fermentation tanks are vented, irrespective of the position of the tank. Likewise, while the vent durations are almost always 30 min, it is likely that the vented volume of CO_2 is significantly different in each case, due to differences in flow rate. It would be interesting in future to equip the vessels with flowmeters to record both the volume and rate of CO_2 introduction into the brewery, rather than the time. Equally, there is no indication that longer venting times, e.g., 8a and 10a, lead to higher levels of recorded CO_2.

While it is perhaps surprising that clearer trends are not apparent, this can also be likely explained by the complicated air movements within the brewery space, influenced by the movement of people, the use of fans, the use of an office door and the presence of a large roller door that remains mostly open during working hours, meaning outdoor air flow (wind speed and direction) can play a significant role in how the vented gas moves within the brewery space. This complex air movements can most likely create scenarios that are not identical even if the venting events are, for example venting from storage tank top-ups results in non-identical CO_2

increases in all cases due to variations in air movements that are non-identical even though the amount of CO_2 being toped-up should roughly be the same.

4.1.2 Maximum CO_2 Concentrations

Figure 51 depicts that the maximum CO_2 levels recorded for each node are 18,420 ppm for Node 1 (fermentation tanks), 5,538 ppm for Node 2 (the canning line) and 13,100 ppm for Node 3 (the office). It should be noted that the sensor remains accurate to an upper limit of only 10,000 ppm, so values above this are indicative only. That said, the maximum CO_2 levels are well above the 1,000 and 10,000 ppm benchmarks, and it can also be seen from the results that almost every vent, approximately 65% (11/17), have directly influenced excessive CO_2 levels above 1,000 ppm, strengthening the correlation between venting events and increased CO_2 concentrations.

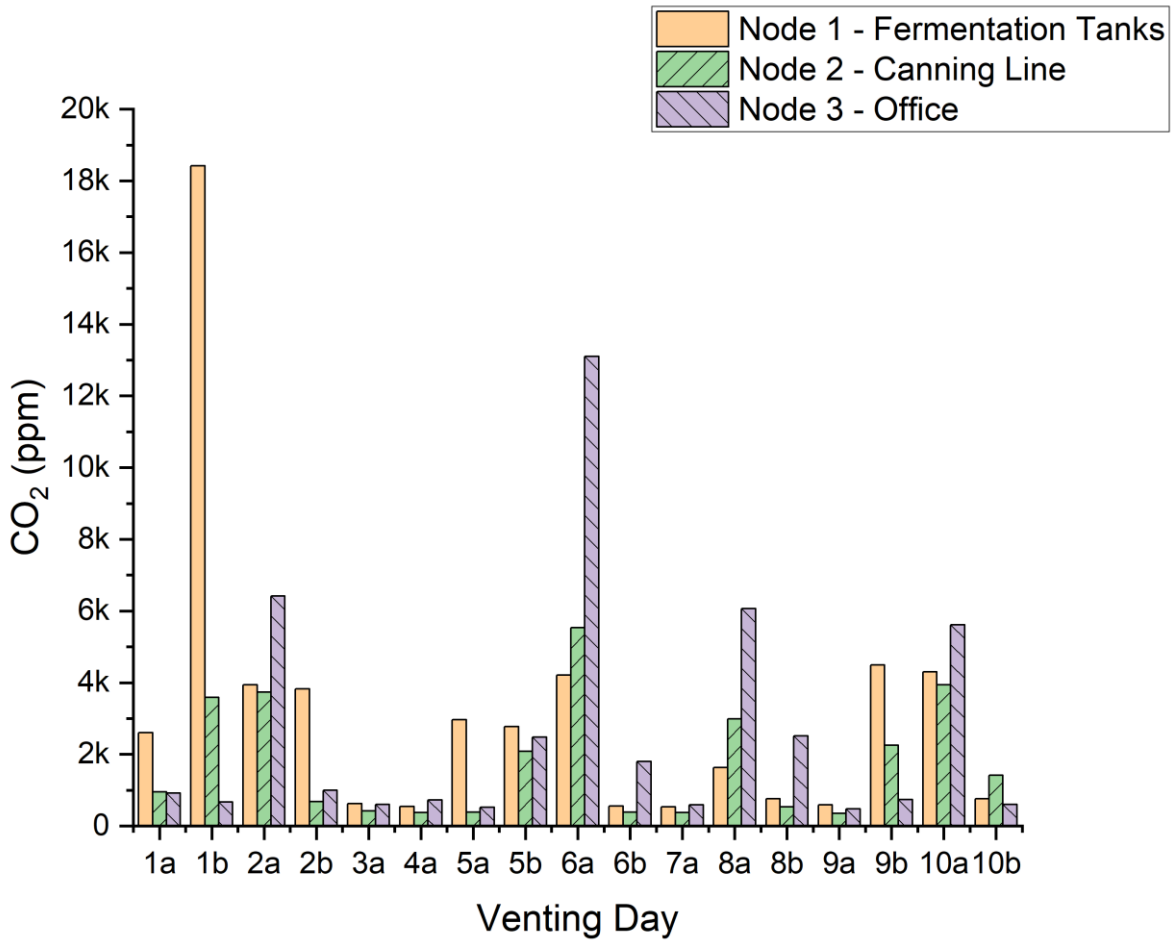

Figure 51. Maximum CO_2 measured by each sensor node for every venting event.

It is likely that the observation of the maximum CO_2 level of 18,420 ppm results from a "perfect storm" of influencing factors. The corresponding venting event took place at 7 pm, therefore the main source of ventilation (roller door) was not present, as it was shut at roughly 5 pm every working day. At the canning line, the CO_2 peak reaches almost 4,000 ppm for the same venting event. For the sensor in the office, a peak is not noticed since the door to the office was also closed at approximately 5 pm, likely impeding the transfer of air from the main brewery zone. Importantly, it was indicated by the staff that venting after 5 pm is not an uncommon occurrence. This leads to the possibility of very high and dangerous levels of CO_2 being present in the brewery space.

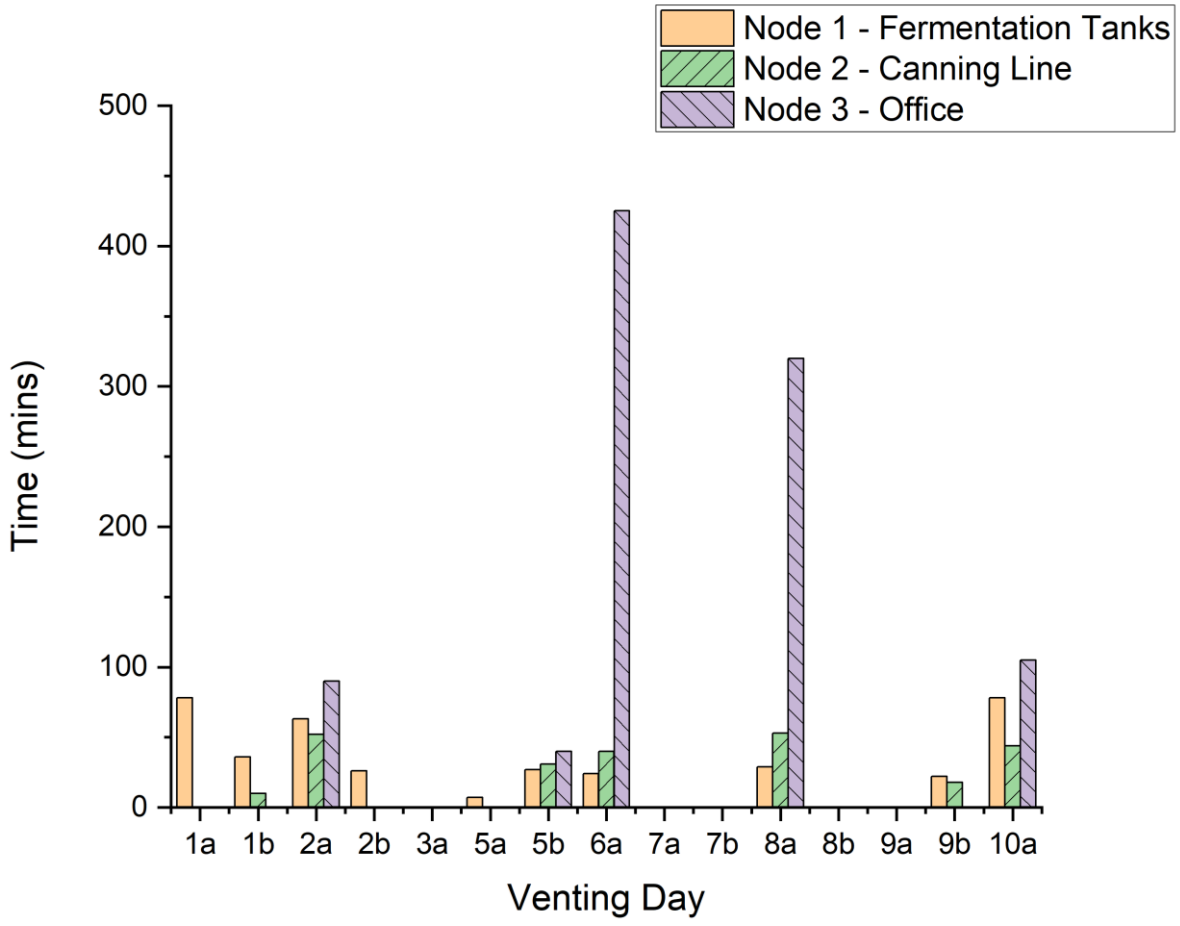

Figure 52. Consecutive time the CO_2 concentration remained above 1,000 ppm for each venting event.

Venting event 6a also generates large concentrations of measured CO_2. This occurs as a result of a refill of CO_2 storage tanks within the building and is most likely due to vapor from liquid

CO_2 unintentionally being released. Since this process occurs close to the office (Node 3), it is not surprising that Node 3 detects the highest concentration of CO_2 approximately 13,000 ppm. This again raises a concern for office staff working in the office, as the CO_2 level remains above 10,000 ppm for 26 min in this case.

The time (mins) that the CO_2 level remained above 1,000 ppm for each node for each venting occurrence is presented in Figure 52. The maximum consecutive amount of time CO_2 levels exceed 1,000 ppm for each node is 425 min for Node 3, 78 min for Node 1 and 53 min for Node 2. 10,000 ppm is exceeded in two cases for durations of 26 min for Node 3 and 3 min for Node 1. High CO_2 levels coupled with the extended periods of potential exposure have the potential to create a hazardous working environment for the brewery staff due to physiological and/or cognitive effects, combined with the nature of work, as discussed in Section 1.1.

For venting events 2a, 6a, 8a, and 10a, where all 3 nodes exceed 1,000 ppm, sensor Node 3 measures the longest period for CO_2 levels above 1,000 ppm, further indicating that the office area is not well ventilated compared to other areas of the workplace and strategies should be considered to reduce the excessively long periods (up to 425 min) when CO_2 exceeds 1,000 ppm, to prevent staff from being exposed to potential unsafe working environments.

Huizen (2020) [56] measured the CO_2 level inside several breweries ranging from small (<10,000 bbls) to large (>100,000 bbls), with the brewery in this research project being equivalent to a small brewery. Huizen (2020) recorded CO_2 ranging from 2,422 - 2,851 ppm within tested small breweries for 95% of the time tested. This result reinforces the results and corroborates the finding that high concentrations of CO_2 well above 1,000 ppm can be found in breweries, however, it is difficult to directly compare the results received in this research project with that of Huizen's system for two reasons, firstly, Huizen's system consisted of a wearable, mobile sensor, not a network of static sensors, secondly, and perhaps of most significance, the work in this research project focuses on the peaks of CO_2 exposure for periods of CO_2 venting. It can be assumed that Huizen might also have noted extremely high peaks had the mobile sensors been close to fermentation tanks during indoor exposure, using high sampling frequency.

4.1.3 Beyond a Single Hard-Wired Sensor

The concentration of CO_2 within the air in the brewery is clearly influenced by the venting of fermentation/stored CO_2 tanks, creating potential hazardous environments, however, the identification of differences in measured CO_2 at different times and locations throughout the brewery (Nodes 1–3) also reveals that a single hard-wired CO_2 sensor may be inadequate to support IAQ monitoring. This strengthens the need to have a network of CO_2 sensors inside a craft brewery. For this purpose, portable CO_2 sensor nodes might be more suitable, imitating the approach taken to radiation dosimetry, for example, this would allow the monitoring of CO_2 levels for the purpose of protecting the workforce and could safeguard the entire workplace, including inside fermentation tanks where workers often have to place their head, without the need for multiple hard-wired sensors in each area which may be unfeasible. They could also allow the workers to be warned in real-time of potential CO_2 dangers that may occur if they proceed with a task.

4.2 Sensor Power Testing

4.2.1 Battery Life

For portable sensors, the battery life (hours) for each sensor node is a key consideration. While a hard-wired sensor receives constant power, a portable sensor would create a battery recharge/replacement burden, therefore, a relatively long battery life is required in order to remove this burden allowing for feasible implementation. In Figure 53, the average battery life for the 3 wireless Wi-Fi sensor nodes used in Section 4.1 is presented.

The largest battery life was measured for Node 2, at approximately 240 hours (10 days), however, Node 3 had a battery life of approximately 200 hours, while the battery life of Node 1 was only approximately 120 hours. During experimentation, the batteries for each node had to be changed every 120 hours for consistency. The total battery capacity of each node was equal to 14,000 mAh, therefore Node 1 consumed the most average current of approximately 116 mA, while Node 3 consumed 70 mA on average, and finally, Node 2 had an average current consumption of 58 mA.

The large difference in battery life was mainly attributed to differences in current draw that resulted from different and variable obstacles in the workplace between the sensor nodes and

wireless access point, such as piled up cans and kegs. This, along with the fact that the brewery had 2 floors, made it difficult to determine any relationship between sensor node location and current consumption. For example, Node 3 is the furthest away from the access point, however it did not have the most current consumption due to being in direct line of sight while Node 2 was the closest to the access point but did not have the least current consumption due to not being in direct line of sight and under the walkway as depicted in Figure 29.

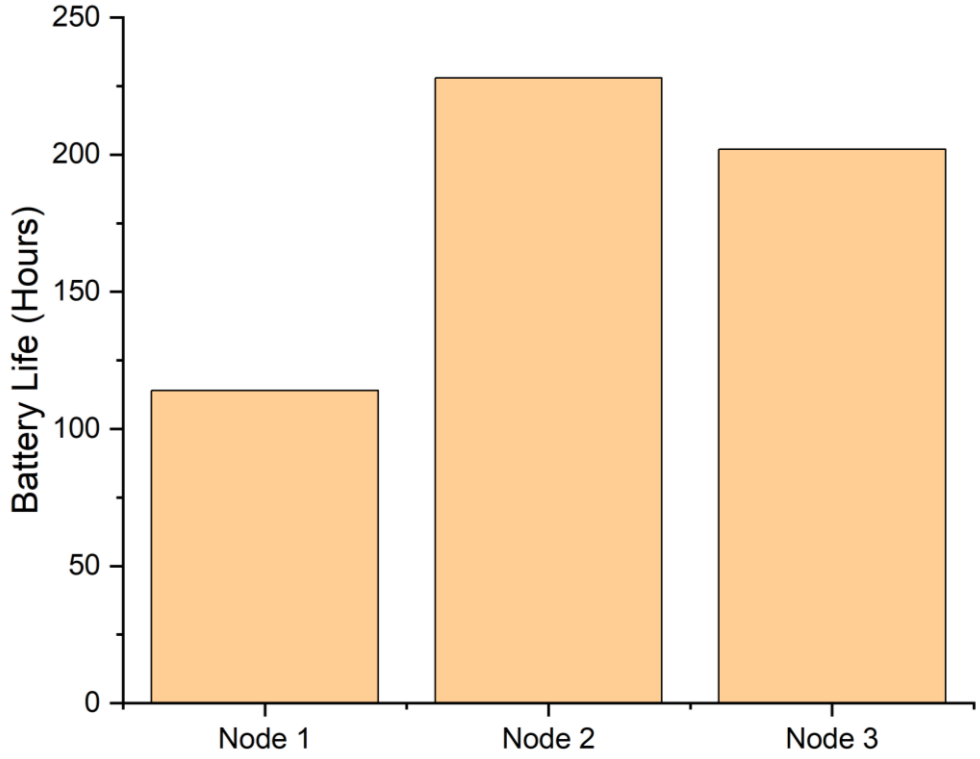

Figure 53. Sensor node battery life.

The increase in average current consumption when objects are introduced between the sensor nodes and access point is expected due to the objects reducing the signal strength of the Wi-Fi connection as highlighted in [63], therefore more current is required in order to produce a consistent Wi-Fi signal.

The relatively short battery life of the current sensor network leaves a lot of room for improvement, and such a short battery life would not be feasible for workplaces adopting IoT technologies, since they would need to recharge or replace the batteries in each sensor node roughly every 5 days [43]. A low-power sensor and communication protocol could be utilized to significantly extend the battery life of sensors [43], making the principle more feasible. This

will be investigated in future sections of this thesis. Other strategies to mitigate exposure to CO_2 in breweries might include careful consideration of ventilation of the vented CO_2 during brewery design, the possibility of technology that vents the CO_2 to the outside, personal protective equipment (PPE) for brewery staff, or the enforcement of regular "fresh air" breaks to prevent exposure over significant time frames.

4.2.2 Minimizing Power Draw

Measuring the CO_2 values across several workspaces in an Australian brewery from the previous section led to the conclusion that the concentration of CO_2 within the air in the brewery is clearly influenced by the venting of fermentation/stored CO_2 tanks, creating potential hazardous environments while the identification of differences in measured CO_2 at different times and locations throughout the brewery (Nodes 1 - 3) revealed that a single hard-wired CO_2 sensor may be inadequate to support IAQ monitoring. This strengthens the need to have a network of CO_2 sensors inside a craft brewery, however the battery life of the Wi-Fi sensor nodes used previously was inadequate and therefore created a battery recharge/replacement burden that needs to be removed in order for a network of wireless IoT sensors to be feasibly implemented.

This section will address research question 2, namely "can a network of wireless IoT-enabled sensors be created to monitor CO_2 in various locations in parallel with low power consumption and long battery life?" This research question will be addressed by attempting to reduce the battery recharge/replacement burden of the aforementioned Wi-Fi sensor nodes by implementing LoRa, a low powered wireless protocol that has been shown in previous literature to drastically reduce the power consumption of IoT technology. The created LoRa sensor node will firstly be optimised for low-power CO_2 measurement applications, it will then be compared to a similar Wi-Fi sensor node to outline and highlight its effectiveness at removing the battery recharge/replacement burden of IoT technology.

4.2.2.1 Data Rate

The first attempt at reducing the power draw of the grasshopper LoRaWAN board used in the LoRa sensor nodes included the adjustment of the data rate of the signal, alongside a CO_2 sampling rate of 7 s. Optimizations were done alongside the LoRa LP3 node, as well as the

LoRa SCD30 node reported in future sections. The average current draw with regards to data rate variability DR(0 - 5) + TX(30) for the LoRa (LP3) sensor node is depicted in Figure 54 with DR and TX representing the data rate and transmission power setting used, respectively. Increasing the data rate from 0-5 of the LoRa connection decreased average current draw exponentially. DR(0) + TX(30) and DR(5) + TX(30) resulted in average current draws of 26.24 mA and 11.12 mA respectively, indicating that a decrease in average current of 57.62% was achievable simply by adjusting DR values.

Comparing the average current consumption of the LoRa (LP3) node with the Wi-Fi node from Section 4.1 indicates that a substantial drop in average current from 58 mA to 11.12 mA has already been achieved via LoRa optimizations alongside the implementation of a low powered LP3 CO_2 sensor, this is a drop of over 80% in average current, due to LoRa's low powered capabilities, however further improvements are required in order to extend battery life beyond that which creates a battery recharge/replacement burden.

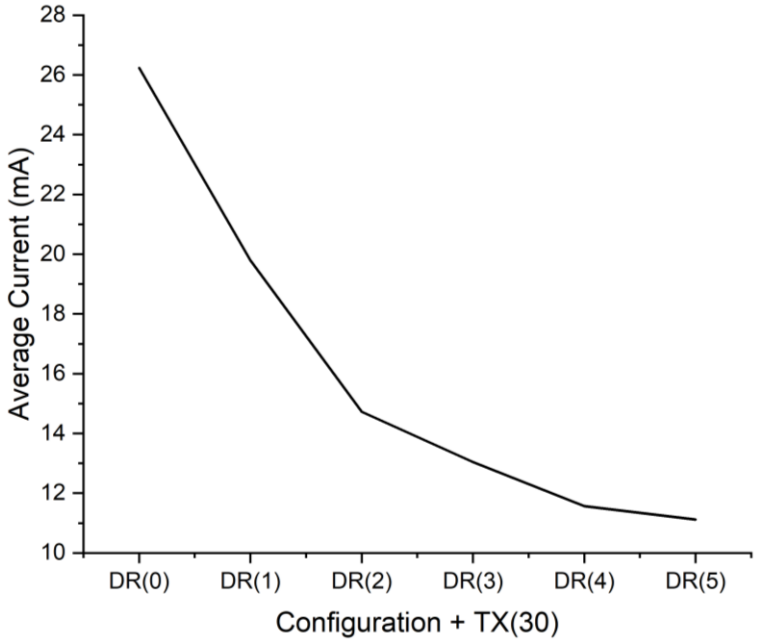

Figure 54. LoRa (LP3) sensor node - average current for DR(0 - 5) + TX(30) configurations.

Figure 55 depicts the current draw over time for DR(0) + TX(30) and DR(5) + TX(30) to highlight the reasoning behind the increased data rate leading to decreased current draw, Figure 55 also contains a breakdown of the particular processes experienced by the LoRa (LP3) sensor node to create a better understanding of the current draw data. Step 1 appears to be the boot up

stage of the sensor node were a large but short amount of current has been consumed. Step 2 is the idle stage, where the sensor node sits idles until 150 s. There we can clearly see the current consumption of the CO_2 sensor, which is depicted as multiple triangular peaks. Lastly, Step 3 is the transmission stage where multiple peaks can be seen, alongside sensor consumption, pertaining to transmission of the CO_2 data to the LoRa gateway. The steps mentioned above were present in every LoRa (LP3) trial, therefore the 150 s interval until first reading was consistent and has been taken into account for every average current calculation.

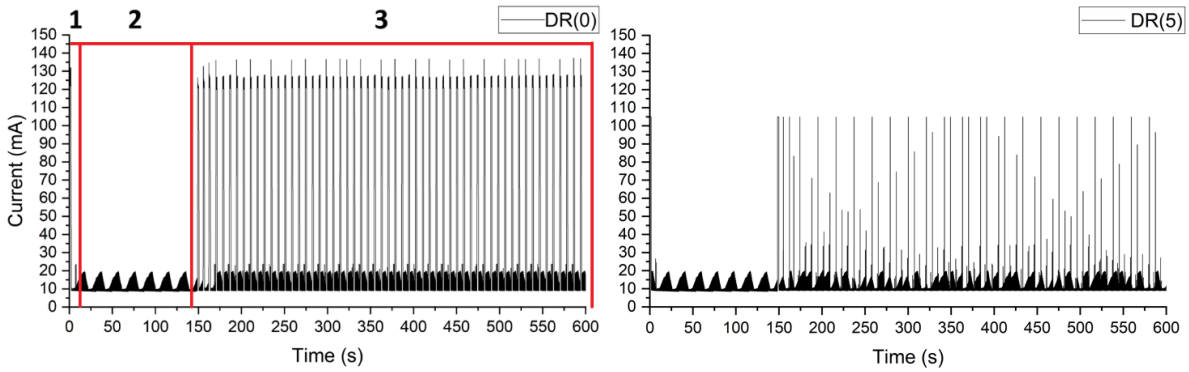

Figure 55. LoRa (LP3) sensor node - current vs time for DR(0, 5) + TX(30) configurations, 1: start-up, 2: idle, 3: transmission.

Figure 55 shows that DR(0) + TX(30) appears to have larger maximum current peaks, within the transmission step, of approximately 130 mA as opposed to 110 mA at DR(5) + TX(30), while also containing more frequent and prolonged (bolder) maximum peaks. This is most likely due to the lower bitrate of DR(0) increasing packet transmission times which was also evident by the observation of 8 s intervals between CO_2 measurement data being sent to TTN as opposed to 7 s with DR(5) + TX(30), therefore more current is required for a prolonged period (during Transmission) with lower DR values/bitrate due to longer times to transmit sensor data.

It is evident from the data rate results that DR(5) + TX(30) resulted in the least amount of average current draw equivalent to 11.12 mA, therefore the next step with regards to reducing the power consumption of the grasshopper LoRaWAN board included varying transmission power alongside a data rate value of 5.

It should be noted that DRs above 5 were tested and resulted in an inconsistent payload interval being received by TTN, which is most likely attributed to the faster bandwidth/bitrate not being completely supported by the grasshopper board, therefore only DR(0-5) was documented.

In reference [43], tests varying DR were conducted on the Grasshopper LoRaWAN board and it was concluded that, similar to the results recorded above, an increase in DR led to an exponential decrease in power consumption, this trend is therefore as expected and corroborates the results and experimental process.

4.2.2.2 Transmission Power

The next step in attempting to remove the battery recharge/replacement burden included varying the transmission power of the Grasshopper LoRaWAN board with the hopes of reducing average current even further. The average current draw with regards to transmission power variability TX(10 – 30) + DR(5) for the LoRa (LP3) sensor node is depicted in Figure 56. An increase in TX resulted in an exponential increase of average current draw for TX(10-22) + DR(5) and an inverse exponential increase for TX(22-30) + DR(5), however TX(10) + DR(5)) and TX(30) + DR(5) resulted in average current draws of 10.10 mA and 11.12 mA respectively, indicating that a decrease in average current of 9.17% was achieved by simply decreasing the TX value.

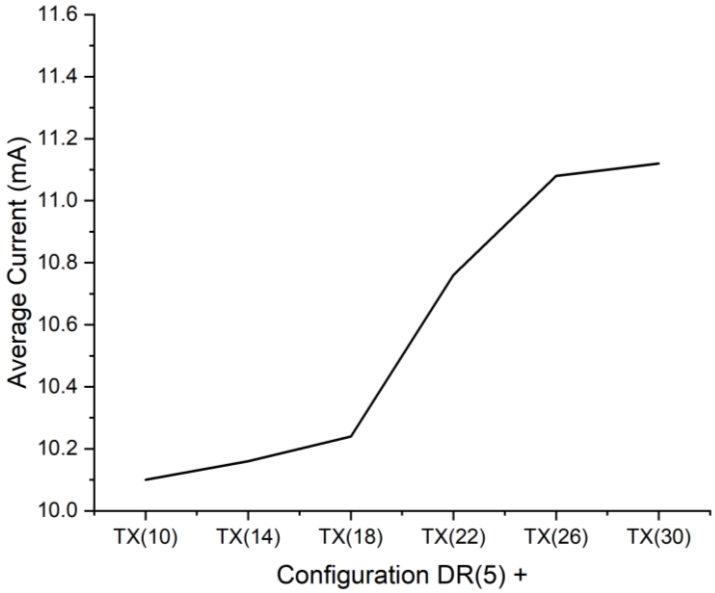

Figure 56. LoRa (LP3) sensor node - average current for DR(5) + TX(10-30) configurations.

Figure 57 depicts the current draw over time for TX(10) + DR(5) and TX(30) + DR(5) of the sensor node to highlight the reasoning behind increased transmission power leading to increased current draw. The prominent reason for increased TX values leading to increased average current draw is attributed to higher TX values having larger maximum current peaks during the transmission step, TX(10) + DR(5) and TX(30) + DR(5) have peak values of 30 mA and 100 mA respectively, this is due to the larger TX values being directly related to increasing the range of the LoRa signal, therefore requiring more power.

The configuration of TX(10) + DR(5) resulted in the least amount of average current draw equivalent to 10.10 mA, however this average current draw is likely too large to remove the battery recharge/replacement burden of the sensor node, therefore further optimizations are required.

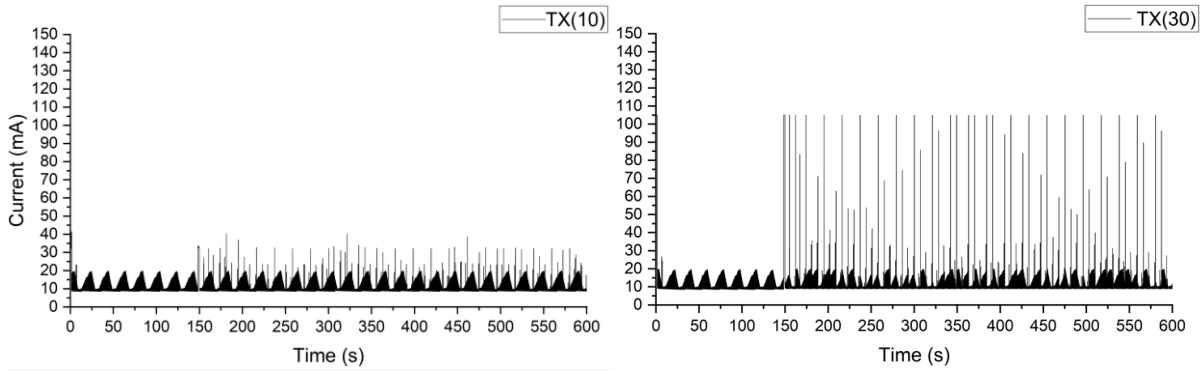

Figure 57. LoRa (LP3) sensor node - current vs time for DR(5) + TX(10, 30) configurations.

Ould and Bennett (2022) [43] conducted tests by varying TX on the Grasshopper LoRaWAN board concluding, similar to the results recorded above, that an increase in TX led to an increase in power consumption, this trend is therefore as expected and increases the validity of the above results and experimental procedure.

4.2.2.3 Arduino IDE Coding Optimization

The LoRa (LP3) sensor node's average current draw of 10.10 mA with TX(10) + DR(5) was optimized next by adjusting the Arduino IDE code and removing the if loop below from the void loop, that is *if (!LoRaWAN.busy() && LoRaWAN.joined())*.

This resulted in a decrease of average current draw from 10.10 mA to 4.54 mA which is equivalent to a decrease of 55.05%. More than half the current consumption has been saved by removing 1 simple line of code, indicating the need for code optimization. The if loop was most likely increasing current draw due to the board consistently checking if the LoRaWAN connection was active every void loop cycle, therefore its omission resulted in no discernible side effects. This truly highlights the need to optimize Arduino code to ensure the particular board in use is performing within optimal conditions.

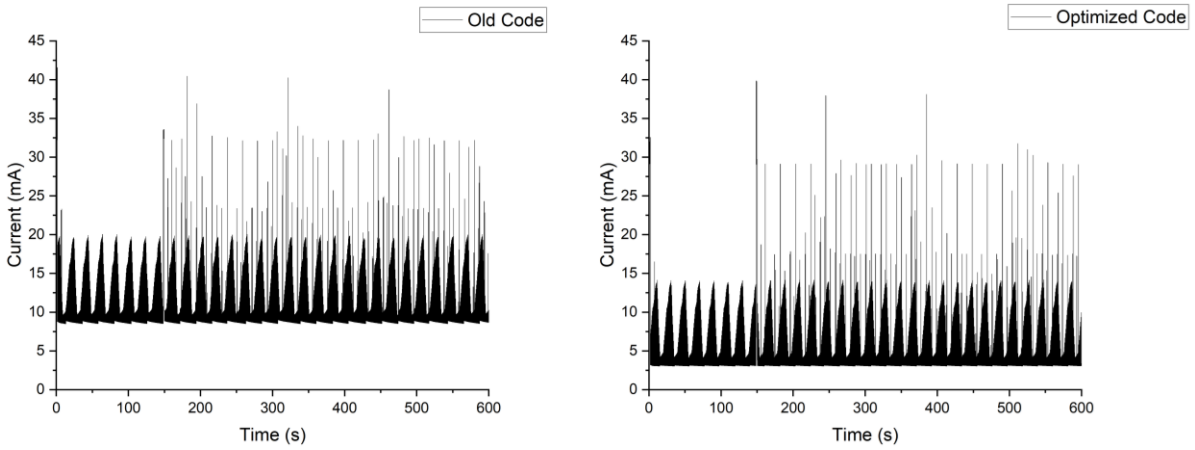

Figure 58. LoRa (LP3) sensor node - current vs time for old and optimized Arduino IDE code.

Figure 58 depicts the current draw over time for the sensor node with the Old and Optimized Arduino codes applied to highlight the reasoning behind the current consumption decrease with the new code. It can be seen that the baseline current has decreased by over 5 mA due to the removal of the if loop which was consuming unnecessary current. It can also be seen that there are no discernible side effects due to only the baseline current differing and not the CO_2 sensor or transmission current trends as highlighted in Figure 55, therefore evidencing the fact that the LoRa (LP3) sensor node was performing as expected.

Although the LoRa (LP3) sensor nodes average current was reduced from 26.24 mA to 4.54 mA, a decrease of over 82%, this is most likely not a large enough decrease in average current to remove the battery recharge/replacement burden, therefore further optimizations were pursued.

4.2.3 LoRa, Wi-Fi Power Comparison

4.2.3.1 Sensor Frequency

Comparing the Wi-Fi (LP3), LoRa (LP3), and LoRa (SCD30) sensor nodes average current consumption required the testing of different sampling rates of the varying CO_2 sensors. This was done as the final attempt to reduce the average current consumption of the LoRa (LP3) sensor node while also highlighting the advantages of using it as opposed to the other nodes tested.

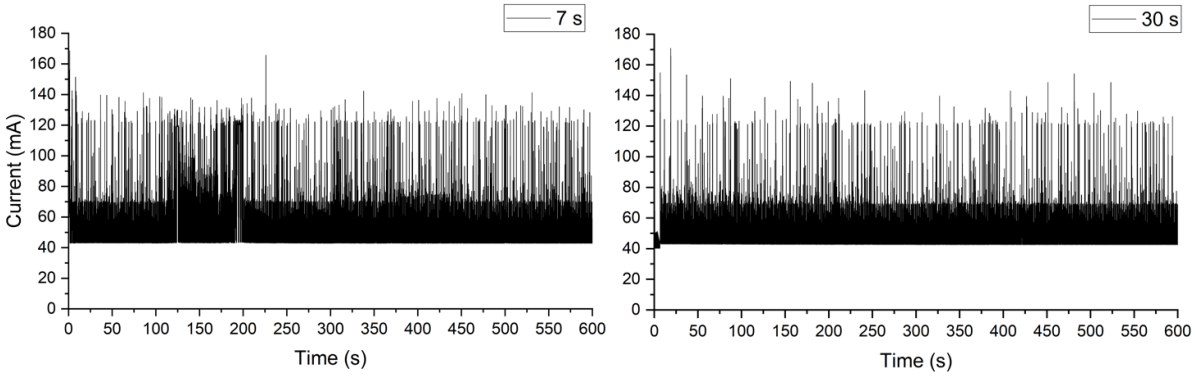

Figure 59. Wi-Fi (LP3) sensor node - current vs time for 7 and 30 s CO_2 measurement intervals.

The Wi-Fi (LP3) sensor node was tested first with Figure 59 depicting the current draw over time for the Wi-Fi (LP3) sensor node at CO_2 measurement intervals of 7 s and 30 s to highlight the advantages/disadvantages of increasing measurement interval. It appears that the Wi-Fi (LP3) sensor node has no idle step and therefore contains transmission from start to power off, this can be seen as an advantage due to the ease of connection when it comes to initial readings, however it was practically harder to connect the Wi-Fi (LP3) sensor node due to it having to connect to both the Wi-Fi and an MQTT server which adds another layer of complication. Maximum peak current appears to be the same in both cases throughout transmission, however the frequency at which the peaks occur decreases for the 30 s interval, as expected, due to the decrease in packets being sent, this ultimately results in decreased average current draw. An increase in measurement intervals for the LoRa sensor nodes will therefore most likely lead to a decrease in average current consumption for the same reasons as aforementioned, however this will be further tested next.

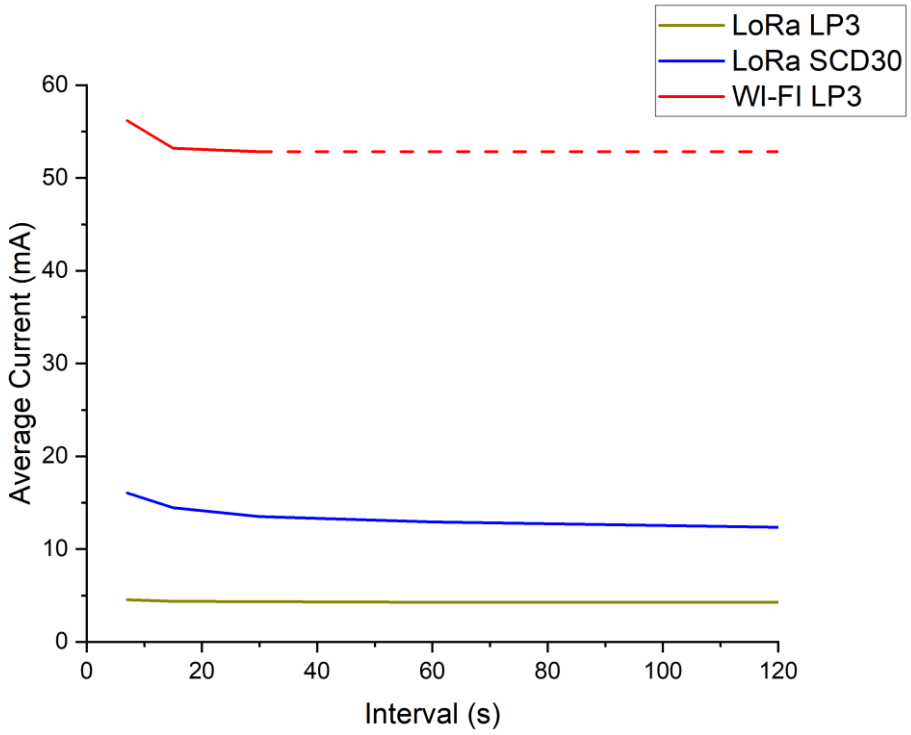

Figure 60. Average current draw of sensor nodes for CO_2 measurement intervals of 7 - 120 s, dashed line: expected values.

The LoRa sensor nodes were tested next with the average current draw of varying CO_2 measurement intervals for all 3 sensor nodes depicted in Figure 60. An increase in measurement interval resulted in a decrease of average current draw for all 3 sensor nodes, however the Wi-Fi (LP3) sensor node appeared to decrease more compared to both LoRa sensor nodes with TX(10) + DR(5) configurations, this is most likely due to Wi-Fi's high-power usage when sending packets due to its larger bandwidth capabilities which are suited to other use cases such as video streaming. The Wi-Fi (LP3) sensor node resulted in the largest average current draw at 30 s of 52.81 mA compared to 4.33 mA and 13.51 mA for the LoRa sensor nodes with the LP3 and SCD30 configurations respectively. It can also be seen that LoRa draws at least 74.42% less average current than Wi-Fi at a 30 s measurement interval strengthening LoRa's feasibility to be used for wireless IoT technology. It should be noted that tests passed a 30 s interval were not possible with the Wi-Fi (LP3) sensor node due to disconnection as a result of the Sparkfun board entering sleep mode, hence the dashed line in Figure 56 indicated expected results only.

Increasing the measurement interval of both LoRa sensor nodes from 7 s to 120 s resulted in decreased average current draws of 4.54 mA to 4.26 mA for the LP3 configuration, and 16.05 mA to 12.35 mA for the SCD30, or 6.17% and 23.05% respectively. It can be seen that the SCD30 configuration did result in a greater decrease in average current with increased measurement interval, however baseline current without packet transmissions was averaged by removing the measurement interval form the Arduino IDE code and resulted in approximately 8.71 mA for the SCD30 configuration as opposed to 4.26 mA for the LP3 configuration, therefore the new innovative LP3 CO_2 sensor requires below 50% of the average current used with traditional sensing methods, therefore the LoRa (LP3) sensor node was used for future comparison tests.

The relatively slim average current decrease with an increase in measurement interval for the LoRa (LP3) sensor node, although demonstrating LoRa's exceptional power efficiency, indicates that it is best to set the measurement interval at 7 s due to the increase in measurement resolution with minimal increase in power consumption, therefore the final average current consumption of the LoRa (LP3) sensor node after all optimizations was equivalent to 4.54 mA which is a decrease of over 82%. this is most likely not a large enough decrease in average current to remove the battery recharge/replacement burden of IoT technology completely, however fit is a significant improvement.

Comparing the optimizations made to the LoRa (LP3) sensor node in this section with the Wi-Fi wireless IoT sensor nodes used in Section 4.1, it is evident that the maximum battery life of the Wi-Fi nodes was equal to approximately 240 hours (10 days) with an average current consumption of 58 mA, while the LoRa (LP3) node consumes approximately 4.54 mA on average. If the LoRa (LP3) node was therefore connected to the same 14,000 mAh batteries it should achieve approximately 3084 hours (128 days) of battery life, a substantial increase of almost 13 times the battery life.

4.2.3.2 Obstacle and Distance Testing

Decreasing the current consumption of the IoT sensor nodes used to measure CO_2 is advantageous for removing the battery recharge/replacement burden of IoT technology, however is it practical? The next experiment will analyse the Wi-Fi (LP3) and LoRa (LP3) sensor nodes to determine whether LoRa is practical in real world applications with regards to

obstacle and distance testing. Both nodes had a sampling frequency of 7s set, while the LoRa (LP3) node had a configuration of TX(10) + DR(5).

The obstacle and distance testing was done by moving the Wi-Fi and LoRa gateway around the UTS Tech Lab in the locations as depicted in Figure 35. The average current draw at different locations of the UTS Tech Lab for the LoRa (LP3) sensor node with the TX(10) + DR(5) configuration and Wi-Fi (LP3) sensor node is depicted in Figure 61. It is evident that the LoRa wireless protocol outperformed Wi-Fi with regards to maximum average current consumption due to the LoRa (LP3) sensor node having less maximum average current draw which was equivalent to 4.56 mA as opposed to the Wi-Fi (LP3) sensor node's 102.51 mA, therefore the LoRa (LP3) sensor node consumed 4.45% of the average current required for the Wi-Fi (LP3) sensor node.

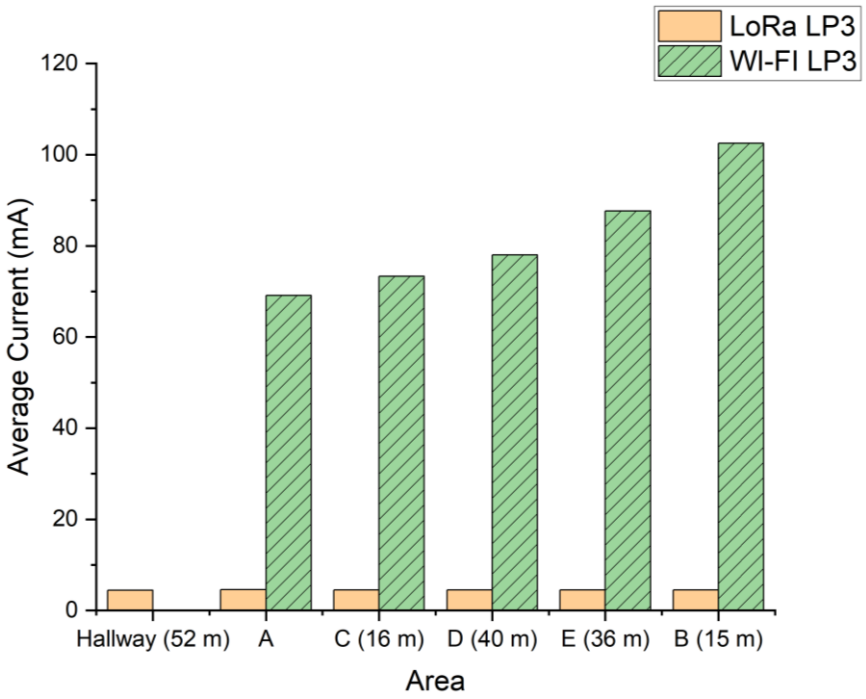

Figure 61. Sensor node average current draw at different locations within UTS tech lab.

The average current draw of the LoRa (LP3) sensor node also remained relatively constant at the different locations tested within the lab, this can be attributed to LoRa's remarkable propagation and penetration capabilities as expected and outlined in reference [64], while the Wi-Fi (LP3) sensor node's average current draw increases exponentially with an increase in both distance and building materials between the sensor node and hotspot, this is due to the

large impact that aforementioned can have on the Wi-Fi signal as expected and discussed in reference [63]. The Wi-Fi gateway at Point B seemed to be an exception to this trend however, as it resulted in the largest average current draw at the closest location to the desk, an influencing factor for this could be the space were Point B is located being fully enclosed with no potential opening for the Wi-Fi signals to propagate around the obstacles between the hotspot and sensor node as expected and outlined by [63], therefore the signal must propagate through all obstacles between the sensor node and hotspot. Reflective material can help in cases where obstacles are present and preventing line-of-sight [63], and is most likely the reason why locations such as the Wi-Fi gateway at Point E, which are further from the desk, do not result in an average current draw greater than that which is recorded at Point B as expected. It can also be seen that increasing the distance and/or obstacles, similar to tested, between the LoRa (LP3) sensor node and gateway has little to no effect on average current consumption as opposed to using Wi-Fi which resulted in an increase of 48.4%.

It should be noted that although the hallway location was the upper limit for the LoRa connection range, it managed to result in the least amount of average current draw, signifying that an increase in average current draw from the LoRa (LP3) sensor node, beyond that which was tested, is highly unlikely within practical applications, LoRa therefore consumes less average current, than Wi-Fi, while being capable of increased range and signal penetrability, therefore highlighting that LoRa is indeed better than Wi-Fi for the chosen application of IoT technology.

4.2.4 Optimized Battery Life

Testing the battery life of the Wi-Fi (LP3) and LoRa (LP3) was done to compare and highlight the advantages of using LoRa over Wi-Fi while also determining if the LoRa (LP3) sensor node's battery recharge/replacement burden was successfully removed with optimizations. Battery life results were achieved by creating an empirical model for a 1000 mAh battery using the Keithley 2281S battery simulator. This was then used to simulate consistent behaviour of a battery while connected to the sensor nodes, as depicted in Figure 37.

Figure 62 and Figure 63 depict the battery life results for the LoRa (LP3) sensor node with the TX(10) + DR(5) configuration and the Wi-Fi (LP3) sensor node. Figure 62 includes current and voltage versus time for a 10-minute extract of the total runtime. It can be seen from the

voltage plot in Figure 62 that both nodes initially discharge in a linear pattern as expected due to the linear decrease in voltage over time, however, the Wi-Fi (LP3) sensor node appears to discharge at a faster rate than its LoRa counterpart due to the larger decrease in voltage within the same 10-minute timeframe. It can also be seen that the current draw over time are fairly similar to that encountered in the previous sections, as expected since the sensor nodes are programmed to perform in exactly the same way.

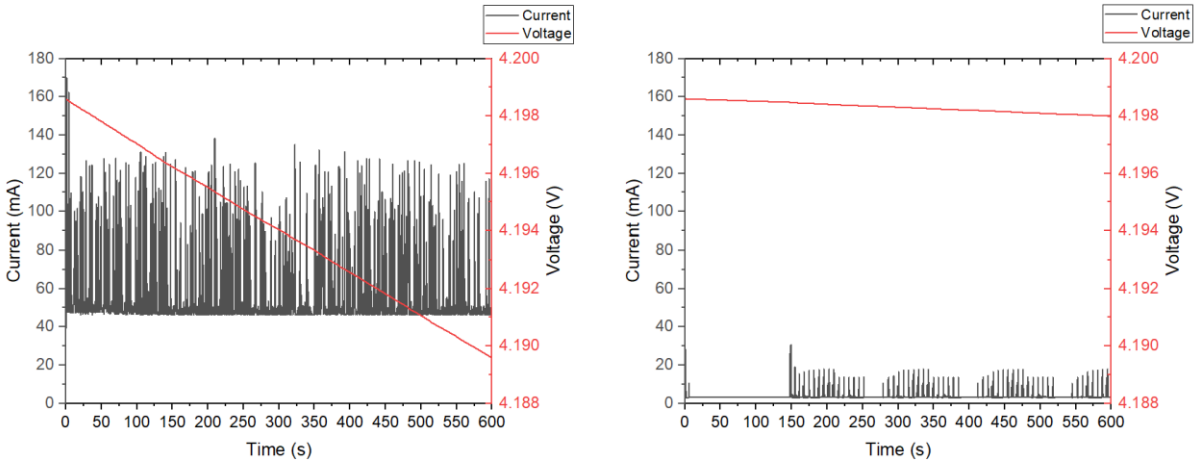

(a) (b)

Figure 62. Current & voltage vs time, a: Wi-Fi (LP3), b: LoRa (LP3).

Figure 63 depicts the voltage versus time of both sensor nodes. The Wi-Fi (LP3) sensor node achieved a total runtime of 16.98 hours while the LoRa (LP3) sensor node achieved 292.44 hours, therefore the Wi-Fi (LP3) node discharged at a rate that was 17.22 times faster than its LoRa counterpart. When taking the modelled battery capacity of 947 mAh and dividing it by the average current consumption of the LoRa (LP3) sensor node (4.56 mA) determined in previous tests in Section 4.2.3.2, the expected battery life of the LoRa (LP3) sensor node is approximately 207.7 hours, therefore the LoRa (LP3) sensor node's battery life is better than expected with that achieved being approximately 85 hours longer indicating that the LoRa (LP3) sensor node used even less average current with a longer runtime. This can mostly be attributed to the large current requirement with first boot-up of the sensor node that has less impact on average current as runtime is increased. It can also be seen that battery voltage in both cases discharges with a similar linear trend up to about 3.5 V as expected due to both batteries being sharing the same model using the battery simulator.

Overall if the nominal voltage of the battery used in the simulation (3.7 V) and the average current consumption over time for the sensor nodes is used to calculate the power required. The LoRa (LP3) sensor node with the TX(10) + DR(5) configuration would need approximately 11.96 mW, while the Wi-Fi (LP3) sensor node would require 202.05 mW. It is therefore evident from the results that implementing LoRa within a wireless IoT sensor network could lead to sensor node power consumption that is 94.08% less than a Wi-Fi network. It should be noted that if batteries were to be used with both sensor nodes, in order to get the same runtime out of the Wi-Fi (LP3) sensor node, you would need to recharge the same battery at least 18 times.

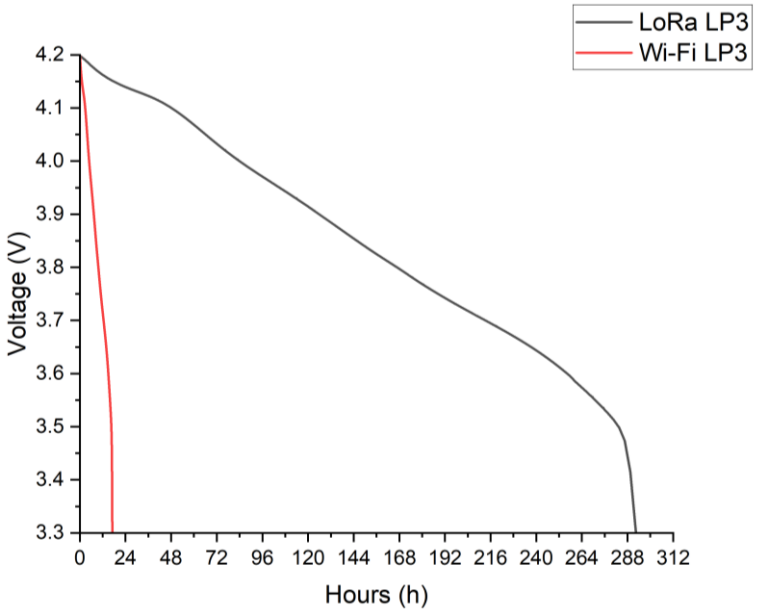

Figure 63. Voltage vs time for Wi-Fi (LP3) and LoRa (LP3) sensor nodes.

LoRa was successful at increasing the battery life of a wireless CO_2 sensor node, however approximately 290 hours of battery life is still not adequate to provide means for creating wireless IoT sensor networks that are feasible and free from battery recharge/replacement burdens, therefore future sections of this thesis project will investigate if LoRa can be practically implemented with thermoelectric energy harvesting to produce IoT sensor nodes that can be powered indefinitely.

Utilizing LoRa to decrease the power consumption of the developed wireless IoT sensor network to a fraction of a traditional Wi-Fi system, increases the feasibility of energy

harvesting to completely remove the recharge/replacement burden of attached batteries that may hinder IoT adoption. Advantages may also be present in systems where batteries are not used, such as in the case of hardwired sensors where wires may be removed completely, allowing for sensors to be placed in locations without powered lines making them more portable.

4.3 Developing a TEG

This section will attempt to address the final research question of this research project, namely "can thermoelectric energy harvesting be used to power sensors to monitor CO_2 with a long battery life, thus removing the battery recharge/replacement burden of IoT technology?"

This research question will be address by determining a waste heat source within an Australian brewery that can be implemented with a developed TEG to recharge the developed LoRa sensor node depicted in Section 3.3.1.2 and remove its battery recharge/replacement burden to furthermore demonstrate the removal of aforementioned burden for similar IoT technology as a whole, thus allowing for the creation of feasible wireless IoT sensor networks that will prevent unsafe workplace environments.

4.3.1 Pipe Temperature and Predicted Power Output

The pipe outlet of two Simons 500 kW boilers as depicted in Figure 40 was identified as a potential waste heat source that could be utilized with a developed TEG to harvest waste heat and convert it into electricity. The first step to determine if the waste heat source was suitable included testing the boiler's outlet pipe temperature throughout a single working day to ensure that the temperature was firstly sufficient for energy harvesting and secondly below the maximum operating temperature of the chosen thermoelectric modules. The boiler's outlet pipe temperature results versus time for a single working day are depicted in Figure 64. It can be seen from Figure 64 that once the boilers were turned on (approx. 7 am), the pipe temperature increased to approximately 150 °C for the duration of their operation, until the boilers were turned off (approx. 4 pm), after which, residual heat remains, allowing the temperatures to remain above 40 °C for an extended period. It can also be seen however, that the ambient temperature also increased within the brewery due to the abundance of heat produced by the

boilers, this was as expected and may reduce energy harvesting capabilities of a TEG due to reduced convection cooling capabilities.

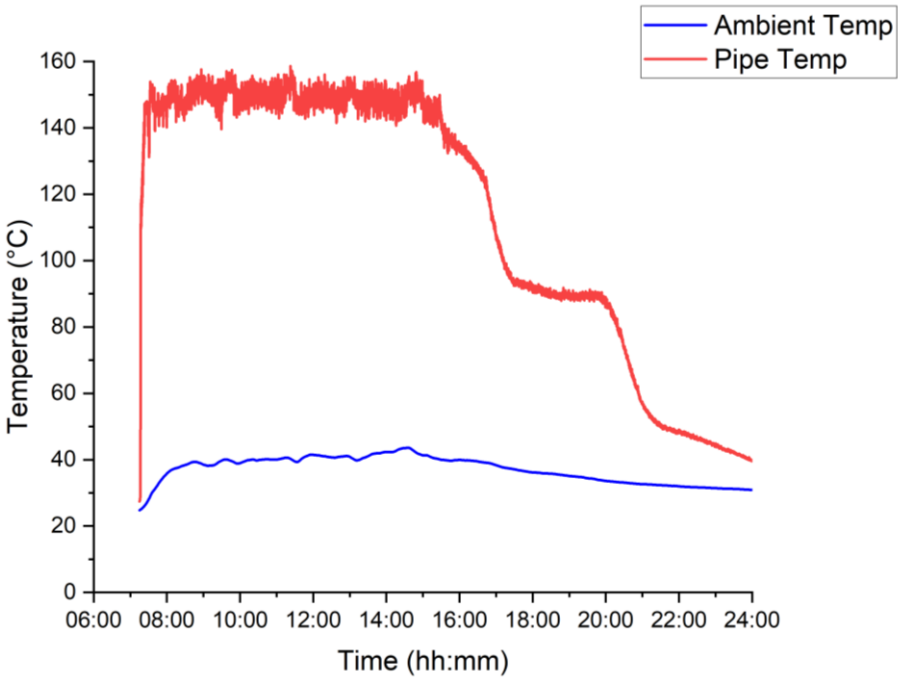

Figure 64. Boiler hot pipe temperature versus time during a single day of operation.

Expanding on the lab experiments conducted using the Noctua NH-P1 heatsink mentioned in Section 3.3.1.1, the combination of hot and cold-side temperatures, 150 °C and 90 °C respectively, produced a predicted power output of 2.2 W for the developed TEG according to the thermoelectric module datasheet. If it is conservatively predicted that this peak power output would be available for 1 working day (8 hours per week), a predicted energy supply of 17.6 Wh can be estimated. The estimated Wh usage of the LoRa (AH1) sensor node can then be determined by taking its approximate average current consumption and multiplying it by a Li-Ion batteries nominal voltage of 3.7 V and 24 hours. It is stated in the datasheet of the AH1 CO_2 sensor that it consumes the same amount of current as the LP3 CO_2 sensor, therefore the average current consumption of the LoRa (AH1) sensor node should be equivalent to 3.24 mA determined by taking the LoRa (LP3) sensor node's battery life of 292.44 hours, determined in Section 4.2.4, and dividing it by the modelled battery capacity of 947 mAh, determined from Figure 38, while also assuming the Steval harvesting board consumes little to no current. The expected daily Wh usage of the LoRa (AH1) sensor node is therefore 0.29 Wh which could be supported by the predicted 17.6 Wh of the developed TEG, therefore it can be predicted that

the Noctua NHP1 is sufficient for this particular use case, however further practical tests are required to confirm that the developed TEG can indeed remove the battery recharge/replacement burden of the LoRa (AH1) sensor node.

4.3.2 Temperature and Open-Circuit Voltage Results

The first practical experiment with regards to validating the developed TEG included testing the temperatures and open-circuit voltage of the entire system. The temperature and open-circuit voltage results versus time recorded for 4 working days are depicted in Figure 65. 4 working days of results were essential in highlighting the consistency of the results. It can be seen from Figure 65 that the temperatures of the hot and cold-sides of the TEG, as well as the boiler's pipe, immediately increased when the boilers were activated for all 4 working days, resulted in temperatures that remain consistently elevated at close to 150 °C for anywhere from 7 - 9 h, strongly depending on how long the brewery was active per working day. The ambient temperature also seemed to increase with a more gradual trend throughout the time the boilers are active in all 4 cases. This is due to the reasons highlighted in the aforementioned section above. The boilers are then deactivated, resulting in a decrease of temperature in all 4 cases, however residual heat allows temperatures to remain above room temperature for extended periods of time which varies for each case.

The shape of the cooling curves are interesting, they show a sudden temperature drop as soon as the boilers were deactivated, followed by a plateau at around 100 °C, where steam in the boiler appears to be condensing. This phase change enabled the hot-side temperatures to remain roughly constant for extended periods in all 4 cases, after which, the temperature of water in the boiler cools down as expected for working days 2 and 4, however working days 1 (23:00) and 3 (68:00) appear to have a spike in temperatures long after the boilers are deactivated, this was most likely due to some trapped steam within the boilers being released from the lines as the boilers were cooled down.

The hot-side temperature of the chosen thermoelectric module closely tracked the pipe temperature in all 4 cases, being consistently 5-10 °C cooler during the operational phase, while the cold-side of the module was consistently 80-90 °C less than the pipe temperature. The ambient temperature in proximity to the boilers appeared to be higher than that in other parts of the brewery, being in excess of 30 °C most of the time on all 4 days and rising to be above

40 °C in some cases throughout the time the boilers were operational. As can be seen from Figure 65 the temperature-time plots were very consistent for days that the boilers were operational, but start and end times of boiler operation were subject to some slight variations, due to the boiler being manually operated.

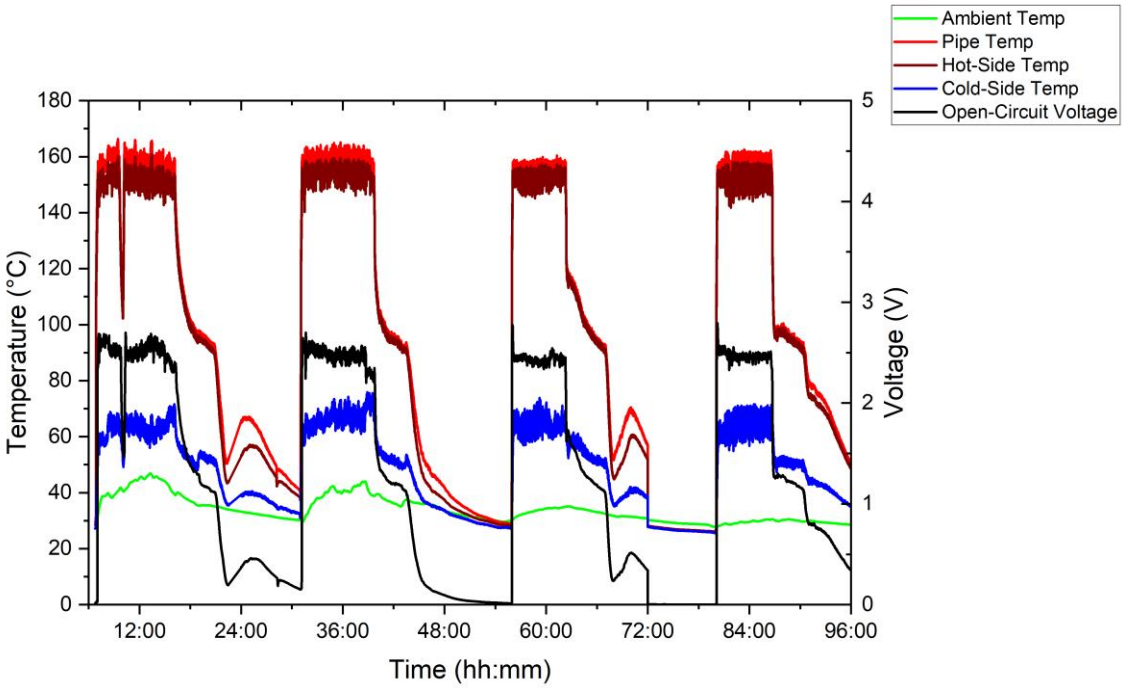

Figure 65. Temperatures and open-circuit voltage versus time across 4 working days of testing.

It should also be noted that the drop in temperatures during working day 1 were due to employee operational error and not due to the boilers themselves.

In order to visualise the consistency of the open-circuit voltage supplied by the TEG, the open-circuit voltages achieved for the previous 4 working days have been plotted with the common time-periods of 00:00 and 24:00 in Figure 66. It is evident from Figure 66 that the open-circuit voltage of the system, in all 4 cases, increases proportionally with the increase in temperature difference between the hot and cold-sides of the TEG, and then decreasing, following a similar trend, when the boilers were deactivated and the temperature difference reduced. Looking closely at the open-circuit voltages while the boilers were active shows that the voltages were indeed very consistent with voltages ranging from approximately 2.3 to 2.6 V. While it does

appear that voltages do decrease slightly as time progresses with the boilers active, this is as expected due to increase ambient temperatures as aforementioned, therefore the only true differing factor between sets of data was the duration that the boilers were active resulting in differing periods of increased open-circuit voltages above 2 V, however it was noted by brewery staff that boiler uptime was mostly between 7-9 hours as can be seen form the results.

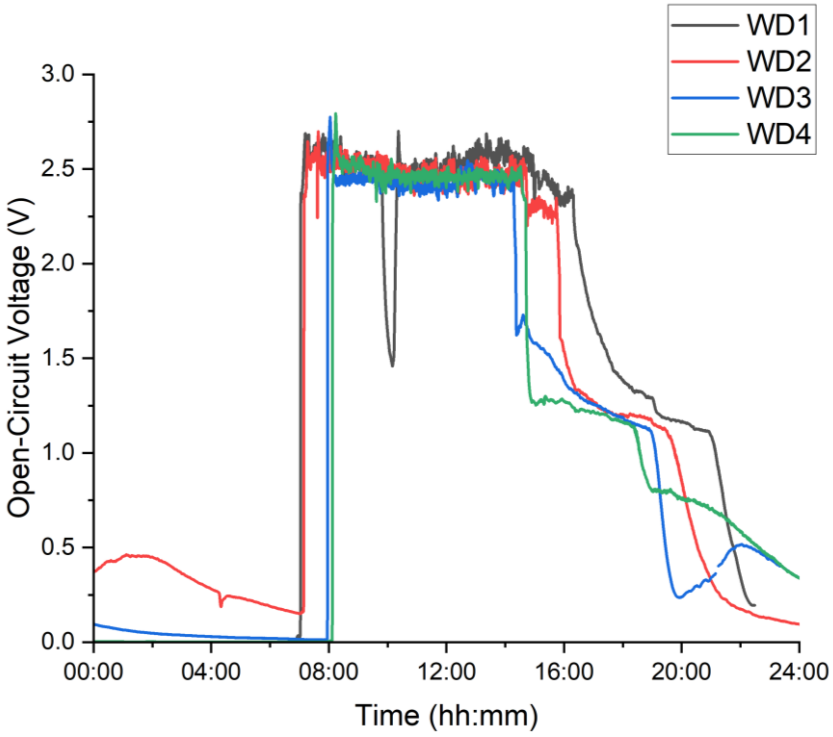

Figure 66. Open-circuit voltage versus time across 4 working days of testing.

4.3.3 Power output

It is evident from the aforementioned section that temperatures and open-circuit voltages are very consistent between working days, however this means little when attempting to address research question 3 without testing the power output of the developed TEG system. The power output over time of the system is extremely important and will create the basis for practically predicting the systems feasibility, while measuring the maximum matched power output of the system will allow for a comparison with the predicted maximum matched power output from previous sections and the maximum power output of previous TEG systems in the literature.

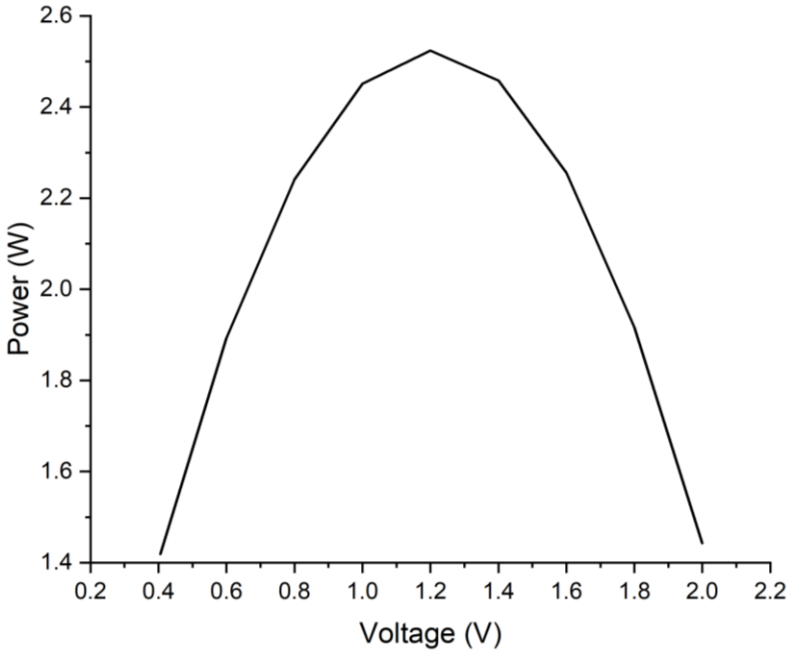

Figure 67. IV curve - maximum power output results.

A thermoelectric module typically has an IV curve that is in the inverse quadratic form with the maximum matched power output of the module in the middle. An example IV curve of the developed TEG system is presented in Figure 67. The IV sweep in this case took place approximately 5 min after the boilers were activated. The IV curve in Figure 67 provides the maximum matched power output of the developed system that was observed throughout testing which was equal to approximately 2.5 W and was present in the middle of the curve as expected. This occurred at a voltage close to 1.2 V and a matched circuit resistance of approximately 0.6 Ω. The maximum matched power output of the developed system was relatively similar to the predicted value of 2.2 W from initial lab experiments outlined in Section 4.3.1, with the difference attributed to the fact that the lab system used thermal pads instead of thermal paste which most likely reduced power output due to having a higher thermal resistance.

Even though the maximum matched power output of the system would be adequate to sufficiently charge the LoRa (AH1) sensor node if it consistently reaches it for at least 8 hours a week, it is of extreme important to practically test the maximum matched power output over time of the developed system to provide further evidence of its capabilities. The temperature and power generated as a function of time for a working day are depicted in Figure 68. It can

be seen that the boiler is active for approximately 10 h, however harvesting, indicated by power generation >0.25 W, occurred for approximately 14 h due to residual heat provided by the boilers. The average power generated from the TEG for the particular working day assessed was approximately 1.02 W, noting that power decreased slightly with an increase in ambient temperature due to the decrease in open-circuit voltage as seen in prior sections. It was evident in previous sections that open-circuit voltage and temperatures were consistent across multiple working days, therefore power should be consistent also and by integrating under the power curve, it was possible to calculate energy generated throughout the working day above which was approximately 18.8 Wh. This energy however, is measured prior to it passing through the energy harvesting board and the battery as seen in Figure 45, therefore a 90% round-trip efficiency, taken from the Steval board's datasheet, would need to be assumed whenever the battery is used, this results in approximately 16.9 Wh of usable energy per working day whenever the boilers were active for approximately 10 hours. Throughout the experimental time-period of 32 days there were 18 working days where the boilers were actively used on average for 7.67 hours a day, therefore on average approximately 12.96 Wh of useable energy was generated across working days where the boilers were active, thus across the entire 32-day time-period on average 7.29 Wh of energy was generated per day. To operate continuously with a measurement interval of 7 s, the LoRa (AH1) sensor node consumed approximately 0.29 Wh of energy each day, therefore it is experimentally predicted that the developed TEG, by providing 7.29 Wh daily. can remove the battery recharge and replacement burden of at least 10 LoRa (AH1) sensor nodes, thus creating a wireless IoT sensor network that can uniformly monitor CO_2 throughout the brewery workplace supporting safe working environments.

It should be noted that a network of LoRa (AH1) sensor nodes, or similar, can utilize the developed TEG to charge their batteries in rotation while continually being active and sensing, for example 1 sensor node can use the TEG to charge its battery then it can be detached from the TEG and be completely portable wherever there is LoRa signal, after which another sensor node can take its place utilizing the TEG as a single point of charging without removing or replacing batteries. Another option would be to have each sensor node fixed to its own TEG, in order to remove the burden of switching out sensor nodes. Whichever option is chosen, it is evident that the developed TEG removes the burden of recharging/replacing the battery of wireless IoT sensor nodes due to its ease of use. It can be said that a traditional portable sensor with a battery pack can be charged from a power outlet similar to using the TEG, however

within a brewery it is extremely difficult to find power outlets and it was stated by some of the brewery workers during experimentation that the use of extension cables is difficult due to the continuous hosing of the brewery floor with water. The TEG also allows the sensor nodes to remain operational and within the brewery workspace when charging.

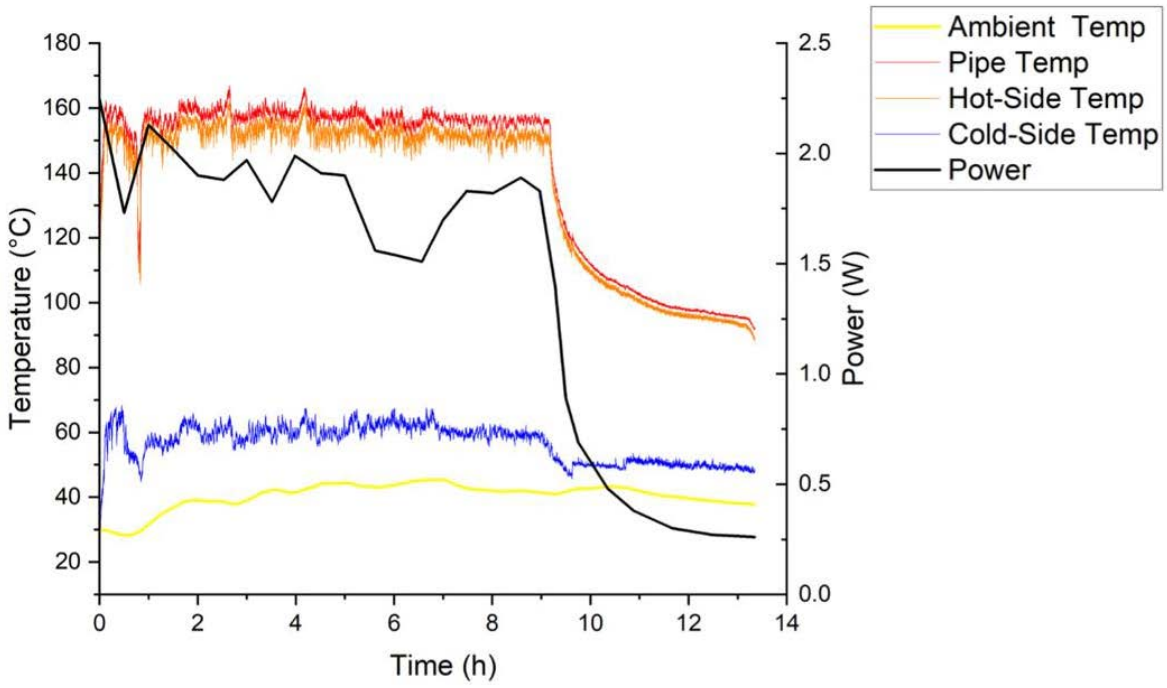

Figure 68. Temperature and power generated versus time results during working day of testing.

It should also be noted that discrepancies in power output while the boilers were active can be attributed to the fact that measuring the maximum matched power output of the system using an IV curve creates a small cooling effect on the module which may cause values to be less than the actual real-world power output.

4.3.4 Battery voltage

It is now important to see how the power generated by the developed TEG system effects the battery connected to the LoRa (AH1) sensor node. The results for battery voltage versus time for day 8 out of the 32-day time-period battery tests were run are plotted in Figure 69. It is evident from Figure 69 that the battery voltage of the LoRa (AH1) sensor node decreased

slowly initially, before the boilers were activated (8 am). This decrease indicated that the sensor node was active, measuring CO_2 values, and consuming power from the battery. Once the boilers were activated, the battery voltage increased, indicating that energy was being harvested from the TEG and the power generated was then used via the energy harvesting board to charge the battery, even though the sensor node was still active, drawing power, and monitoring CO_2 levels.

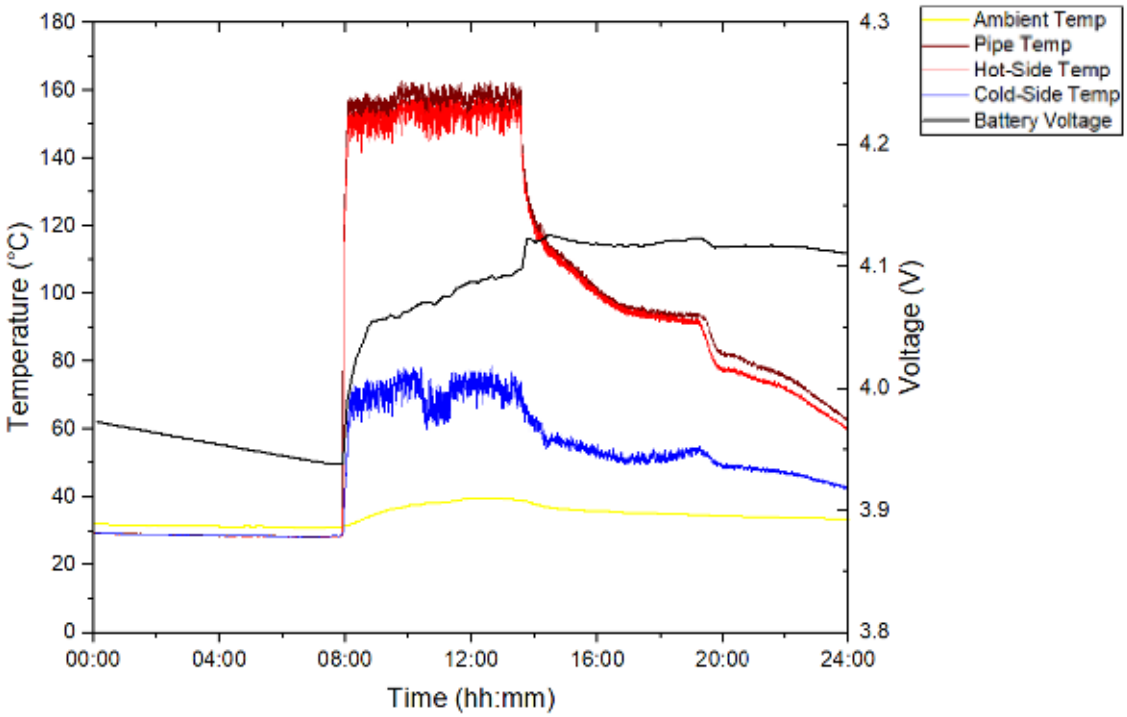

Figure 69. Temperature and battery voltage versus time during Day 8 of testing.

It can also be seen that the battery voltage at the 0-hour mark is approximately 3.95 V, while the battery voltage at the 24-hour mark is approximately 4.1 V, indicating that the battery has been charged more than it has been discharged throughout the working day, even though the sensor node has been active throughout. Lastly, residual heat can be seen to provide energy for the system to maintain the battery charge for extended periods after the boilers were deactivated.

4.3.5 Battery state-of-charge

The final step in determining whether the developed TEG system is feasible requires the monitoring of the LoRa (AH1) battery's state of charge over the entire 32-day time period to highlight whether the sensor node's battery recharge/replacement burden has been removed. The battery SOC over the 768-h time-period (32 days) is plotted in Figure 70.

The SOC at the start of the time-period is equivalent to 70.4 % while the SOC at the end of the period is equivalent to 87.2%, indicating that an increase in SOC has been achieved throughout the time-period of experimentation. It Is also evident that increases in SOC were directly related to the boilers being active, leading to battery charging due to the TEG harvesting waste heat and converting it into electricity. Peaks in the SOC can be directly related to operation of the boilers as outlined in Table 5, likewise, decreases in SOC represent the battery being drained due to no harvesting being available and the sensor node being active. The SOC throughout can also be seen to vary between 50 - 100 %. The SOC drops from 100% to 50% between 264 h and 336 h, during the 3-day period where the boilers are non-operational. Given that the battery has a capacity of 1,000 mAh (3.7-4.2 Wh), this equates roughly to the SOC reduction that would be expected. During hours 480 h and 576 h a power interruption to the Keithley measurement apparatus meant data was not recorded, however during this time the SOC would likely have dropped lower – perhaps as low as 20% − due to 5 days of boiler inactivity. As Figure 71 demonstrates, CO_2 was recorded throughout the 5-day period and the battery was not fully depleted. It was previously determined, as depicted in Figure 63, that the battery should last approximately 292.44 hours (approx. 12 days), however it appears that adding the Steval harvesting board reduced this close to 164 hours as can be seen from Figure 70. This could of course be extended by increasing the battery size to accommodate variations and interruptions in the brewery's brewing schedule, e.g. during festive holiday periods. A larger battery would be advisable since even after extended periods of boiler inactivity, the battery was able to be returned to fully charged relatively quickly. Likewise, during periods of repeated boiler operation (200 h to 280 h), the battery was at full capacity during periods where waste heat was available meaning it could not be stored. The field testing indicates that the LoRa (AH1) wireless IoT CO_2 sensor node could be powered indefinitely via the use of the developed TEG system, strengthening the feasibility of a wireless IoT sensor network that can monitor IAQ

throughout the brewery workplace, thus reducing the possibility of unmonitored CO_2 areas and unsafe workplaces.

It should be noted that the SOC graph does not paint an accurate picture with regards to how many sensor nodes the developed TEG can actually support due to the Steval energy harvesting board of the LoRa (AH1) sensor node being limited to currents below 100 mA as shown in its datasheet, this limited the amount of energy that could be used prior to being harvested from the TEG and can be improved by using better harvesting boards in future work.

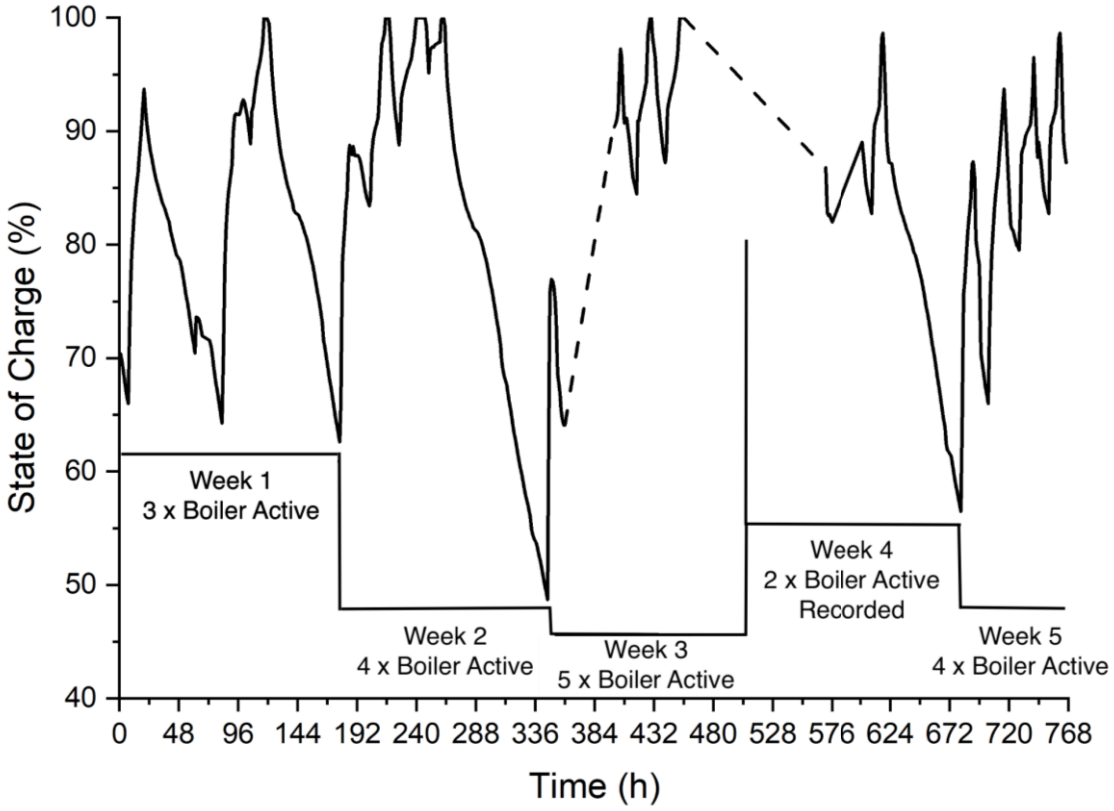

Figure 70. SOC of the system's battery (%) throughout the 32-day test period.

4.3.6 CO_2 monitoring

The CO_2 results over the entire 768-hour (32 days) time-period must be shown in order to stand as evidence that the LoRa (AH1) sensor node was active throughout battery SOC testing. The CO_2 versus time results across the aforementioned time-period are depicted in Figure 71. It can

be seen that the sensor node was active throughout testing, with no battery recharge or replacement, therefore leading to the conclusion that the battery recharge/replacement burden of the LoRa (AH1) wireless IoT CO_2 sensor node has been removed by the developed TEG system. Removing this burden strengthens the feasibility of a wireless IoT sensor network that can monitor IAQ throughout the brewery workplace, thus reducing the possibility of unmonitored CO_2 areas and unsafe workplaces.

It should be noted that the results in Figure 71 show that high CO_2 levels were also detected in this brewery, similar to that seen in Section 4.1. Peak CO_2 concentrations of over 8,000 ppm were reached, which are approaching dangerous levels [11-14]. This finding also strengthens the need for more robust IAQ monitoring within breweries.

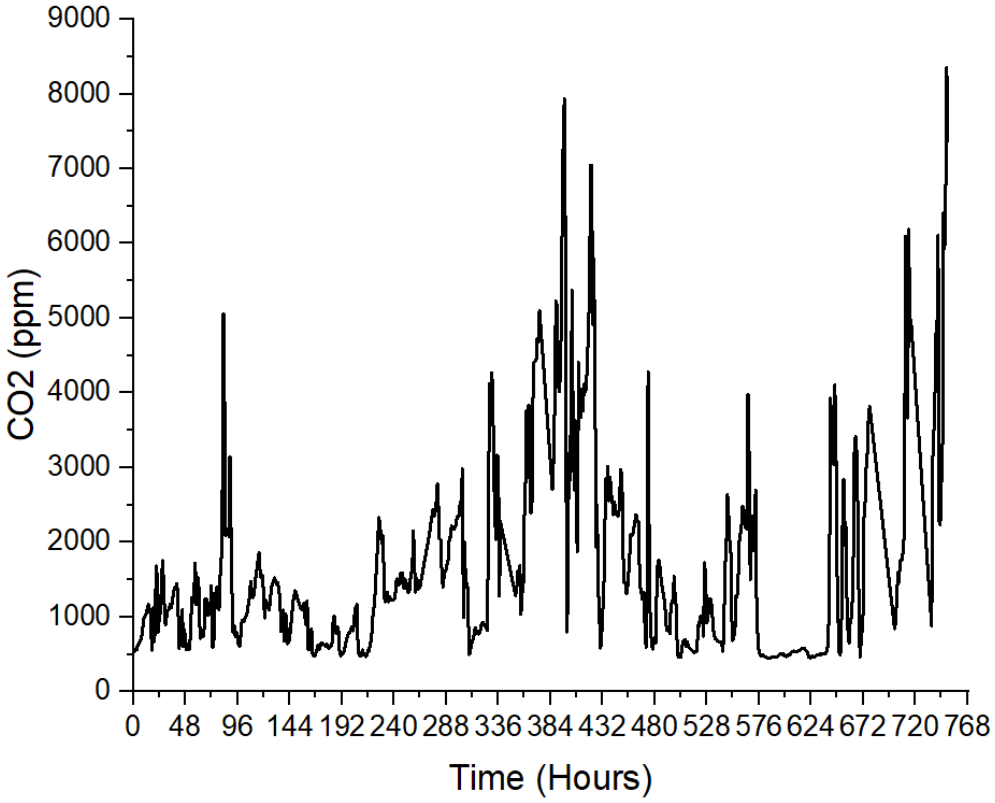

Figure 71. CO_2 versus time throughout the 32-day test period.

4.3.7 Comparison with Previous Systems

Figure 72 contains the power densities for 18 TEG systems in the literature plus the developed TEG system for comparison to determine whether the power density achieved by the current

system is reasonable. A line of best fit has been drawn on the graph to aid with the aforementioned by creating an average trend of the previous systems, if the developed system's power density result was to lie below the line of best fit, it can be concluded that the developed system is performing below expectations, however as can be seen from Figure 72 the developed system, as depicted by the red box, lies above the line of best fit, this, along with the fact that the developed system is within range of similar previous TEG systems and the fact that the systems maximum power output is close to the predicted value, indicates that the developed system is performing within range of expectation. Increasing the temperature delta of the system may improve the maximum power output using the same effective cross-sectional area as can be seen in [91–93], with the maximum power densities depicted in Figure 72, however as explored in previous sections, the power generated by the developed system is already sufficient for removing the battery recharge/replacement burden of wireless IoT sensor nodes and also finding a waste heat source within a brewery that can create a larger temperature delta for a TEG system would be highly unlikely. The developed system however, can be adapted to work in other manufacturing sectors that may be able to provide a greater temperature delta as the Noctua NHP1 did not appear to reach maximum capacity, thus resulting in greater maximum power output.

Comparing the developed TEG system with that developed by Huizen (2020) [56], leads to the conclusion that the system developed in this research project is an improvement on Huizen's system in several ways. Firstly, Huizen's system involved wearing a backpack which can make it difficult for a brewery employee to do their day-to-day acridities due to the need to access tight spaces or due to the high temperature within a brewery creating reluctance to wear extra layers of clothing, while the system developed in this research project can be placed anywhere within the brewery, either portably once charged using the TEG, or coupled with the TEG near a hot surface as outlined in Section 4.3.3. Another advantage of the system developed in this research project is the fact that it does not require the removable, recharging, and replacement of batteries as Huizen's does.

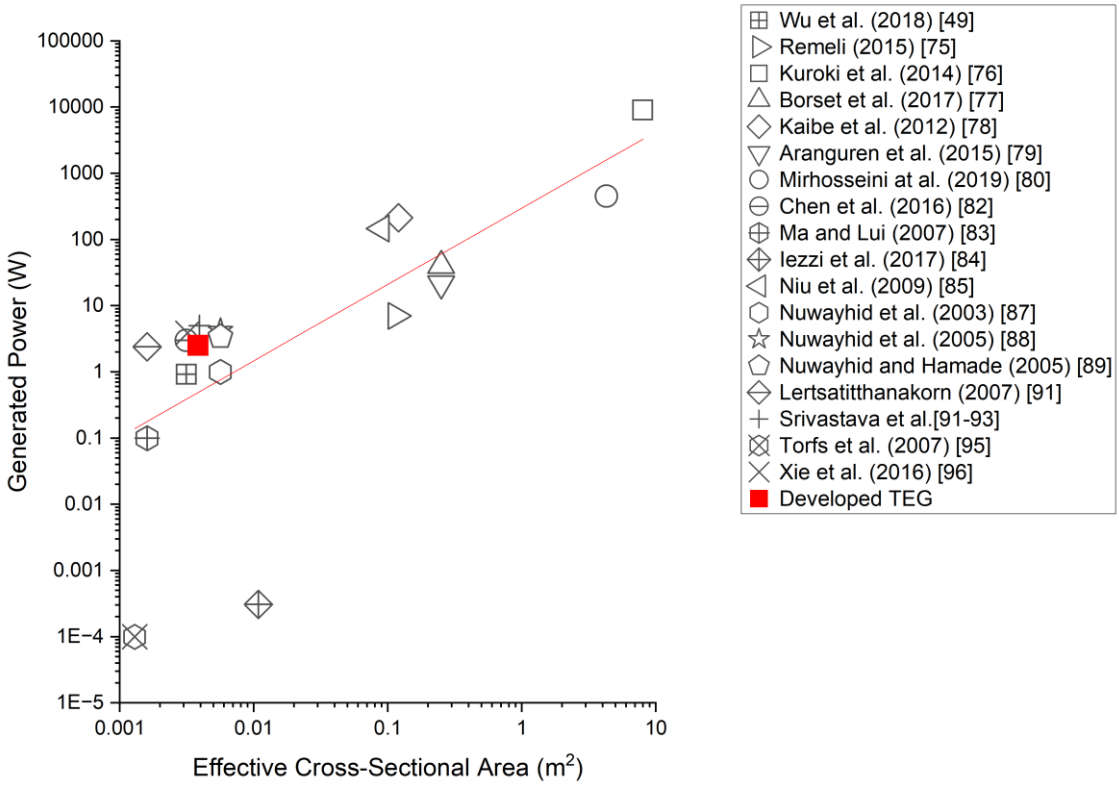

Figure 72: Generated power versus effective cross-sectional area for TEG systems reported in the scientific literature + developed system [49, 75–80, 82–85, 87–93, 95, 96].

Comparing the developed TEG system with other systems in the literature such a [71, 82, 98], shows that some previous systems in the literature required the sensor portion of the system to be coupled with the TEG throughout the entirety of its lifetime, while the system developed in this research project features a sensor node portion that can be detached from the TEG while running completely on its own battery, therefore allowing it to be fully portable. This also means that several sensor nodes can utilize the TEG instead of just one sensor, leading to the creation of a wireless sensor network that can facilitate a safe workplace environment throughout.

4.4 Conclusions

All three research questions have been addressed successfully. Research question one, was addressed by measuring the CO_2 levels inside an Australian brewery in three locations, the fermentation tanks (Node 1), canning line (Node 2), and office (Node 3) using a network of wireless Wi-Fi IoT CO_2 sensor nodes. It was concluded that the venting of fermentation CO_2

and the unintentional venting of CO_2 during the filling of storage tanks, can cause the indoor CO_2 levels in breweries to exceed safe limits (>1,000 and >10,000 ppm) for prolonged periods. The identification of differences in measured CO_2 at different times and locations throughout the brewery also revealed that a single hard-wired CO_2 sensor may be inadequate to support IAQ monitoring. This strengthened the need to have a network of CO_2 sensors inside a craft brewery, however the battery life of the current wireless Wi-Fi IoT sensor nodes was too short. Research question two, was also addressed by attempting to remove the battery recharge/replacement burden of the aforementioned Wi-Fi sensor nodes through implementing LoRa. LoRa was analysed alongside Wi-Fi by developing three wireless sensor nodes that measured the CO_2 concentration indoors. The LoRa (LP3) sensor node achieved a battery runtime that was 17.2 times greater than the Wi-Fi (LP3) sensor node, equalling a decreased power consumption of over 94%, however the battery runtime of approximately 290 hours for the LoRa (LP3) was still not considered long enough, due to battery recharge/replacement burdens. Finally, research question three, was addressed by developing a TEG to recover brewery waste heat from the hot pipe outlet of two steam boilers within an Australian brewery, converting it into electricity to recharge the battery of a LoRa (AH1) wireless IoT CO_2 sensor node. The TEG was successful at removing the battery recharge/replacement burden of the developed LoRa (AH1) sensor node, evidenced by its ability to keep the battery charged with no input from any user/source over the (32 days) test period, while the sensor node was active and continuously monitoring CO_2 levels. The TEG was also capable of producing a maximum power output of approximately 2.5 W, while generating approximately 7.29 Wh of useable energy daily, allowing for the prediction that it can support as many as ten wireless LoRa IoT sensor nodes, thus creating a wireless IoT sensor network that can uniformly monitor CO_2 throughout the brewery workplace supporting safe working environments.

It should be noted that, while this use case focussed on brewery waste heat and CO_2 monitoring, similar TEG systems may be developed and applied in other manufacturing sectors. This is particularly true for those that offer abundant waste heat and where it would be advantageous for wireless sensor networks to monitor other parameters, such as temperature, humidity, etc.

Finally, the limiting factor of the developed TEG that still needs to be overcome in order for it to be commercially viable is its cost.

The cost of the TEG was approximately $600 AUD, which would need to be minimized to improve the feasibility of purchasing the system for consumers.

5. Conclusions and Future Work

Maintaining a high standard of indoor air quality (IAQ) is vital to ensuring good human health since many humans spend the majority of their time indoors. The measured concentration of CO_2 in air is a good proxy for IAQ. Likewise, high levels of CO_2, above 1,000 and 10,000 ppm, have been shown to cause cognitive impairment and physiological impairment, respectively. Work environments that generate CO_2 as an inherent part of their business present a unique and significant risk in terms of poor IAQ. Craft breweries generate CO_2 and, unlike larger breweries, often lack the technology to capture and re-use the fermentation CO_2 for beer carbonation. This research project demonstrated that the venting of fermentation CO_2 and the unintentional venting of CO_2 during the filling of storage tanks can cause the indoor CO_2 levels in breweries to exceed safe limits. This was shown by monitoring CO_2 levels inside an Australian craft brewery using a network containing three wireless Wi-Fi IoT sensor nodes, positioned strategically in different sections of the brewery. The maximum CO_2 level recorded was in excess of 18,000 ppm, with the maximum time period levels exceeded 1,000 and 10,000 ppm for a single venting event were 425 min and 26 min, respectively. The identification of differences in measured CO_2 at different times and locations throughout the brewery revealed that a single hard-wired CO_2 sensor may be inadequate to support IAQ monitoring. This strengthens the need to have a network of CO_2 sensors inside a craft brewery. For this purpose, wireless sensor nodes would be most suitable, however the battery life of the sensor nodes is a key consideration, and the battery life of the wireless Wi-Fi IoT sensor nodes used initially were far too short.

LoRa was then analysed alongside Wi-Fi with regards to the wireless IoT sensor node use-case, by developing three sensor nodes that measured the CO_2 concentration indoors and forwarded the information to their respective gateways. The LoRa (LP3) sensor node consumed, with the configuration being TX(10) + DR(5), the least average current of 4.33 mA at a measurement interval of 30 s, while the Wi-Fi (LP3) and LoRa (SCD30) (same configuration as LP3) consumed 52.81 mA and 13.51 mA, respectively. Propagation capabilities were also analysed, and it was evident that the LoRa wireless protocol outperformed Wi-Fi due to the LoRa (LP3) sensor node having less maximum average current draw which was equivalent to 4.56 mA as opposed to the Wi-Fi (LP3) sensor node's 102.51 mA. The LoRa (LP3) sensor node therefore achieved a battery runtime that was 17.2 times

greater than the Wi-Fi (LP3) sensor node, equalling a decreased power consumption of over 94%. That said, a battery runtime of approximately 290 hours for the LoRa (LP3) was still not considered feasible due to battery recharge/replacement burdens occurring every 10 or so days. The significant decrease in power consumption of wireless IoT sensor nodes using LoRaWAN, in conjunction with no decrease in signal range and penetrability, did however increase the feasibility of utilizing energy harvesting technologies, such as thermoelectrics, to remove battery recharge/replacement burdens, increasing the willingness for adoption and increasing sensor node portability.

A thermoelectric generator (TEG) was then developed to recover brewery waste heat from the hot pipe outlet of two steam boilers within an Australian brewery, converting it into electricity to recharge the battery of the developed LoRa (AH1) wireless IoT CO_2 sensor node. The TEG was successful at removing the battery recharge/replacement burden of the developed LoRa sensor node, evidenced by its ability to keep the battery charged with no input from any user/source over the (32 days) test period in the field, while the sensor node was active and monitoring CO_2 levels. The TEG was also capable of producing a maximum power output of approximately 2.5 W, while generating approximately 7.29 Wh of useable energy daily, allowing for the prediction that it can support a network of wireless IoT sensor nodes that can uniformly monitor CO_2 throughout the brewery workplace, thus supporting safe working environments.

5.1 Future Work

The research presented has made a step forward towards improving IAQ monitoring within craft breweries by combining CO_2 monitoring and thermoelectric energy harvesting technologies. Despite these advancements, several areas warrant further investigation to expand upon findings and address remaining challenges. Future work includes the following:

1. **TEG Optimizations:** Optimizations to the current TEG design to improve power output, such as improved cold-side heat exchanger design.
2. **IoT Sensor Network Development:** Creating a network of wireless IoT sensor nodes that can utilize a single TEG. This can be implemented by firstly placing the sensor nodes in different locations throughout the brewery while creating a cloud based alert system that notifies employees via mobile phone notifications when a particular node

is low in battery, it can then be connected to the TEG for charging. Throughout this entire process it should be noted that the sensor node will always be actively monitoring for CO_2 even within the charging location, something that can be beneficial in craft breweries which contain fermentation tanks in proximity of the boiling areas such as is the case with the craft brewery depicted in Section 3.1.1. When compared with traditional charging which requires the removal of batteries from sensor nodes or the connection to hardwired wall outlets, which can be difficult to access, this would be an improvement.

3. **Sensor Deployment:** Future studies should also explore strategies for optimizing the deployment and accuracy of the CO_2 sensor nodes within the IoT sensor network. Investigating various sensor placements, beyond that of which has been presented in this research project, including those in non-obvious locations where CO_2 accumulation might be more prevalent, could enhance the accuracy and effectiveness of the IoT sensor network.
4. **Vented CO_2 Volume Monitoring**: The volume of vented CO_2 can be monitored in future. This may allow for the determination of trends with regards to the amount of vented CO_2 and its effects on overall CO_2 concentrations within different workspaces of the brewery.
5. **Advanced Data Analysis and Machine Learning Integration:** To maximize the utility of the measured and databased CO_2 data. Future research should integrate advanced data analysis techniques and machine learning algorithms, thus facilitating the development of predictive models that analyse databased CO_2 data to forecast potential spikes or trends and enable proactive IAQ management. Machine learning algorithms could also identify patterns and correlations between CO_2 levels and operational activities, leading to predicted targeted interventions beforehand.
6. **Real-Time IAQ Management Integration:** Future research should investigate how the IoT CO_2 monitoring network can be integrated into real-time IAQ management platforms to automatically adjust ventilation, cooling, or other environmental controls based on advanced data analysis techniques and machine learning algorithms to enhance overall air quality management. This integration could include developing user interfaces that allow operators to monitor and control IAQ parameters remotely.

7. **Different Sensor Types:** Investigating other TEG powered sensor types that could be beneficial for use within a brewery such as temperature sensors which can be used to monitor the surface temperatures of brewing equipment to ensure workers do not contact surfaces which may cause injury. Another sensor type would be motion sensors which can be used to open ventilation systems when employees are in proximity of high CO_2 concentration areas.
8. **Exploration of Sensor Fusion Techniques:** Integrating data from multiple types of sensors, such as temperature, humidity, and VOC sensors, alongside CO_2 measurements could provide a more comprehensive understanding of IAQ. Future research should explore sensor fusion techniques to combine data from different sources and enhance the accuracy of IAQ assessments.
9. **Scalability and Adaptability to Diverse Environments:** Expanding the research to evaluate the scalability of the proposed technologies in larger or different brewery settings is recommended. Studies can also assess how the IoT sensor network can be adapted for use in various industrial environments, such as food processing facilities, manufacturing plants, or large commercial buildings. Additionally, exploring the application in residential settings could provide valuable insights into broader applicability.
10. **Long-Term Performance and Reliability of Sensor Nodes:** A thorough evaluation of the long-term performance and reliability of the LoRa sensor node and TEG is essential. Future work should assess how sensor nodes perform under varying conditions over extended periods, including different temperature ranges, humidity levels, and potential exposure to corrosive environments. This will help determine their durability and operational stability in real-world scenarios.
11. **Economic and Environmental Impact Analysis:** A comprehensive analysis of the economic and environmental impacts of implementing a TEG and IoT sensor network may be essential for promoting adoption. Future work should include cost-benefit analyses that consider installation, maintenance, and operational costs versus potential savings and benefits.
12. **User-Centric Design and Usability Studies:** Engaging with end-users to gather feedback on the usability and functionality of the sensor networks can be advantageous. Future research should involve user-centred design approaches, including usability

testing and surveys, to identify practical challenges and improve system interfaces. Ensuring that the technology is user-friendly and meets the needs of brewery staff will be critical for successful implementation and adoption.

13. **Development of Hybrid Energy Harvesting Systems:** While the TEG successfully addressed battery recharge/replacement issues, exploring hybrid energy harvesting systems could provide a more robust solution. Combining multiple energy sources, such as thermoelectrics and indoor solar panels might offer more consistent and sustainable power.
14. **Commercial Potential:** Exploring the commercial potential of the developed TEG system could be done by creating a UTS startup company from the developed TEG prototype that could then be used, with the assistance of UTS, to bring the product forward for commercialisation.
15. **Development of Standards and Guidelines:** Finally, developing industry standards and guidelines for IAQ monitoring in craft breweries and similar environments could help standardize practices and ensure consistent quality. Future work could focus on establishing best practices for sensor deployment, data analysis, and system integration.

In summary, while this research has made progress in IAQ monitoring for craft breweries, addressing the diverse areas of future work highlighted above will enhance the effectiveness, reliability, and practical application of CO_2 monitoring networks. By exploring these avenues, researchers can contribute to safer and healthier indoor environments for employees across a range of workplaces.

References

[1] Indoor Air Quality - Joseph M. Seguel, Richard Merrill, Dana Seguel, Anthony C. Campagna, 2017, https://journals.sagepub.com/doi/full/10.1177/1559827616653343 (accessed 21 January 2023).

[2] Morawska L, Allen J, Bahnfleth W, Bennett B, Bluyssen PM, Boerstra A, Buonanno G, Cao J, Dancer SJ, Floto A, Franchimon F, Greenhalgh T, Haworth C, Hogeling J, Isaxon C, Jimenez JL, Kennedy A, Kumar P, Kurnitski J, Li Y, Loomans M, Marks G, Marr LC, Mazzarella L, Melikov AK, Miller SL, Milton DK, Monty J, Nielsen PV, Noakes C, Peccia J, Prather KA, Querol X, Salthammer T, Sekhar C, Seppänen O, Tanabe S, Tang JW, Tellier R, Tham KW, Wargocki P, Wierzbicka A, Yao M. Mandating indoor air quality for public buildings. *Science* 2024; 383: 1418–1420.

[3] Persily A, de Jonge L. Carbon dioxide generation rates for building occupants. *Indoor Air* 2017; 27: 868–879.

[4] Emmerich SJ, Persily AK. *State-of-the-art review of CO2 demand controlled ventilation technology and application*. NIST IR 6729, Gaithersburg, MD: National Institute of Standards and Technology.

[5] Ramalho O, Wyart G, Mandin C, Blondeau P, Cabanes P-A, Leclerc N, Mullot J-U, Boulanger G, Redaelli M. Association of carbon dioxide with indoor air pollutants and exceedance of health guideline values. *Building and Environment* 2015; 93: 115–124.

[6] Satish U, Mendell MJ, Shekhar K, Hotchi T, Sullivan D, Streufert S, Fisk WJ. Is CO2 an Indoor Pollutant? Direct Effects of Low-to-Moderate CO2 Concentrations on Human Decision-Making Performance. *Environmental Health Perspectives* 2012; 120: 1671–1677.

[7] Allen JG, MacNaughton P, Cedeno-Laurent JG, Cao X, Flanigan S, Vallarino J, Rueda F, Donnelly-McLay D, Spengler JD. Airplane pilot flight performance on 21 maneuvers in a flight simulator under varying carbon dioxide concentrations. *J Expo Sci Environ Epidemiol* 2019; 29: 457–468.

[8] Allen JG, MacNaughton P, Satish U, Santanam S, Vallarino J, Spengler JD. Associations of Cognitive Function Scores with Carbon Dioxide, Ventilation, and Volatile Organic Compound Exposures in Office Workers: A Controlled Exposure Study of Green and Conventional Office Environments. *Environ Health Perspect* 2016; 124: 805–812.

[9] Zhang X, Wargocki P, Lian Z, Thyregod C. Effects of exposure to carbon dioxide and bioeffluents on perceived air quality, self-assessed acute health symptoms, and cognitive performance. *Indoor Air* 2017; 27: 47–64.

[10] ACGIH. Carbon Dioxide. In Threshold Limit Values for Chemical Substances and Physical Agents and Biological Exposure Indices with 7th Edition Documentation. Cincinnati, OH, USA: American Conference of Governmental Industrial Hygienists, 2017.

[11] DFG. Kohlendioxid [MAK Value Documentation, 2002]. In Documentations and Methods; MAK Collection for Occupational Health and Safety. Weinheim, Germany: Wiley-VCH Verlag GmbH, 2012.

[12] HSDB. Carbon Dioxide. In: *In Hazardous Substances Data Bank Number: 516*. Bethesda, MD, USA: U.S. National Library of Medicine, 2015.

[13] Rice SA. Health Effects of Acute and Prolonged CO2 Exposure in Normal and Sensitive Populations*. Alexandria, VA, USA, 2003.

[14] Australia Standards. AS 5034-2005: Installation and use of inert gases for beverage dispensing.

[15] Haxhibeqiri J, De Poorter E, Moerman I, Hoebeke J. A Survey of LoRaWAN for IoT: From Technology to Application. *Sensors* 2018; 18: 3995.

[16] Reynaud CA, Clerc R, Lechêne PB, Hébert M, Cazier A, Arias AC. Evaluation of indoor photovoltaic power production under directional and diffuse lighting conditions. *Solar Energy Materials and Solar Cells* 2019; 200: 110010.

[17] Tran VV, Park D, Lee Y-C. Indoor Air Pollution, Related Human Diseases, and Recent Trends in the Control and Improvement of Indoor Air Quality. *International Journal of Environmental Research and Public Health* 2020; 17: 2927.

[18] Brook RD, Rajagopalan S, Pope CA, Brook JR, Bhatnagar A, Diez-Roux AV, Holguin F, Hong Y, Luepker RV, Mittleman MA, Peters A, Siscovick D, Smith SC, Whitsel L, Kaufman JD, American Heart Association Council on Epidemiology and Prevention, Council on the Kidney in Cardiovascular Disease, and Council on Nutrition, Physical Activity and Metabolism. Particulate matter air pollution and cardiovascular disease: An update to the scientific statement from the American Heart Association. *Circulation* 2010; 121: 2331–2378.

[19] Miller MR, Shaw CA, Langrish JP. From particles to patients: oxidative stress and the cardiovascular effects of air pollution. *Future Cardiology* 2012; 8: 577–602.

[20] US EPA O. Volatile Organic Compounds' Impact on Indoor Air Quality, https://www.epa.gov/indoor-air-quality-iaq/volatile-organic-compounds-impact-indoor-air-quality (2014, accessed 22 January 2023).

[21] Dunagan SC, Dodson RE, Rudel RA, Brody JG. Toxics use reduction in the home: lessons learned from household exposure studies. *Journal of Cleaner Production* 2011; 19: 438–444.

[22] Huang Y, Ho SSH, Ho KF, Lee SC, Yu JZ, Louie PKK. Characteristics and health impacts of VOCs and carbonyls associated with residential cooking activities in Hong Kong. *Journal of Hazardous Materials* 2011; 186: 344–351.

[23] Lee K, Choi J-H, Lee S, Park H-J, Oh Y-J, Kim G-B, Lee W-S, Son B-S. Indoor levels of volatile organic compounds and formaldehyde from emission sources at elderly care centers in Korea. *PLoS One* 2018; 13: e0197495.

[24] Liu S, Li R, Wild RJ, Warneke C, de Gouw JA, Brown SS, Miller SL, Luongo JC, Jimenez JL, Ziemann PJ. Contribution of human-related sources to indoor volatile organic compounds in a university classroom. *Indoor Air* 2016; 26: 925–938.

[25] Tang X, Misztal PK, Nazaroff WW, Goldstein AH. Siloxanes Are the Most Abundant Volatile Organic Compound Emitted from Engineering Students in a Classroom. *Environ Sci Technol Lett* 2015; 2: 303–307.

[26] Brickus LSR, Cardoso JN, de Aquino Neto FR. Distributions of Indoor and Outdoor Air Pollutants in Rio de Janeiro, Brazil: Implications to Indoor Air Quality in Bayside Offices. *Environ Sci Technol* 1998; 32: 3485–3490.

[27] Bernstein JA, Alexis N, Bacchus H, Bernstein IL, Fritz P, Horner E, Li N, Mason S, Nel A, Oullette J, Reijula K, Reponen T, Seltzer J, Smith A, Tarlo SM. The health effects of nonindustrial indoor air pollution. *Journal of Allergy and Clinical Immunology* 2008; 121: 585–591.

[28] Weschler CJ. Roles of the human occupant in indoor chemistry. *Indoor Air* 2016; 26: 6–24.

[29] Huang Y, Yang Z, Gao Z. Contributions of Indoor and Outdoor Sources to Ozone in Residential Buildings in Nanjing. *International Journal of Environmental Research and Public Health* 2019; 16: 2587.

[30] Katsouyanni K, Touloumi G, Spix C, Schwartz J, Balducci F, Medina S, Rossi G, Wojtyniak B, Sunyer J, Bacharova L, Schouten JP, Ponka A, Anderson HR. Short-term effects of ambient sulphur dioxide and particulate matter on mortality in 12 European cities: results from time series data from the APHEA project. Air Pollution and Health: a European Approach. *BMJ* 1997; 314: 1658–1663.

[31] Seow WJ, Downward GS, Wei H, Rothman N, Reiss B, Xu J, Bassig BA, Li J, He J, Hosgood HD, Wu G, Chapman RS, Tian L, Wei F, Caporaso NE, Vermeulen R, Lan Q. Indoor concentrations of nitrogen dioxide and sulfur dioxide from burning solid fuels for cooking and heating in Yunnan Province, China. *Indoor Air* 2016; 26: 776–783.

[32] Hänninen O, Goodman P. Outdoor Air as a Source of Indoor Pollution. In: Harrison RM, Hester RE (eds) *Issues in Environmental Science and Technology*. Cambridge: Royal Society of Chemistry, pp. 35–65.

[33] WHO. . In: *Air Quality Guidelines: Chapter 7.4 Sulfur Dioxide*. WHO Regional Oce for Europe: Copenhagen, Denmark, 2000.

[34] World Health Organization: Geneva, Switzerland. International Programme on Chemical Safety. Carbon Monoxide. 1999.

[35] Raub JA, Mathieu-Nolf M, Hampson NB, Thom SR. Carbon monoxide poisoning--a public health perspective. *Toxicology* 2000; 145: 1–14.

[36] Alonso-Moreno C, García-Yuste S. Environmental potential of the use of CO2 from alcoholic fermentation processes. The CO2-AFP strategy. *Sci Total Environ* 2016; 568: 319–326.

[37] D'alberti V, Cammalleri I, La Bella S, Ragusa M, Pavan M, Ragusa R. PRODUCTION OF ALGAE WITH CO2 FROM WINE FERMENTATION: AN IMPORTANT WAY TO REDUCE EMISSIONS. EXPERIMENTAL TESTS ON 4 ALGAL STRAINS. 2019. Epub ahead of print 6 December 2019. DOI: 10.5071/23rdEUBCE2015-1CV.1.51.

[38] Sehrawat D, Gill NS. Smart Sensors: Analysis of Different Types of IoT Sensors. In: *2019 3rd International Conference on Trends in Electronics and Informatics (ICOEI)*, pp. 523–528.

[39] Jiang Y, Li K, Tian L, Piedrahita R, Yun X, Mansata O, Lv Q, Dick RP, Hannigan M, Shang L. MAQS: a personalized mobile sensing system for indoor air quality monitoring. In: *Proceedings of the 13th international conference on Ubiquitous computing*. New York, NY, USA: Association for Computing Machinery, pp. 271–280.

[40] Marques G, Ferreira CR, Pitarma R. Indoor Air Quality Assessment Using a CO2 Monitoring System Based on Internet of Things. *J Med Syst* 2019; 43: 67.

[41] Kodali RK, Pathuri S, Rajnarayanan SC. Smart Indoor Air Pollution Monitoring Station. In: *2020 International Conference on Computer Communication and Informatics (ICCCI)*. 2020, pp. 1–5.

[42] Fernández-Ramos MD, Moreno-Puche F, Escobedo P, García-López PA, Capitán-Vallvey LF, Martínez-Olmos A. Optical portable instrument for the determination of CO2 in indoor environments. *Talanta* 2020; 208: 120387.

[43] Ould S, Bennett NS. Energy Performance Analysis and Modelling of LoRa Prototyping Boards. *Sensors* 2021; 21: 7992.

[44] Seller, O.B.; Sornin, N. *Low Power Long Range Transmitter*. US Patent 9,252,834, 2016.

[45] Sforza, F. *Communications System*. US Patent 720139, 2009.

[46] LoRa Alliance. LoRaWAN R1.0. Open Standard Released for the IoT. *LoRa Alliance: Fremont, CA, USA*.

[47] Petäjäjärvi J, Mikhaylov K, Pettissalo M, Janhunen J, Iinatti J. Performance of a low-power wide-area network based on LoRa technology: Doppler robustness, scalability, and coverage. *International Journal of Distributed Sensor Networks* 2017; 13: 1550147717699412.

[48] LoRa Alliance. RP002-1.0.3 LoRaWAN® Regional Parameters. *LoRa Alliance: Fremont, CA, USA*.

[49] Wu F, Rüdiger C, Redouté J-M, Yuce MR. WE-Safe: A wearable IoT sensor node for safety applications via LoRa. In: *2018 IEEE 4th World Forum on Internet of Things (WF-IoT)*. 2018, pp. 144–148.

[50] Lee H-C, Ke K-H. Monitoring of Large-Area IoT Sensors Using a LoRa Wireless Mesh Network System: Design and Evaluation. *IEEE Transactions on Instrumentation and Measurement* 2018; 67: 2177–2187.

[51] Abraham S, Li X. A Cost-effective Wireless Sensor Network System for Indoor Air Quality Monitoring Applications. *Procedia Computer Science* 2014; 34: 165–171.

[52] Kim J-Y, Chu C-H, Shin S-M. ISSAQ: An Integrated Sensing Systems for Real-Time Indoor Air Quality Monitoring. *IEEE Sensors Journal* 2014; 14: 4230–4244.

[53] Pitarma R, Marques G, Ferreira BR. Monitoring Indoor Air Quality for Enhanced Occupational Health. *J Med Syst* 2017; 41: 23.

[54] Moon YS, Choi HR, Kim JJ, Kim DW, Cho JH, Kim JW, Jeong JW. Development of IoT-Based Sensor Tag for Smart Factory. *IRJECE* 2017; 3: 28.

[55] Husein NAA, Hadi A, Putri D. Evaluation of LoRa-based Air Pollution Monitoring System. *IJACSA*; 10. Epub ahead of print 2019. DOI: 10.14569/IJACSA.2019.0100753.

[56] Huizen D. The Assessment of Co2 Exposures, Workload Demands, and Musculoskeletal Disorder Risk on Heart Rate for Select Craft Brewery Job Tasks. *Dissertations*, https://scholarworks.wmich.edu/dissertations/3644 (2020).

[57] Twahirwa E, Mtonga K, Ngabo D, Kumaran S. A LoRa enabled IoT-based Air Quality Monitoring System for Smart City. In: *2021 IEEE World AI IoT Congress (AIIoT)*. 2021, pp. 0379–0385.

[58] Syafrudin M, Alfian G, Fitriyani NL, Rhee J. Performance Analysis of IoT-Based Sensor, Big Data Processing, and Machine Learning Model for Real-Time Monitoring System in Automotive Manufacturing. *Sensors* 2018; 18: 2946.

[59] Salamone F, Danza L, Meroni I, Pollastro MC. A Low-Cost Environmental Monitoring System: How to Prevent Systematic Errors in the Design Phase through the Combined Use of Additive Manufacturing and Thermographic Techniques. *Sensors (Basel)* 2017; 17: 828.

[60] Lee J, Noh SD, Kim H-J, Kang Y-S. Implementation of Cyber-Physical Production Systems for Quality Prediction and Operation Control in Metal Casting. *Sensors (Basel)* 2018; 18: 1428.

[61] Calderón Godoy AJ, González Pérez I. Integration of Sensor and Actuator Networks and the SCADA System to Promote the Migration of the Legacy Flexible Manufacturing System towards the Industry 4.0 Concept. *Journal of Sensor and Actuator Networks* 2018; 7: 23.

[62] Li J, Xie J, Yang Z, Li J. Fault Diagnosis Method for a Mine Hoist in the Internet of Things Environment. *Sensors (Basel)* 2018; 18: 1920.

[63] Suherman S. WiFi-Friendly Building to Enable WiFi Signal Indoor. *Bulletin of Electrical Engineering and Informatics* 2018; 7: 264–271.

[64] Liang R, Zhao L, Wang P. Performance Evaluations of LoRa Wireless Communication in Building Environments. *Sensors* 2020; 20: 3828.

[65] ESP32 Thing Hookup Guide - SparkFun Learn, https://learn.sparkfun.com/tutorials/esp32-thing-hookup-guide/hardware-overview# (accessed 30 July 2024).

[66] Adafruit SCD-30 - NDIR CO2 Temperature and Humidity Sensor - STEMMA QT / Qwiic, https://core-electronics.com.au/adafruit-scd-30-ndir-co2-temperature-and-humidity-sensor-stemma-qt-qwiic.html (accessed 30 July 2024).

[67] Marin-Garcia G, Vazquez-Guzman G, Sosa JM, Lopez AR, Martinez-Rodriguez PR, Langarica D. Battery Types and Electrical Models: A Review. In: *2020 IEEE International Autumn Meeting on Power, Electronics and Computing (ROPEC)*, pp. 1–6.

[68] Gilbert JM, Balouchi F. Comparison of energy harvesting systems for wireless sensor networks. *Int J Autom Comput* 2008; 5: 334–347.

[69] Starner T. Human-powered wearable computing. *IBM Systems Journal* 1996; 35: 618–629.

[70] HoSung Lee. Thermoelectrics. In: *Thermal Design*. John Wiley & Sons, Ltd, pp. 100–179.

[71] Wu Y. Thermoelectric Energy Harvesting for Sensor Powering, https://vtechworks.lib.vt.edu/handle/10919/90891 (2019, accessed 23 January 2023).

[72] Dalala ZM, Saadeh O, Bdour M, Zahid ZU. A New Maximum Power Point Tracking (MPPT) Algorithm for Thermoelectric Generators with Reduced Voltage Sensors Count Control †. *Energies* 2018; 11: 1826.

[73] Cook E. The Flow of Energy in an Industrial Society. *Scientific American* 1971; 225: 134–147.

[74] Lu H, Price L, Zhang Q. Capturing the invisible resource: Analysis of waste heat potential in Chinese industry. *Applied Energy* 2016; 161: 497–511.

[75] Remeli MF. *Simultaneous industrial waste heat recovery and power generation using heat pipe assisted thermoelectric generator*. RMIT University, https://researchrepository.rmit.edu.au/esploro/outputs/doctoral/Simultaneous-industrial-waste-heat-recovery-and-power-generation-using-heat-pipe-assisted-thermoelectric-generator/9921863933801341 (2015, accessed 23 January 2023).

[76] Kuroki T, Kabeya K, Makino K, Kajihara T, Kaibe H, Hachiuma H, Matsuno H, Fujibayashi A. Thermoelectric Generation Using Waste Heat in Steel Works. *Journal of Elec Materi* 2014; 43: 2405–2410.

[77] Børset MT, Wilhelmsen Ø, Kjelstrup S, Burheim OS. Exploring the potential for waste heat recovery during metal casting with thermoelectric generators: On-site experiments and mathematical modeling. *Energy* 2017; 118: 865–875.

[78] Kaibe H, Makino K, Kajihara T, Fujimoto S, Hachiuma H. Thermoelectric generating system attached to a carburizing furnace at Komatsu Ltd., Awazu Plant. *AIP Conference Proceedings* 2012; 1449: 524–527.

[79] Aranguren P, Astrain D, Rodríguez A, Martínez A. Experimental investigation of the applicability of a thermoelectric generator to recover waste heat from a combustion chamber. *Applied Energy* 2015; 152: 121–130.

[80] Mirhosseini M, Rezania A, Rosendahl L. Power optimization and economic evaluation of thermoelectric waste heat recovery system around a rotary cement kiln. *Journal of Cleaner Production* 2019; 232: 1321–1334.

[81] Wu Y, Zhang H, Zuo L. Thermoelectric energy harvesting for the gas turbine sensing and monitoring system. *Energy Conversion and Management* 2018; 157: 215–223.

[82] Chen J, Klein J, Wu Y, Xing S, Flammang R, Heibel M, Zuo L. A Thermoelectric Energy Harvesting System for Powering Wireless Sensors in Nuclear Power Plants. *IEEE Trans Nucl Sci* 2016; 63: 2738–2746.

[83] Ma K-Q, Liu J. Heat-driven liquid metal cooling device for the thermal management of a computer chip. *J Phys D: Appl Phys* 2007; 40: 4722.

[84] Iezzi B, Ankireddy K, Twiddy J, Losego MD, Jur JS. Printed, metallic thermoelectric generators integrated with pipe insulation for powering wireless sensors. *Applied Energy* 2017; 208: 758–765.

[85] Niu X, Yu J, Wang S. Experimental study on low-temperature waste heat thermoelectric generator. *Journal of Power Sources* 2009; 188: 621–626.

[86] Gao HB, Huang GH, Li HJ, Qu ZG, Zhang YJ. Development of stove-powered thermoelectric generators: A review. *Applied Thermal Engineering* 2016; 96: 297–310.

[87] Nuwayhid RY, Rowe DM, Min G. Low cost stove-top thermoelectric generator for regions with unreliable electricity supply. *Renewable Energy* 2003; 28: 205–222.

[88] Nuwayhid RY, Shihadeh A, Ghaddar N. Development and testing of a domestic woodstove thermoelectric generator with natural convection cooling. *Energy Conversion and Management* 2005; 46: 1631–1643.

[89] Nuwayhid RY, Hamade R. Design and testing of a locally made loop-type thermosyphonic heat sink for stove-top thermoelectric generators. *Renewable Energy* 2005; 30: 1101–1116.

[90] Lertsatitthanakorn C. Electrical performance analysis and economic evaluation of combined biomass cook stove thermoelectric (BITE) generator. *Bioresource Technology* 2007; 98: 1670–1674.

[91] Srivastava A, Duran D, Pinder M, Raghav V, Komerath N. Conceptual design of a thermoelectric Edu-Kitchen system. In: *Controls and Computation 2012 International Conference on Power, Signals*. 2012, pp. 1–6.

[92] Srivastava A. Design of a thermoelectric edu-kitchen system, https://smartech.gatech.edu/handle/1853/46910 (2013, accessed 1 February 2023).

[93] Srivastava A, Pinder M, Shah S, Raghav V, Komerath N. Thermoelectric and Thermophotovoltaic Micro-Renewable Power Systems for Home Use. In: *10th International Energy Conversion Engineering Conference*. American Institute of Aeronautics and Astronautics. Epub ahead of print 2012. DOI: 10.2514/6.2012-3900.

[94] Kim SJ, We JH, Cho BJ. A wearable thermoelectric generator fabricated on a glass fabric. *Energy Environ Sci* 2014; 7: 1959.

[95] Torfs T, Leonov V, Vullers R. Pulse Oximeter Fully Powered by Human Body Heat. *Sens Transducers J*; 80.

[96] Xie Y, Wu S, Yang C. Generation of electricity from deep-sea hydrothermal vents with a thermoelectric converter. *Applied Energy* 2016; 164: 620–627.

[97] Alegría P, Catalán L, Araiz M, Casi Á, Astrain D. Thermoelectric generator for high temperature geothermal anomalies: Experimental development and field operation. *Geothermics* 2023; 110: 102677.

[98] Samson D, Kluge M, Becker Th, Schmid U. Wireless sensor node powered by aircraft specific thermoelectric energy harvesting. *Sensors and Actuators A: Physical* 2011; 172: 240–244.

[99] Benday NS, Dryden DM, Kornbluth K, Stroeve P. A temperature-variant method for performance modeling and economic analysis of thermoelectric generators: Linking material properties to real-world conditions. *Applied Energy* 2017; 190: 764–771.

Appendix

A.0 Arduino IDE Codes

A.1 Wi-Fi - SCD30

```
#include "EspMQTTClient.h"
#include <Wire.h>
#include <Adafruit_SCD30.h>

Adafruit_SCD30  scd30;

int ledPin = 5;



EspMQTTClient client(
  "Access Point",
  "Password”,
  "IP Address",
  "testclient"
);

void setup() {

  digitalWrite(ledPin, LOW);
  Serial.begin(115200);
  client.enableDebuggingMessages(true);
  client.setWifiReconnectionAttemptDelay(5000);
  client.setMqttReconnectionAttemptDelay(5000);
  // Try to initialize!
  if (!scd30.begin()) {
    Serial.println("Failed to find SCD30 chip");
    while (1) {
      delay(10);
    }
  }
  Serial.println("SCD30 Found!");

  scd30.setMeasurementInterval(30);
  Serial.print("Measurement Interval: ");
  Serial.print(scd30.getMeasurementInterval());
  Serial.println(" seconds");
```

```
  scd30.forceRecalibrationWithReference(400);
}

void onConnectionEstablished() {


}

void loop() {

  if (scd30.dataReady()) {

    Serial.println("Data available!");


    if (!scd30.read()) {
      Serial.println("Error reading sensor data");
      return;
    }


    Serial.print("Temperature: ");
    Serial.print(scd30.temperature);
    Serial.println(" degrees C");


    Serial.print("Relative Humidity: ");
    Serial.print(scd30.relative_humidity);
    Serial.println(" %");


    Serial.print("CO2: ");
    Serial.print(scd30.CO2);
    Serial.println(" ppm");
    Serial.println("");

    client.publish("sensors/CO2-3", String(scd30.CO2));
    client.publish("sensors/temp-3", String(scd30.temperature));
    client.publish("sensors/hum-3", String(scd30.relative_humidity));

    Serial.print("Wifi: ");
    Serial.println(client.isWifiConnected());
```

```
   Serial.print("MQTT: ");
   Serial.println(client.isMqttConnected());


  }

  client.loop();


}
```

A.2 LoRa - SCD30

```
#include <Adafruit_SCD30.h>
#include "LoRaWAN.h"
#include <avr/dtostrf.h>
float inData;
char data[5] = {1, 2, 3, 4, 5};
char buffer[256];

Adafruit_SCD30  scd30;

#define REGION_AU915

const char *appEui  = "0101010101010101";
const char *appKey  = "D325944E9EB28D87DE38D6BB0AA9AA32";
const char *devEui  = "70B3D57ED005A226";

void setup() {
  Serial.begin(9500);

   LoRaWAN.begin(AU915);
    LoRaWAN.setSubBand(2);
    LoRaWAN.setADR(false);
    LoRaWAN.setDataRate(5);
    LoRaWAN.setTxPower(10);
   LoRaWAN.joinOTAA(appEui, appKey, devEui);
    Serial.println("JOIN( )");

  // Try to initialize!
  if (!scd30.begin()) {
    Serial.println("Failed to find SCD30 chip");
    while (1) {
```

```
    delay(10);
   }
  }
  Serial.println("SCD30 Found!");

  scd30.setMeasurementInterval(6);
  Serial.print("Measurement Interval: ");
  Serial.print(scd30.getMeasurementInterval());
  Serial.println(" seconds");

}


void loop() {

 //if (!LoRaWAN.busy() && LoRaWAN.joined()){
  if (scd30.dataReady()) {

   if (!scd30.read()) {
    Serial.println("Error reading sensor data");
    return;
   }
   Serial.println(scd30.CO2);
   inData=scd30.CO2;
    Serial.println(inData);
    dtostrf(inData,5,1,data);
      Serial.print("DR: ");
      Serial.print(LoRaWAN.getDataRate());
      Serial.print(", TxPower: ");
      Serial.println(LoRaWAN.getTxPower(), 1);
      LoRaWAN.beginPacket();
      LoRaWAN.write(data);
      LoRaWAN.endPacket();

    }
  // }

 }
```

A.3 LoRa - LP3

```
#include "LoRaWAN.h"
```

```
char inData='0';
String CO2String="";
int charCounter=0;
char data[5] = {1, 2, 3, 4, 5};
char buffer[256];

#define REGION_AU915


const char *appEui  = "0101010101010101";
const char *appKey  = "D325944E9EB28D87DE38D6BB0AA9AA32";
const char *devEui  = "70B3D57ED005A226";

void setup( void )
{
   Serial.begin(9600);
   Serial1.begin(9600);

   LoRaWAN.begin(AU915);
   LoRaWAN.setSubBand(2);
   LoRaWAN.setADR(false);
   LoRaWAN.setDataRate(5);
   LoRaWAN.setTxPower(30);


   LoRaWAN.joinOTAA(appEui, appKey, devEui);
   Serial.println("JOIN( )");

}

void loop( void )
{

  // if (!LoRaWAN.busy() && LoRaWAN.joined()){
   inData = Serial1.read();
   if (inData!=' '){  //we have a char available


     if (inData=='Z'){  //start of a sequence of chars detected

       charCounter=0; //start looping and recording char on next good read

     }
```

```
  if ((charCounter > 0) && (charCounter < 6)) {
    CO2String.concat(inData);      //if char charCounterber between 0 - 6 then add to string

   }

   if (charCounter==6){
    //when string is full print it and delete contents
    Serial.print("DR: ");
    Serial.print(LoRaWAN.getDataRate());
    Serial.print(", TxPower: ");
    Serial.println(LoRaWAN.getTxPower(), 1);
    Serial.println(CO2String);
    CO2String.toCharArray(data,6);
   delay(7000); //must add delay
    LoRaWAN.beginPacket();
    LoRaWAN.write(data);
    LoRaWAN.endPacket();
    CO2String="";
   }

   charCounter=charCounter+1;
  }


   //}
  }
```

A.4 Wi-Fi - LP3

```
#include "EspMQTTClient.h"
#include <Wire.h>
#include <HardwareSerial.h>
HardwareSerial SerialPort(2);




char inData='0';
String CO2String="";
int charCounter=0;
char data[5] = {1, 2, 3, 4, 5};
char buffer[256];
```

```
int ledPin = 5;


EspMQTTClient client(
  "Access Point",
  "Password”,
  "IP Address",  // MQTT Broker server ip
  "testclient"      // Client name that uniquely identify your device
);

void setup() {

digitalWrite(ledPin, LOW);

  SerialPort.begin(9600, SERIAL_8N1, 13, 12);
 Serial.begin (9600);

  client.enableDebuggingMessages(true);
  client.setWifiReconnectionAttemptDelay(5000);
  client.setMqttReconnectionAttemptDelay(5000);

}
void onConnectionEstablished() {

}


void loop() {


   if(SerialPort.available()){

    inData = SerialPort.read();
    if (inData!=' '){  //we have a char available


      if (inData=='Z'){  //start of a sequence of chars detected

        charCounter=0; //start looping and recording char on next good read

      }
```

```
 if ((charCounter > 0) && (charCounter < 6)) {
    CO2String.concat(inData);      //if char charCounterber between 0 - 6 then add to string
    delay(1400);
  }

  if (charCounter==6){
    //when string is full print it and delete contents
     Serial.println(CO2String);
    CO2String.toCharArray(data,6);


    client.publish("sensors/CO2-1", String(data));
    CO2String="";
  }

  charCounter=charCounter+1;
 }
}
client.loop();

  }
```